Coordination Chemistry Reviews, 78 (1987) 147–251
Elsevier Science Publishers B.V., Amsterdam — Printed in The Netherlands

4 TITANIUM

MARY A. JAMIESON, NICK SERPONE [1], and EZIO PELIZZETTI

CONTENTS

0010-8545/87/$36.75

INTRODUCTION

This article reviews the developments in the chemistry of titanium as well as applications of titanium compounds covered by Chemical Abstracts from Volume 99, number 25 through Volume 101, number 22. In keeping with our most recent review of this subject [2], the material is presented according to the element bonded to titanium.

General reviews on titanium covering the 1981 [3] and 1982 [4] calendar years have appeared in this journal. Additionally, a short review on angle-resolved photoemission experiments and band structure calculations for TiN has been published [5]. Several reviews on titanium oxides have been written, including one on titanium oxide based catalysts by Matsuda and Kato [6], on the kinetics and mechanisms of anodic reactions on oxide electrodes by Krishtalik [7], and others on rare earth perovskites [8], and $K_2Ti_6O_{13}$ [9]. Titanium sulfide polytypes ($Ti_{1+x}S_2$) were reviewed by Legendre and coworkers [10] and by Palosz et al. [11]. The electrochemical behavior and corrosivity of Ti in sulfide-containing aqueous solution have been discussed [12], as have crystal structure and density data of titanium chalcogenides and halides [13]. Newberry has reviewed, for 1982, the compounds of Group IVB, VB, VIB and VIIB [14], while the reactivities and stereochemical aspects of carbon-carbon bond formation reactions using titanium reagents ($TiCl_4$, $RTiX_3$, $R_2Ti(OR)_3$ and $RTi(NR'_2)_3$) was presented by Takahashi [15].

It is worth noting the increasing amount of published material concerning semiconductors and colloids employed in the catalytic and photocatalytic domains.

4.1 TITANIUM HYDRIDES

Surface-sensitive XPS and x-ray induced Auger electron spectroscopy have been employed to analyse surface changes in $TiH_{0.65}/KClO_4$ powders during accelerated aging at 333 and 393K. Cl^- forms at 0.02% per day for powders aged

at 393K for less than 145 days; no decomposition occurs for $KClO_4$ samples without pyrotechnic fuels under similar aging conditions [16]. The amount of hydrogen released during heating up to 800K and the decomposition energy of $TiH_{1.6}$ were determined by the $^{1}H(^{15}N,\alpha\gamma)^{12}C$ method. The decomposition energy depends on sample thickness [17]. The x-ray Raman spectrum from atomic hydrogen in $TiH_{1.9}$ has been interpreted [18] in terms of primarily atomic or molecular hydrogen trapped in the grain boundaries, there being no single storage mechanism at room temperature.

The equation of state for Ag-bonded TiH_2 was calculated over a large range of densities and temperatures. The results agree well with shock-wave data, and reportedly are an improvement over rational-function forms and additive-volume-mixing schemes [19]. Ab initio MO approximations have been employed to calculate the potential inversion barriers, 'h', for tetrahedral and square planar TiH_4, ScH_4^-, TiF_4, ScF_4^- and TiH_4^* (H^* = a pseudo-hydrogen atom in which the nuclear charge is increased to +1.1. In agreement with increasing electronegativities in changing from H to H^*, Sc to Ti and H to F, the 'h' values increase in the series TiH_4-TiH_4^*, ScH_4^--TiH_4, ScF_4^--TiF_4, TiH_4-TiF_4 and ScH_4^--ScF_4^- [20]. A recent study [21] demonstrates the applicability of a geometric model to predict stoichiometries and preferred hydrogen sites in hydrides of intermetallic compounds, specifically hydrides of MBe_2 (M = Ti, Zr, Hf, V) of three different structures.

4.2 TITANIUM BORIDES

Filonenko et al. [22] have studied the gas-free combustion of a pressed mixture of Ti-31%B in an argon-filled bomb at 4 MPa for the preparation of refractory TiB_2. The ratio of combustion rates of pressed and freely suspended specimens decreases from 1.3 to 1.2 with an increase of 80 to 10 mm in diameter. A mathematical model has been developed for the process of gasless combustion, with phase transitions for the Ti-B system as an example [23]. Crystals of TiB_2 can be prepared via reaction of ferrotitanium and ferroboron

at >1973K, having microhardness values of 3650 kgf mm^{-2}. The solubility of Fe in TiB_2 is >3 wt % [24].

An investigation of the steady-state propagation of the combustion wave for Fe-xB-yTi systems with x = 1-6 and y = 0.5-3 reveals that combustion progresses in stages. The results suggest that the combustion rate depends on the phase transition temperature and not on the maximum combustion temperature. For all samples, the final products are TiB_2 granules, TiB_2-Fe eutectics and the nonequilibrium phases Fe_3B, FeB and FeTi [25].

A rotating disk method was employed to determine the diffusion coefficients D and solution rate of titanium, chromium and boron in liquid copper and nickel [26]. The solution rate of $TiCrB_2$ in liquid copper, nickel and Cu-Ni alloys was also determined. The effective D values obtained for $TiCrB_2$ in liquid copper and nickel are 5.6×10^{-5} and 6.5×10^{-5} cm^2sec^{-1}, respectively, with the limiting step assigned to the diffusion of B into the liquid matrix [26]. An investigation of the species formed during solid-phase reaction of Al_2O_3, SiC or cubic BN with TiB_2, B or B_2O_3 indicates that the most stable species are those formed from the reactants with the greatest difference in electrical properties, which is related to the difference in gap energies of the reactants [27]. The stability of AlN, BN and AlN mixtures with BN, Si, ZrB_2, Al_2O_3 or TiB_2 at high temperatures depends on the composition and properties of the compounds forming on the surface of the oxidation product of the refractory and the metal melt [28].

A TiB_2 cathode has been used in the electrochemical reduction of $AlCl_3$ in an equimolar NaCl-KCl mixture at 973-1223K. The reduction of $AlCl_3$ occurs according to reaction (1) [29].

$$AlCl_3 + 3e^- \longrightarrow Al + 3Cl^- \qquad (1)$$

4.3 TITANIUM CARBIDES

Danilenko and coworkers [30] have calculated various thermodynamic properties of the phases and the phase diagram of the titanium-carbon system.

The Fermi surfaces in stoichiometric TiC and TiN were calculated using the constant-energy Korringa-Kohn-Rostoker/Green-function method, based on self-consistent APW potentials and APW Fermi energies [31]. The physicochemical properties of transition metal carbides (e.g., TiC, NbC, $VC_{0.98}$, $TeC_{0.99}$) have been calculated by a statistical method using Chebyshev coefficients for the description of the valence electron energy distribution and of the sublevels of the metal and carbon sublattices in the carbides. Also calculated was the pressure dependence of the physicochemical properties as a function of the electronic structure under compression conditions [32].

Infrared spectra of interstitial TiC and WC were interpreted in terms of a metal-metal-nonmetal bonding type [33]. Konishi et al. [34] have obtained the quasi-instantaneous Auger electron and Auger electron appearance potential spectra (AEAP) of Ti, TiC_x, TiN_x and TiO_2.

Electron microscope studies of the annealing of Ti-C thin films indicate that at <750K only TiC is formed in the film. Saturation of the Ti film by C occurs as a result of C-atom diffusion into Ti. At ∿750K, the formation and growth of TiC_xO_{1-x} is observed, as a result of C- and O-atom diffusion into TiC. At ∿1000K, oxidation of TiC occurs, giving TiO [35]. Oxygen diffusion coefficients in $TiC_{0.97}$ single crystals have been measured by a gas exchange technique. In this method, the amount of stable isotope taken up by the carbide is controlled by introducing a constant gas volume of oxygen-marked CO; secondary ion mass spectroscopy (SIMS) measured the concentration profiles [36]. The effect of added TiC (≤ 50 wt % Ti) on the overvoltage of O_2 and H_2 evolution on graphite in 1N NaOH can be determined from polarization curves [37]. Graphite with ≥ 30 wt % TiC approximates TiC with respect to its electrochemical properties.

AES and x-ray diffraction were used to characterize the thermal stability of Al thin films on Ti_xC films reactively-sputter-deposited on a silicon substrate. The stability increases with increasing C content in the Ti_xC films. An enhanced stability obtained for a $Ti_{3.1}C$ film pre-annealed at 1023K

for 30 min to induce a phase separation yielding a titanium silicide inner layer and a Ti_xC outer layer prior to Al deposition [38].

The reaction products obtained *via* electric explosion of the cubic phases TiC_xO_y and $TiC_xO_yH_m$ include the original phases graphite and TiO_2(rutile and anatase) [39].

Alekseev and coworkers [40] have analysed the physicochemical transformations occurring during the formation of $Ti_xC_yN_z$ from TiO_2 in a nitrogen plasma flow containing hydrocarbons. The formation of $Ti_xC_yN_z$ occurs *via* the formation of titanium clusters with subsequent nitridation and carbidization by the gaseous components, namely N and HCN. The thermodynamics of the preparation of $Ti_xC_yN_z$ films by chemical vapor deposition have been studied, and the relationships between the composition of input gas mixture ($TiCl_4$, CH_4, N_2, H_2) and the deposited film stoichiometry has been discussed [41]. The Ti-C-N phase diagram at 1673K was calculated using the Redlich-Kister substitutional model. Literature data was utilized to construct a phase diagram at 1900K, the temperature for vapor deposition [42].

The microstructures of TiC, TiN and TiC_xN_{1-x} powders before and after polishing were characterized by x-ray diffraction. Deformation induced defects and microstresses were observed, and dislocation densities were determined as a function of x [43]. The relation between the deformation characteristics and the microstructure of $Ti_{1-x}Nb_xC_{0.5}N_{0.5}$ reveal direct correlations between grain size and deformation flow in $TiC_{0.5}N_{0.5}$-$NbC_{0.5}N_{0.5}$ and between the microstress and the deformation in $Ti_{0.77}Nb_{0.25}C_{0.5}N_{0.5}$. The results were interpreted in terms of dislocation motion [44].

4.4 TITANIUM NITRIDES

Ultrafine TiN particles (<0.1 μm) can be prepared using an arc to melt titanium in a nitrogen atmosphere at 0.1 MPa pressure. A plasma gas-molten metal reaction involving activated atomic nitrogen serves an important role in the particle formation [45]. A microwave discharge method was employed to

study the kinetics of the nitridation of titanium and product distribution [46]. The effect of metal particle size and azide content on the amount of nitrogen in titanium nitride prepared from titanium and $Ba(N_3)_2$ has been investigated [47]. The nitrogen content decreases with increasing azide content. The deposition of TiN films from reaction of $TiCl_4$ with N_2 and H_2 on graphite was characterized over the temperature range 700-1673K. At 1373-1473K, single-crystal TiN films of rocksalt-type structure form; at higher temperatures, Ti(C,N) films are formed [48]. The nitridation of Al_3Ti at 873-1573K proceeds to 58% completion at 1273K with TiN and AlN formation, and to 98% completion at 1573K with formation of highly dispersed TiN-AlN powdered mixtures [49]. The kinetics and mechanism of TiN film deposition on porous (4-30%) iron powders were investigated by Kirilyuk and coworkers [50], who observed a maximum deposition rate at 12-18% porosity and TiN coatings inside the pores. At lower temperatures, amorphous films form, while crystalline films form at high temperatures.

The Green-function method has been utilized to calculate the number and nature of TiN(001) surface phonons. The electron-phonon interaction was discussed in terms of the coupling of the electronic charge-density deformations to the nuclear displacements [51]. An x-ray diffraction study of $TiN_{0.89}$ powder at room temperature reveals the electron transfer from the titanium atom to the nonmetal sites is (1.5 ± 0.3) electronic charges [52]. Ti-N films with nickel concentrations of 0-52 atomic % prepared by d.c. magnetron and radio frequency reactive sputtering were examined by transmission electron microscopy. A fully dense structure is confirmed by the maximum in the microhardness and density and the minimum in the electrical resistivity. The sample prepared by magnetron sputtering has a very inhomogeneous and voided microstructure and a lower hardness than the radio frequency sputtered sample with similar Ni content. A theory was proposed [53] for the development of a lamellar microstructure in the films containing two phases. The photo-emission spectra of TiN_{1-x} exhibit strong, resonance-enhanced, conduction-band

emission. The increased enhancement of the conduction-band peaks were indicative of approx. 25% of the vacancy electrons being bound in non-(d-like) states with a binding energy of about 2 eV [54]. Optical and electrical characteristics of TiN films produced by N_2^+ implantation on titanium-coated silicon wafers were studied in an effort to produce films with good transparency and conductivity to be used as antireflection coatings in solar cell manufacturing [55]. Solar selective properties of thin (5-120 nm) TiN films on fused SiO_2 and glass substrates have been determined. Reflectance and transmittance measurements confirm high solar and visible transmission, and sufficiently high infrared reflection [56]. The isobaric heat capacity of TiN was calculated from infrared absorption spectra and elasticity constants, and found to agree fairly well with the experimental data [57].

Valeskalne and coworkers [58] have studied the kinetics of the decomposition of TiN powders in mineral acid and NaOH solutions. The catalytic activity of nitrogen-deficient TiN was investigated in the ortho-para conversion of hydrogen [59]. The phase equilibrium has been determined for two isothermal sections in the ternary system Ti-Al-N. At 1273K, the H-phase Ti_2AlN and the cubic perovskite-type phase Ti_3AlN are found; at 1573K, $Ti_3Al_2N_2$ is also found [60]. The thermal conductivity of Si_3N_4-TiN composites with TiN dispersed uniformly in the Si_3N_4 matrix was measured at 293-1173K [61]. With increasing TiN content, the conductivity of composites having the crystalline Si_3N_4 matrix decreases drastically. The effect of added Ti atoms on the crystallization of amorphous Si_3N_4 thin films has been investigated; precipitated TiN particles enhance the crystallization of β-Si_3N_4 [62].

4.5 TITANIUM SULFIDES AND SELENIDES

Under high pressures at 1273K, stoichiometric TiS_2 formation accompanies non-stoichiometric TiS_2 from a starting stoichiometric mixture of titanium and sulfur. Further reaction yields stoichiometric TiS_2, as does reaction of titanium and TiS_3 at 1273K after 2 hours [63].

The calculation of electronic structure by the X_α method of discrete variation in the numerical basis of atomic orbitals, and x-ray spectra of clusters of $[Ti_7S_6]^{14+}$ in TiS_2 have been obtained. Additionally, $K_\beta S$ and $L_{II,III}Ti$ emission spectra, and the L_{III} quantum yield of Ti and L_{III} spectra of Ti in TiS_2 have been interpreted [64]. Raman spectra reported [65] for 2H-$Ti_{1.06}S_2$, 4H-$Ti_{1.16}S_2$, 12R-$Ti_{1.16}S_2$ and 4H-$Ti_{1.54}S_2$ at 300K were interpreted in terms of results obtained for TiS_2. With increasing titanium content, bands due to the A_{1g}-type mode become weaker compared to bands due to the R_g-type mode. Palosz [66] has discussed the effect of titanium layers on the process of ordering of sulfur and titanium hexagonal layers in polytypic $Ti_{1.2}S_2$ crystals. The stability of different arrangements of molecular S-Ti-S layers causing structural polytypism in Ti-S crystals may be influenced by fluctuations of the density of extra titanium atoms in the TiS_2 lattice.

Measurements of velocity and attenuation of ultrasonic plate mode waves were carried out on TiS_2, $TiSe_2$ and $TiS_{0.5}Se_{1.5}$ at 4-300K [67]. $TiSe_2$ exhibits large anomalies associated with the occurrence of a charge-density-wave transition near T_c = 200K. The temperature dependence of the velocity in $TiSe_2$ below T_c was accounted for by anharmonic and electron-phonon contributions, which reflect the opening of an energy gap on the Fermi surface by the charge-density wave. Above the T_c, the observed velocity changes affected by fluctuations over a wide temperature range were associated with phonon mode softening near the L point of the Brillouin zone as T_c is approached [66].

Holleck and coworkers [68] have reported test results obtained with hermetically sealed prototype secondary lithium batteries employing TiS_2, $Cr_{0.5}V_{0.5}S_2$ and MoS_3 cathode materials. The results indicate that cells based on amorphous MoS_3 exhibit the highest quasi-theoretical energy density. Charge-discharge characteristics of lithium anodes and TiS_2 cathodes were investigated in $LiBF_4$ solutions of THF and/or 1,3-dioxolane [69]. Charge-discharge potentials at the Li electrode are most stable in THF/1,3-dioxolane/$LiBF_4$, while the charging efficiency with respect to the TiS_2 electrode is best

in THF/$LiBF_4$. The discharge properties of Li/Ti_xS_2 (x = 1.00 - 1.13) batteries have been studied in several organic solvents (THF being the most favorable), and x-ray powder diffractometry was employed to characterize the discharged products [70]. Problems affecting discharge voltage profile, current density and energy density of solid state batteries incorporating vitreous solid electrolytes have been shown to be decreased by using layered cathodes. Those investigated included a structure consisting of distinct layers of a halogen (I, Br) and an intercalating cathode material (TiS_2), sandwich structures of the type TiS_2/X/TiS_2 (X = I, Br), and X layers encapsulated in a TiS_2 shell. Reportedly, the halogen enhances the removal of Li ions from the intercalating TiS_2 layer by controlling the continuous regeneration of the TiS_2 until all the halogen is converted to LiX [71]. Kikkawa and coworkers [72] have studied the effect of TiS_2 nonstoichiometry on the discharge of a Li-TiS_2 battery, and found it to be controllable. The effects of lithium anode passivation on the performance of Li/$LiAsF_6$--3-methylsulfolane/TiS_2 rechargeable cells were studied by SEM, XPS and FTIR spectroscopy in order to identify the chemical species formed on the anode [73]. A detailed mechanism for electrolyte degradation has been proposed. A current-pulse relation method was employed to determine the chemical diffusivity of Li in Li_xTiS_2 ($0 < x < 1$) cathodes in a Li/1.5M $LiAsF_6$--3-methylsulfolane/TiS_2 battery [74].

Atomic hydrogen is intercalated into the interlayers of TiS_2 *via* reduction of TiS_2 with granular zinc in dilute HCl. A pressure-jump technique with conductivity detection was employed to observe double relaxation in TiS_2(H). The fast relaxation time increases with pH and decreases with particle concentration, while the slow relaxation time remains approximately constant. The fast and slow relaxations were attributed to protonation-deprotonation of protonated surface sites and proton intercalation-deintercalation in the interlayers of TiS_2(H), respectively. The kinetic parameters reveal that the proton intercalated into TiS_2(H) interlayers serves as a strong solid acid comparable to a mordenite [75]. Kozinkin *et al.* [76] have found that the amine

nitrogen atom in TiS_2, containing interstitial Bu_2NH, Et_2NH and cyclohexylamine, is coordinated directly to the Ti atom. The amine-containing TiS_2 is easily oxidized in air at 293K, with formation of TiO_2 and S_8.

Three-fold superlattice structures have been observed [77] at $Li_{0.33}TiX_2$ during the Li intercalation of TiX_2 (X = S, Se). A satisfactory match between observed and calculated x-ray powder diffraction intensities was obtained; a model with a tripled 'c'-axis was proposed for these complexes. Lithium and sodium intercalations in TiS_2 have been investigated by transmission electron microscopy (TEM) using lattice imaging and diffraction contrast techniques. Observations on both Na_xTiS_2 and chemically prepared Li_xTiS_2 reveal highly dislocated structures. A model was proposed wherein the dislocations are introduced to accommodate misfit strains caused by nonuniform intercalation and, for Na_xTiS_2, to initiate phase transformations, leading to potentially irreversible structural changes in cycled material [78]. TEM studies in intercalation in solid-battery materials point to a model in which battery intercalation in Na_xTiS_2 leads to a highly nonuniform microstructure with complex intergrowths of different phases. The misfit between different phases and phase transformations were described by dislocations which are capable of achieving very high densities [79].

The topochemical reaction of Na_xTiS_2 solid phases with I_2 in MeCN leads to several modifications of TiS_2. The 1T-TiS_2 modification is found by deintercalation of the rhombohedral phases 3R(I)-Na_xTiS_2 and 3R(II)-Na_xTiS_2. Deintercalation of the hexagonal phase 2H(1)-Na_xTiS_2 leads to a strongly disordered 2H-TiS_2 phase with a "chch" stacking of S. The structure was found to be compatible with a mechanism of deintercalation consisting of parallel displacements of TiS_2 sandwiches [80]. A structural study of $Na_xV_xTi_{1-x}S_2$ reveals only the 3R(Ib)-type phase in the composition range $0.3 < x < 1$. Electrical, nmr and magnetic measurements confirmed a metallic-type behavior [81].

Ba_2TiS_4 has been obtained from Ba_2TiO_4 and CS_2 at high temperatures and

characterized by Ir, Raman and UV/VIS spectroscopies, powder x-ray diffractometry and magnetic susceptibility measurements [82].

Crystal growth, characterization and photoelectrochemical properties of $Zr_{1-x}Ti_xS_3$ ($0 < x < 0.33$) have been determined and compared to those of pure ZrS_3. Resistivity decreases with increasing Ti content, and the onset of photoresponse shifts to lower energies with a significant rise in quantum efficiency. The results were related to the formation of a lower energy band consisting of Ti-like orbitals [83]. Angle-resolved XPS has been employed to study self-intercalated single crystals of $Ti^{I}_{x}V^{I}_{1-x}V^{II}_{y}S_2$. A polar-angle distribution curve of photoelectrons emitted from interstitial lattice sites was reported [84]. Its shape differed significantly from that of the electrons emitted from regular sites. Several techniques were employed to intercalate Mn metals into TiS_2 crystals with a 1T-CdI_2-type layered structure [85]. The EPR signals of the intercalated species reveal a Mn^{2+} state with a 'g'-value of $\sim$ 2 and a hyperfine structure constant $A = 80 \times 10^{-4}$ cm^{-1}, indicative of a strong ionic crystalline environment [85]. Layered $LiTi_{1-y}M_yS_2$ (M = V, Cr, Fe) have been prepared directly from a mixture of Li_2S and M [86]. The structure is 1T for M = V and Cr, and 3R for M = Fe. Magnetic and Moessbauer data indicate that Fe is high-spin and divalent for $y < 0.5$, that Cr is trivalent, and that V is nonmagnetic.

Vol'pin and coworkers [87-89] have performed an extensive x-ray emission spectroscopic study of the electronic structure of the titanium disulfide-metal intercalation compounds M_xTiS_2 (M = Fe, Co, Ni). They found that the interstitial Fe atoms in Fe_xTiS_2 ($0 \leq x \leq 1$) interact with the matrix atoms in such a way that the electron density from Fe atoms is transferred into the vacant 3d-band of TiS_2, and the degree of oxidation of the Ti atoms decreases while that of the S atoms remains constant [87]. $TiK\beta_5$ x-ray fluorescence spectra of Fe_xTiS_2 (x = 0.25, 0.50, 0.75) show that the interstitial Fe atoms present in the interlayer regions of TiS_2 are responsible for decreasing the oxidation state of Ti. This effect increases as x increases, reaching a 3+

oxidation state at x = 0.75. The appearance of a short-wavelength maximum in the Ti $K_{\beta 5}$ spectra is indicative of the presence of Ti-Fe interactions [88]. The Ti $K_{\alpha 1}$ x-ray fluorescence spectra of M_xTiS_2 (M = Fe, Co, Ni; x = 0.15, 0.25, 0.33, 0.50, 0.75, 1.00) and $Li_{1.0}TiS_2$ reveal that the introduction of M atoms into TiS_2 results in an electron density transfer from M to the Ti atoms. The magnitude of the transfer depends on the reduction capability of M and decreases as Ti > Fe > Co > Ni [89].

A spontaneous intercalation/corrosion reaction of TiS_2 occurs upon the placement of 1T-TiS_2 crystals in aqueous $AgNO_3$. The reaction is reduced or eliminated on using dilute electrolyte or an organic solvent. Open-curcuit emf potentials of the Ag_xTiS_2/Ag^+(glycerol)/Ag electrochemical cell was reported as a function of x, and the observed features correspond to the structural changes induced in the host TiS_2 lattice by the intercalating Ag ions [90]. Scholz [91] has also investigated the silver intercalated 1T-TiS_2 system. Ag_xTiS_2 can serve as a reversible electrode in contact with electrolytes. It can be prepared <u>via</u> reaction of metallic Ag with TiS_2 at 1090K and by the reaction of Ag_2S with metallic Ti and S at 1000K. Emf measurements were performed on the electrochemical cell with solid electrolytes: Ti/Ag/ Ag_4RbI_5/Ag_xTiS_2/Ti. Depending on the x value, the Ag_xTiS_2 exists in the form of three different phases [92]. The electronic component of the thermoelectric power was measured for Ag_xTiS_2 and $Li_xTi_{1.03}S_2$ (0 < x < 1, 323K < T(temp) < 473K). The heat of transport of Ag^+ ions was much smaller than the activation enthalpy for Ag^+ conduction, suggesting a high ionic polaron binding energy in these materials [93].

The specific heat of 1T-$Ta_{0.93}Ti_{0.07}S_2$ in the Anderson localized states was measured from 0.2 to 5.0K in magnetic fields up to 60 kOe. Below 3.5K, a Schottky-type excess specific heat was observed, and explained on the basis of Coulomb interactions [94]. The preparation and crystal structures of Tl_4TiS_4 and Tl_4TiSe_4 reveal them to be isostructural. They are characterized by isolated tetrahedral thioanions connected to each other by Tl^+ ions. The Tl

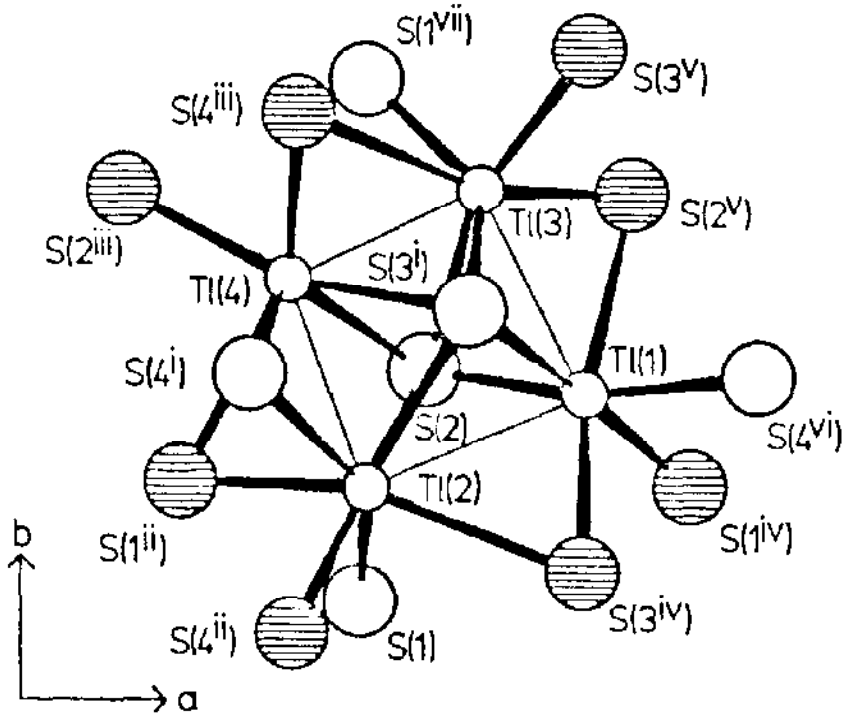

FIGURE 1: The structure of Tl_4TiS_4, which is isostructural with Tl_4TiSe_4. The projection shown is that parallel to [001] [94].

atoms are surrounded by six and seven chalcogen atoms, respectively, in an irregular and polar arrangement, indicative of stereochemical activity of the lone electron pair of the Tl^+ ions (Figure 1) [95]. Huntley [96] has discussed the structural and magnetic properties of transition metal intercalated titanium diselenide.

4.6 TITANIUM HALIDES

a. FLOURIDES

Thermographic and visual-polythermal studies have defined crystallization fields of initial components and solid solutions formed from K_3TiClF_6 and K_3NbClF_7 [97]. A ternary eutectic occurs at 927K with the composition K_2TiF_6 (41 mol%)/K_2NbF_7 (41 mol%)/KCl (18 mol%). In the presence of KCl, the continuous solid solutions formed by K_2TiF_6 and K_2NbF_7 are unstable [97]. In solution, Na_2TiF_6 reacts with ammonia in the presence of HCl to initially form $Ti(OH)F_5^{2-}$ and $TiClF_5^{2-}$, and subsequently $Ti(OH)_4$ [98].

The progression rate versus temperature for the supercooled structural transformation in $NiTiF_6 \cdot 6D_2O$ has been compared to that of $NiTiF_6 \cdot 6H_2O$. Deuteration lowers the critical temperature by about 14K, and a second transition, seen in the hydrated salt, was not unambiguously observed. Energy parameters were calculated from a fit to a nucleation and growth model [99]. The temperature dependence of the zero-field transverse susceptibility, $\chi_\perp$, of the isostructural compounds $NiMF_6 \cdot 6H_2O$ (M = Ti, Zr, Si, Sn) has been studied and found to be nonordering as these compounds are easy-axis ferromagnets [100]. The synthesis and crystal structure of $YbTi_2O_5F$ has been reported by Lobkovskaya and coworkers [101]. $YbTi_2O_5F$ is orthorhombic with Yb atoms in archimedian antiprismatic coordination and the Ti ion in octahedral coordination. The F is coordinated to some Ti polyhedra and some Yb polyhedra [101].

b. CHLORIDES

(i) $TiCl_3$

The vibtational spectrum and normal coordinate analysis of β-$TiCl_3$ have been performed [102]. The A_2u mode is lower in frequency than that in α-$TiCl_3$ and one of the Ti-Ti stretching vibrations (at 281 cm^{-1}) corresponds to a Ti-Ti stretching force constant of 81.6 N/m [102].

$TiCl_3$ is known to reduce N-hydroxy imidazoles (1) (R = $PhCH_2$, Me_3C, Me_2CHCH_2, Bu, pentyl) in methanol/water to yield the N-protio derivatives (2) which are useful precursors of chiral amino acids [103]. In aqueous solution,

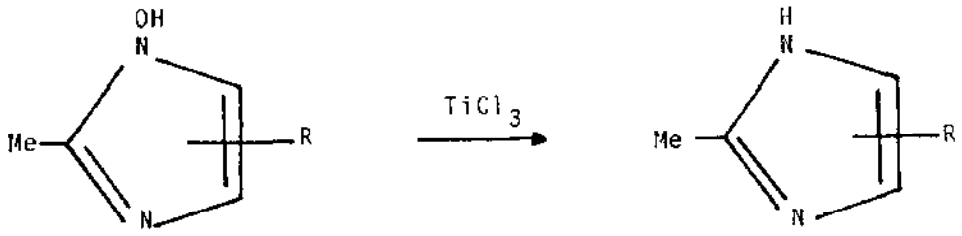

(1) (2)

selected nitrosoamines of the type RR'NNO {R = R' = C_{1-4} alkyl; RR' = $(CH_2)_4$, $(CH_2)_5$, $(CH_2CH_2)_2O$} are reduced by $TiCl_3$ to give the aliphatic hydrazines RR'NNH_2 in good yield. Reduction of $MeOCH_2NMeNO$ produces $MeNHNH_2$ as the major reaction product, whereas other reducing agents give a mixture of primary and secondary amines [104].

Mixed crystals of $TiCl_3 \cdot 1/3AlCl_3$ (commercially known as TAC-141) have been employed successfully as a catalyst for the polymerization of propylene [105]. An increase in isostereospecificity and activity is observed when the catalyst is treated in a nitrogen atmosphere at 343-363K for several hours with diethyl ether in heptane. The optimum quality is achieved at a $Et_2O/TiCl_3$ ratio of approximately 0.15 - 0.20 mole/l [105]. Diffractometry and infrared spectroscopy were used to characterize the reaction of $TiCl_3$ with polymeric support in combined grinding. The grinding of $TiCl_3$ with polyethylene or polypropylene supports, having methacrylate or polyacrylonitrile, significantly

affects the structure and catalytic properties. The activity and stereospecificity of the catalyst increase simultaneously when a shortage of functional groups is present on the support [106]. Corradini and coworkers [107] explain the similar properties of $TiCl_3$- and $MgCl_2$-Lewis base catalysts in the isospecific polymerization of α-olefins in terms of the analogous structure of catalytic sites resulting from the epitactic growth of small $TiCl_3$ units on unsaturated surfaces of $MgCl_2$. Computations of the non-bonded energies of different diastereoisomeric complexes of these sites suggest that the main factor in determining their stereospecific properties is the fixed chiral orientation into which the growing polymeric chain is forced.

In the presence of visible light, the reduction of CO_2 in aqueous solution in the presence of $TiCl_3$-treated zeolite CaA affords HCO_2H, HCHO and oxalic acid. The yields increase when reducing agents (e.g., Cr^{2+}, V^{2+}, Mo^{5+} and metallic Al, Zn or Mg) are present [108].

(ii) $TiCl_4$

The quantum yield for the photoreduction reaction (2) in ethanol depends on the concentration of $TiCl_4$, H_2O and HCl in the ethanol solutions [109]. A complex mixture of photoproducts is obtained upon photolysis (λ =

$$Ti^{4+} + h\upsilon \xrightarrow{254\ nm} Ti^{3+} \qquad (2)$$

254 nm) of $TiCl_4$ in H_2O/EtOH solutions. The mixture is composed of (a) a binuclear complex containing Ti(III), Ti(IV) and OH, (b) a monomeric hydroxo complex of Ti(III), (c) $[TiO(H_2O)_5]^+$, and (d) a mixed complex of formula $[TiCl_x(H_2O)_y(EtOH)_z]^{n+}$. The composition of the mixture and the concentration of the single product depend on many factors, including water concentration, irradiation time, and system acidity [110]. Kryukov and coworkers [111] have experimentally confirmed the formation of molecular hydrogen in the photocatalytic reduction of Ti^{4+} in $TiCl_4$ solutions in ethanol. A mechanism

assuming complexation of EtOH with the Ti ion and formation of atomic hydrogen has been proposed. The photolysis of $TiCl_4$ in a frozen ethanol matrix leads to the formation of Ti^{3+} complexes possessing the same coordination sphere as the initial Ti^{4+} complex [112].

The electrochemical reduction of Ti^{4+} from a solution of $TiCl_4$ in DMSO has been examined to determine the possibility of depositing metals that cannot be deposited from aqueous solution [113]. The reduction products of graphite laminar compounds with $TiCl_4$ were studied by x-ray diffraction, DSC, Auger electron microanalysis, and Moessbauer spectroscopy. The reduction leads to decomposition of the laminar compound and the formation of titanium chloride on the sample surface [114]. A 91% yield of 1-dodecanol is obtained *via* reaction of equimolar amounts of 1-dodecene and $TiCl_4$-$2KBH_4$ in $MeOCH_2CH_2OMe$, followed by hydrolysis with 5% H_2O_2 [115]. The reaction of methylene bromide with dicyclopropyl ketone in the presence of $TiCl_4$ in CH_2Cl_2/THF yields 1,1-dicyclopropylethylene and 1,1-dicyclopropylcyclopropane. The analogous reaction with $n\text{-}C_7H_{15}COMe$ gives $n\text{-}C_7H_{15}CMe{=}CH_2$ (3) [116]. The reaction of

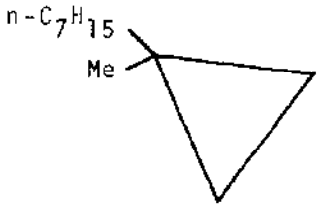

(3)

$TiCl_4$ with formamide has been reported by Aspandiyarova [117].

A kinetic study of the reaction of the alkyl sulfonates RSO_3CH_2R' (R = alkyl, Ph; R' = alkyl) with $TiCl_4$ to give alkyl chlorides suggests the formation of a complex which decomposes in the rate-determining step *via* nucleophilic attack by Cl^-. The large negative activation entropies are indicative of a highly ordered transition state, characteristic of S_N2 reactions [118]. A related investigation reveals complex formation *via*

reaction of the alkyl sulfonates RSO_3R' (R = Me, Bu, Ph, substituted phenyl; R' = Me, Et) with $TiCl_4$ in protoinert solvents. The complexes react with benzene to produce alkylbenzenes and alkyl halides [119].

The activation energies of the $TiCl_4$ vapor phase reaction with copper, coated by an oxide film of variable thickness, have been determined. The reaction rate increases in the presence of molecular oxygen [120]. The kinetics of the reaction of copper films with $TiCl_4$ vapor have been studied gravimetrically in a flow of dry air at 298-453K. The rate curve obtained is initially logarithmic and then becomes parabolic. Those $TiCl_4$-copper films prepared at temperatures below 353K are subject to hydrolysis, while those prepared at higher temperatures are stable in a humid atmosphere [121].

Gaseous TiO_2 and $TiOCl_2$ are yielded from the reaction between $TiCl_4$ and H_2O. A vibrational infrared spectroscopic analysis shows that TiO_2 is non-linear with Ti-O stretching frequencies of ∿944 and 965 cm^{-1}; $TiOCl_2$ has a Ti-O stretching frequency of 818 cm^{-1} and a Ti-Cl stretching frequency of ∿535 cm^{-1} [122]. $TiCl_4$ reacts with the dialkoxy silanes $R_{3-n}R'_nSiNHR''$ (R = $ClCH_2CH_2O$; R' = $ClCH_2CH_2O$, EtO, PrO, BuO, Me; R'' = Ph, $C_6H_5CH_2$; n = 1,2) at different molar ratios to give $R_{4-n-m}R'_nSi(NHR'')_mxTiCl_4$ (n = 0, 1; m = 2,3; x = 1, 2). The adducts were characterized by elemental analysis, and infrared and nmr spectroscopies; the nitrogen atoms are the coordinating atoms [123]. Infrared spectroscopy was also employed to examine the solid-state configurations of the 1:1 and 1:2 adducts which result from reaction of $TiCl_4$ with β-amino thiones and β-keto amines. The results suggest that the bi- and tetra-dentate amino thiones coordinate through the nitrogen atoms where β-keto amines coordinate through oxygen [124].

The cyanamides R'R''NC=N (R ' = R'' = Pr^i) react with $TiCl_4$ to give $R'R''NC{=}NTiCl_4$ [125].

The crystal structures and spectroscopic properties (UV and IR) of the complexes formed by $TiCl_4$ with esters have been investigated in an ongoing study of the structures of highly efficient polypropylene polymerization

catalysts. For example $TiCl_4$ and PhCOOEt (=L) yield two complexes, $TiCl_4 \cdot L$ and $TiCl_4 \cdot 2L \cdot MgCl_2$. The x-ray powder diffraction analysis reveals that the former complex is formed in the catalyst preparation process by the milling-soaking method [126]. The chemical composition of a $MgCl_2$-supported polymerization catalyst has been determined at every stage of its preparation, which involved ball milling of $MgCl_2$ with ethyl benzoate, reaction with p-cresol, addition of $AlEt_3$, and reaction with $TiCl_4$ [127]. Highly active catalysts for the polymerization of ethylene and propylene are obtained from the interaction of organic and hydride compounds of Ti, Zr, Hf, V or Cr with silica and alumina. Results of a study of Ziegler-type catalysts prepared by supporting $TiCl_4$ on silica and $MgCl_2$ and activating by an organo-aluminum compound were also reported [128]. Addition of alkylaromatic esters to the $TiCl_4/MgCl_2 + AlR_3$ system yields a highly active propylene polymerization catalyst. A study of the kinetics of ethylene polymerization catalysed by $TiCl_4/MgCl_2$ and $TiCl_4$-$Ti(OBu)_4/MgCl_2$ in the absence of hydrogen reveals greater propagation rate constants and lower apparent activation energies when compared to ordinary $TiCl_4$ and AlR_3 catalysts [129]. On the other hand, a study of the rate of ethylene polymerization catalysed by $TiCl_4$-phenetole-Et_2AlBr shows it to depend only on the Al-Ti ratio. At constant $TiCl_4$ content, an increase in the Al:Ti ratio gives rise to accelerated catalyst formation and increased catalyst activity [130]. The kinetics of isoprene polymerization in the presence of Ziegler catalysts have been reported by Bresler *et al.* [131]. The catalysts employed were prepared *via* the reduction of $TiCl_4$ by PhMgBr or 5 $Bu_2Mg \cdot AlEt_3$. Both the catalyst activity and polymerization decrease on addition of either *iso*-Bu_2AlCl or *iso*-Bu_3Al to the catalyst system.

The treatment of the unsaturated alcohols 3-butyne-1-ol and 4-pentyn-2-ol with Et_2AlCl, followed by treatment with $TiCl_4$ under various conditions, selectively gives (E)-3-hexen-1-ol and (E)-4-hepten-1-ol, respectively. The reaction results from a *syn*-ethylmethylation of the multiple bond, with no complications observed from *in situ* β-hydride elimination [132]. A kinetic

investigation of the $TiCl_4$-catalysed Friedel-Crafts benzylation of $PhCH_2Cl$ in excess aromatic hydrocarbon suggests the reaction to be first-order with respect to $PhCH_2Cl$ and second-order with respect to catalyst. The reaction mechanism involves attack by $PhCH_2^+$ or a $PhCH_2^+Ti_2Cl_9^-$ ion pair on the aromatic [133]. Pozdnyakovich and coworkers [134] reported that benzylation of m- and p-tert-alkyl toluenes ($PhCH_2Cl$) give mixtures of the corresponding 2,4-, 2,5-, 4,2-, 5,2-, and 5,3-$Me(RCMe_2)C_6H_3CH_2Ph$ (R = Me, Et). Less than 4% o-, m- and p-$MeC_6H_4CH_2Ph$ were formed in the presence of $TiCl_4$.

Thermal analytical data were employed to construct a phase diagram for the $TiCl_4/TiBr_4$ system. A continuous series of solid solutions is formed with a minimum melting point of 247K and 13 mol % $TiBr_4$ [135]. Chikanova and Vorontsov [136] have determined the thermodynamic conditions for producing an electrolyte melt of the binary system $TiCl_4$-PCl_5. Various two-component oxide structures have been prepared with the use of $TiCl_4$, PCl_3, $VOCl_3$ and CrO_2Cl_2 by a method of molecular stratification on a silica surface. The $(:SiO)_3TiOH$ surface group consists of a series in which $TiCl_4$ substitutes the metal-oxo groups [137].

Intracavity laser spectroscopy has been used to determine the spectral bands $Ti^{14}N$, $Ti^{15}N$ and TiO in the absorption spectra of $TiCl_4$-N_2 pulsed discharge plasma [138].

An investigation of the current and nature of the ester solvents (E = EtOAc, BuOAc, PrOAc) on the anodic dissolution of titanium in ester solutions of $TiCl_4$ reveals two types of processes occurring. These processes are related to the electrochemical discharge of anions with a $[TiCl_5 \cdot E]^-$ composition, and to the chemical process of oxidation of the metals of the cations $[TiCl_3 \cdot 3E]^+$ and $[TiCl_3 \cdot E]^+$. At lower current density values, the electrochemical process predominates, while the chemical process dominates at higher (>1 A/dm^2) current densities. The rate of electrochemical dissolution of the metals is determined by the electron-donor properties of the ester ligands and increases with decreasing overall Taft constant of the acid and alcohol radicals of the

complex ester molecules [139].

(iii) Miscellaneous Chlorides

An attempt has been made to calculate the stability constant of $TiCl_6^{2-}$ in concentrated HCl using spectrophotometric data. However, the extinction coefficient of $TiCl_6^{2-}$, calculated by extrapolation, was not sufficiently accurate to allow stability constant calculations [140]. The infrared and low-temperature Raman spectra of $Cs_2TiCl_5 \cdot 4H_2O$ have been measured in the 4000-200 cm^{-1} region. Additionally, normal coordinate calculations were performed for trans-$[TiCl_2(H_2O)_4]^+$. The presence of this ion in $Cs_2TiCl_5 \cdot 4H_2O$ was reportedly [141] confirmed by the similarities in their vibrational spectra. Auger electron microanalysis and x-ray phase analysis of the reduction products of the layered graphite $C_kTi_{1.0(1)}Cl_{4.5(1)}$ (k = 57-78) indicate the formation of titanium and graphite [142]. The electronic structure of the dibenzotetrathiofulvalene ion-radical salt with $Ti_2Cl_9^-$ has been determined from x-ray emission spectroscopy [143]. The stability constants of $TiOCl^+$ and $TiOCl_2$ (1.04 and 0.29, respectively) have been determined using an ion-exchange method [144].

c. BROMIDES

A reinvestigation of the violet emission bands of TiBr reveals the production of five band systems when $TiBr_4$ and argon are passed through a microwave discharge. Three of the systems reportedly arise from TiBr, one from $TiBr_2$ or $TiBr^+$, and one from $TiBr_3$. Vibrational analyses are given for two of the TiBr systems [145]. An effective Hamiltonian has been developed for the treatment of exchange interactions in a pair of transition metal ions with orbitally degenerate ground states [146]. The Hamiltonian retains a partial degeneracy of singlet and triplet pair states, and was applied to $Ti_2X_9^{3-}$ (X = Br, Cl) dimers. The gross experimental features of $Rb_3Ti_2Br_9$ and $Cs_3Ti_2Cl_9$ agree fairly well with the theoretical model, with strongly antiferromagnetic

coupling and rationalization of exchange parameters by an approximate MO calculation [146]. Employing molecular kinetic constants and the Wilson's FG matrix method, the general quadratic valence field was applied to the solid-state metal-hexahalo species R_2TiX_6 (R = $(C_2H_5)_4N$, Cs). For the first time, the compliance constants, vibrational mean amplitudes, shrinkage constants, Coriolis coupling constants and rotation distortion constants are reported for these ions [147].

4.7 TITANIUM OXIDES

a. TITANIUM OXIDES, EXCEPT TiO_2

Nonstoichiometric TiO_x films have been prepared by dual ion beam sputtering, and have been characterized by a high absorption index. Additionally, deposition conditions are reported for obtaining either TiO_x films with an adequate reproducibility of film properties [148]. Theoretical studies of optical scattering show that transparent layers deposited on a rough surface may possess an antiscattering effect. Roche and coworkers [149] have experimentally shown that such predictions are true for titanium oxide provided exceptionally stable deposition conditions are employed. Thermodynamic properties have been calculated for the nonstoichiometric titanium oxide TiO_x ($0.85 \leq x \leq 1.25$) by the method of cluster components [150]. The overlap molecular integrals and the Ti-Ti bond screening energy, 'V', in TiO were calculated by solving a four-electron problem which accounts for the interaction of the electron of the d orbital from each Ti atom and two electrons of the 2p orbitals of the oxygen ion. The resulting 'V' values exhibit a direct relation to the formation of structural vacancies [151].

Structural defects occurring in plastically-deformed, nonstoichiometric rutile, TiO_{2-x} ($0 \leq x \leq 0.0035$), have been characterized by high-resolution electron microscopy. The observed crystallographic shear planes possess considerable local disorder in orientation and structure, implying a different precipitation mechanism for these defects compared to those in quenched

nondeformed materials of similar composition [152]. The extrinsic and/or intrinsic nature of extended defects in TiO_{2-x} have been analysed by drawing Burger's circuits directly onto high-resolution electron micrographs. Above the extended defect precipitation temperature, an essentially interstitial and/or vacancy nature of the small defects responsible for TiO_{2-x} are implied. Images suggestive of a partial wall of anion vacancy defects were also obtained [153]. Chemical diffusion coefficients have been measured for various nonstoichiometries of TiO_{2-x} at 1323K. The results were compared with those in the literature, and were interpreted in terms of a major constituent, interstitial Ti^{3+}, being responsible for the diffusion. As a consequence, oxygen vacancies possibly associated with shear planes in the $TiO_{1.99}$-$TiO_{1.995}$ part of the nonstoichiometric domain are expected to be minor defects in this oxide [154]. High-resolution electron microscopy along with controlled specimen preparation were employed to investigate the nature and structures of {100} platelet defects observed in TiO_{2-x} ($0 \leq x \leq 0.0035$). The platelet defect precipitation was explained in terms of new linear cationic interstitial defect models which exist within the nonstoichiometric phase [155].

A method involving in situ annealing using an electron microscope was reported to study the phase transition of evaporated $TiO_{0.5}$ films. Single crystals of the δ-phase precipitate during annealing; also, appearing during annealing were two transition structures possessing ordered vacancies of Ti and O, respectively. Differences in lattice distortion of the two transition structures, relative to the parent rock-salt type lattice, suggest that the effective atomic volume of Ti is larger than that of O in the transition structure crystal [156]. The effect of thermobaric treatment on the magnetic susceptibility of TiO_x ($x = 0.84, 1.05, 1.27$) has been studied. The observed changes in the magnitude of the magnetic susceptibility are interpreted in terms of a change in the structural characteristics and charge state of atoms subsequent to the action of high temperatures and pressures [157]. Kutzler and Ellis [158] have calculated the x-ray 'K'-edge photoabsorption cross

section of TiO employing the self-consistent one-electron local-density theory. Additionally, energy levels, charge distribution, and cross sections are reported from a 27-atom microcrystal with a molecular-cluster approach in the discrete-variational method.

Micrometric particles of powdered titanium oxides (TiO_2, Ti_2O_3, TiO) were characterized by laser microprobe mass analysis (LAMMA). The stoichiometry of the sample can be correlated with the relative intensity distributions of the positive or negative cluster and atomic ions. Variations in laser energy density and in ion lens potential also affect the ion intensity distributions. Similar conclusions were reached via application of the valence model [159]. The structural chemistry of Magneli phases in Ti_xO_{2x-1} ($4 \leq x \leq 9$) at 115, 140 and 298K has been examined by LePage and Marezio [160]. At 140K, a significant cell-parameter change at the lower transition and a 5-fold superstructure occur. The 140K phase is triclinic and corresponds to long-range order of the titanium valences. Expansion and contraction of the Ti-Ti distances in the rutile-like chains can be correlated with the electrostatic repulsion of the titanium ions. Chemical transport experiments on the phase Ti_xO_{2x-1} with $HgCl_2$ reveal a neighbor phase with higher oxygen content ($Ti_{x+1}O_{2x+1}$) deposited at a lower temperature T_1. Similar results were obtained using $TeCl_4$ as the transporting agent. These results and thermodynamic calculations suggest it is possible to calculate the composition of a compound deposited at Ti in systems with numerous close-neighbor phases and for given experimental conditions [161]. Similar experiments showed that in the presence of traces of H_2O, the neighboring phases with a higher oxygen content are deposited in the zone with the lower temperature T_1. The transport is due to the formation of HCl from $HgCl_2$ or $TeCl_4$, as confirmed by the use of HCl or NH_4Cl as the transporting agent [162].

b. MIXED METAL OXIDES

Canali and coworkers [163] have studied the interactions and compounds formed between titanium and $LiNbO_3$ which occur before the true

titanium in-diffusion process for optical waveguide production. Lithium insertion into various close-packed TiO_2 frameworks has been investigated using neutron diffraction. A simple model based on minimizing cation repulsion was employed to rationalize the structures and diffusion of lithium in lithium inserted anatase, $Li_{0.5}TiO_2$, the spinel $LiTi_2O_4$, and the lithiated spinel $Li_2Ti_2O_4$ [164]. Crystal structure determinations of these oxides reveal that lithium partially occupies the highly distorted octahedral interstices in the anatase framework in five-fold-coordination with oxygen in $Li_{0.5}TiO_2$ (Figure 2). A normal spinel structure obtains for cubic $Li_2Ti_2O_4$ with Li in the tetrahedral sites. In $Li_2Ti_2O_4$, the Ti remains in the spinel positions but the Li is displaced, filling all of the available octahedral sites [165]. The

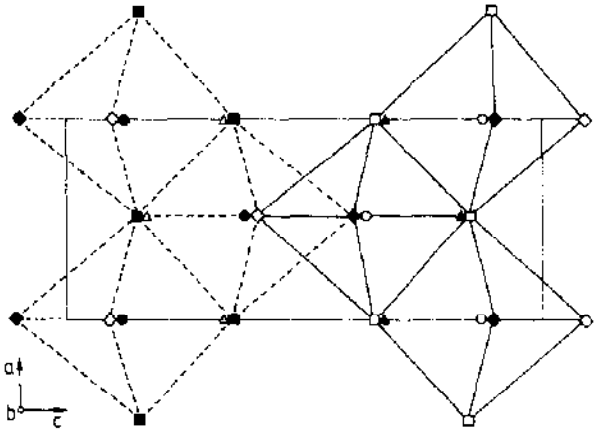

FIGURE 2: The structure of $Li_{0.5}TiO_2$, anatase form. The anatase framework is accentuated by outlining the TiO_6 octahedra. Triangles, Li; open circles, Ti; diamonds, O1; squares, O2 [164].

metallic nature of $LiTi_2O_4$ has been confirmed by the presence of a Fermi edge in the helium I-excited valence-band UPS spectrum. However, the measured density of states at the Fermi energy is significantly lower than expected from an independent-electron interpretation of the magnetic susceptibility. The difference is due [166] to a strong interaction between the conduction electrons and lattice vibrations. The localization of conduction electrons observed in the final state in the Mg K_α-excited Ti-2p XPS spectrum of $LiTi_2O_4$ is the result of a Coulomb interaction with a core hole [166]. ESR spectroscopy and magnetic susceptibility were used to characterize the $Li_{1+x}Ti_{2-x}O_4$ spinel. The two types of localized moments observed were associated with two types of defects; an oxygen vacancy and an OH^- ion. Unpaired electrons are trapped as Ti^{3+} ions adjacent to these defects, and the strong tetragonal field is likely associated with the formation of a static $(TiO)^+$ ion *via* displacement of the Ti ion from the defect. Spin relaxation then occurs through thermal ionization of the trapped electron, which apparently is related to a static-dynamic transition in the Ti ion displacement [167]. Porotnikov *et al.* [168] have recorded the infrared and Raman spectra (33-1000 cm^{-1}) of Li_2TiO_3, and compared the data to a group theory analysis and to an isotopically-substituted $^{6,7}Li_2TiO_3$. The effective coordination numbers and the Madelung part of the lattice energy have been calculated for the isotypic compounds KLi_3TiO_4 and KLi_3SiO_4 [169]. At temperatures of 573-773K, the electrical conductivity is significantly increased upon partial replacement of Si^{4+} in Li_4SiO_4 by larger ions (Ti^{4+}, Ge^{4+}) to give $Li_4Si_{1-x}Ti_xO_4$. There appears to be an optimum ratio of the size of the migrating Li^+ ion and the size of the migration channel, as determined by the size of the Ge^{4+} or Ti^{4+} ions [170]. Belinskaya and Filina [171] have studied the formation conditions, composition and ion-exchange properties for the alkaline hydrolysis products in the $TiCl_4$-H_2O-MOH (M = Li, Na, K) systems at pH 10 and greater than 12. The M:Ti molar ratio in the precipitate depends on the aging time of the precipitate in its mother liquor. X-ray phase analysis was employed to

characterize the major calcined precipitates, identified as $Li_4Ti_{15}O_{12}$, $Na_2Ti_3O_7$ + $Na_2Ti_5O_{11}$, and $K_2Ti_6O_{13}$.

Berdowski and Blasse [172] have investigated the nonradiative relaxation by multiphonon emission for the $^5D_1$ ($\rightarrow{}^5D_0$) level of Eu^{3+} in $NaGdTiO_4$ in the temperature range 4.2-298K. The temperature of the relaxation rate is indicative of a fifth-order process, while the frequency of the emitted phonons corresponds with that of Gd-O stretching vibrations. The static structure factor S(q) for the Frenkel-Kontorova model Hamiltonian has been treated on the basis of a high-temperature expansion of the transfer-integral equation (TIE). Application to the potassium hollandite $K_{1.54}Mg_{0.77}Ti_{7.23}O_{16}$ reveals that experimental results are not reproducible for S(q) at substrate potential $U\beta \lesssim 1$, though it gives consistent results for $U\beta = 8$ and a correlation length $A_a = 3.1$ [173]. A study of the character of the magnetic conversion of diluted ferrites, including $Mg_{1.5}FeTi_{0.5}O_4$ (Mg-Ti), shows the existence of ordered and disordered spins (mictomagnetism) [174]. X-ray powder diffraction was employed to obtain the crystal structure of $CaTiO_3$ containing R_2O_3 (R = La, Dy, Pr, Lu, Y, Cr). The R_2O_3 additives do not affect the lattice parameters, as they apparently are not situated in the lattice but at grain boundaries [175]. The difficult-to-prepare monoclinic crystals $CaTi_3Al_8O_{19}$ and $LaTi_2Al_9O_{19}$ have been successfully produced by a relatively simple method [176]. The reaction between molten Al_2O_3 and TiO_2 in a solar furnace gives β-Al_2TiO_5, which has been characterized by x-ray diffractometry and Raman spectroscopy. The 900 cm^{-1} band in the Raman spectrum of β-Al_2TiO_5 corresponds to valence vibrations of the Al-O bonds in distorted [AlO_6] octahedra, as confirmed by the Raman spectra of $Al_{2x}Ga_{2(1-x)}TiO_5$ solid solutions [177].

Infrared spectroscopy and x-ray diffractometry have also been employed to determine the effect of acidic or basic molecules and of the structure of a V-Ti-O (V_2O_5/TiO_2) catalyst on the catalytic oxidation of alcohols. With increasing V_2O_5 concentration (V:Ti = 2-11) the concentration of the active surface V=O groups increases [178]. TEM studies of the ternary system $VTiO_x$

($x \approx 1.750$-1.900) at 1373-1473K reveal the formation of a homologous series of oxides which have been formulated as $V_2Ti_{n-2}O_{2n-1}$ ($5 \leq n \leq 10$). The new phases are described as derived from the rutile structure through the application of the crystallographic shear on the (121)r planes. Unit cell parameters are reported for the $V_2Ti_7O_{17}$ and $V_3Ti_6O_{17}$ phases, which also possess micro-synthetic intergrowths [179]. Kidoh and coworkers [180] have characterized the structure and electron density distribution in the ilmenite-type $MnTiO_3$ crystal (Figure 3). A small amount of partial disorder occurs in the cation arrangement of the rhombohedral crystal examined. The electron cloud about the Ti^{4+} ion is deformed so as to shield the positive charge of the Mn^{2+} ion, as in $CoTiO_3$. A positive-density region spreads between the nearest Mn^{2+} ions in the deformation density map, which suggests direct interaction between Mn and Ti. The antiferromagnetic order observed in the (0001) plane at low temperatures does not contradict the presence of such direct interaction. The

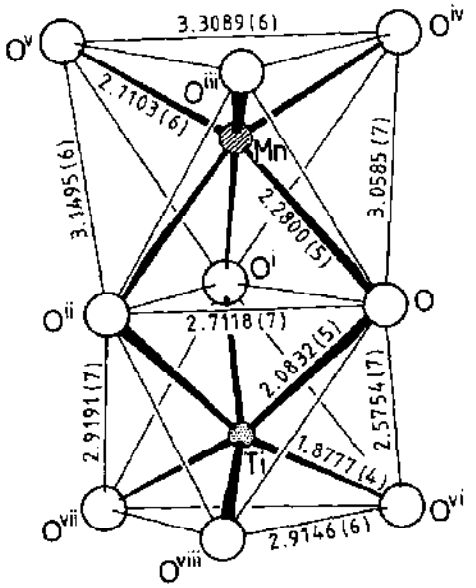

FIGURE 3: Bond lengths, in Å, in the MnO_6 and TiO_6 octahedra of the ilmenite-type $MnTiO_3$ crystal [180].

electrochemical behavior of the natural ilmenite $FeTiO_3$ has been investigated by cyclic voltammetry [181]. The valences of the metal ions in $FeTiO_3$ are Fe(II) and Ti(IV), based on analyses of current-voltage curves. The preparation and the electro- and photoelectro-chemistry of $Fe_xTi_{1-x}O_y$ ($x \leq 0.9$) have been reported [182]. Data from Moessbauer spectra of $Fe_{1-x}M_xO_{1+5}$ (M = Ti, V, Cr, Co, Ca) have been interpreted in terms of the oxidation state of Fe being between +2 and +3 which depends on the composition of the solid solution [183]. The monoclinic Fe_2TiO_5 system has been characterized by high-resolution electron microscopic images and by their computer simulated images, with the aid of electron and x-ray powder diffractometric methods [184]. X-ray phase analysis, infrared spectra, electrical conductivities, photoelectron emission and diffuse reflection spectra of $(Ti_xFe_{1-x})_2O_3$ (x = 0-0.1) solid solutions reveal the samples to be true substitutional solid solutions with a uniform distribution of Ti between the surface and the bulk. Electronic conduction occurs *via* ionization of the donors Ti^{4+}-Fe^{2+}, situated 0.5eV below the conduction band [185].

Porous metallic supports (stainless steel PNS, Nichrome PNKh, Ti and Ni) corrode by molten $M(NO_3)_m \cdot nH_2O$ during the preparation of the oxide catalysts Co_3O_4, $Co_{1-x}M_xO$ (M = Ti, Ni, Cr, Fe), Fe_2O_3, and $Fe_{1-x}M_xO$ (M = Ti, Ni, Cr). The corrosion is accompanied by inclusion of the support metal ions into the lattice of the catalytically-active oxide and by a change in its phase composition [186]. The electron density distribution in a $CoTiO_3$ crystal was examined by single-crystal x-ray diffractometry. The observed deformation densities about the Co^{2+} ion are explained in terms of the high-spin d^7 ion electron configuration in an octahedral field. The Ti^{4+} ion lies in a negative region of the deformation density map, and a positive peak exists on the three-fold axis [187]. The thermal decomposition (1300-1700K) of $CoTiO_3$ apparently proceeds *via* two steps, with $CoTi_2O_5$ an an intermediate product having a standard heat of formation of -2162.7 kJ-mole^{-1} (from the elements). The decomposition was examined by mass spectrometric Knudsen cell determinations

and by vacuum thermobalance experiments, with subsequent x-ray analysis of the residues [188]. For the first time, an electrical field induced texture effect has been observed in the Moessbauer spectra of $NiTiO_3$-Fe_2O_3 pellets [189]. Thermogravimetry, DTA, isothermal studies, x-ray diffraction and chemical analysis have been utilized to study the thermal decomposition of $ZnTiO(C_2O_4)_2 \cdot 2.5H_2O$. The decomposition occurs via three steps: (a) a two-stage dehydration of $ZnTiO(C_2O_4)_2 \cdot 2.5H_2O$ between 295K and 453K; (b) the second step involves decomposition of the oxalate at 450-573K, while (c) the third step results in the formation of oxides as the end product. The end product, when isothermally heated at 973(20)K, is the cubic $Zn_2Ti_3O_8$, which on further heating (1173(25)K) gives cubic Zn_2TiO_4 [190].

The formation of strontium titanate, $SrTiO_3$, has been examined by thermogravimetry (TG) and by x-ray diffractometry. The reactivities of several starting materials [$Sr(NO_3)_2$, $SrCO_3$, $Sr(OH)_2$, $TiO_2 \cdot nH_2O$, anatase, rutile] were also studied; the reactivity decreases in the order OH^-, NO_3^-, CO_3^{2-} and anatase, $TiO_2 \cdot nH_2O$, rutile [191]. A three-terminal capacitance dilatometer was employed to determine the linear thermal expansion of $SrTiO_3$ at 10-150K. The temperature at which the dilation is minimal (37.5K) is very close to a transition point (T_c = 32 ± 5K) predicted by Cowley [192]. Mueller and Berlinger [193] have measured the effect of uniaxial [100], [111] and [110] stresses on the EPR fine-structure lines of Cr^{3+} at 300K on octahedral Ti^{4+} sites in $SrTiO_3$ and Mg^{2+} sites in MgO. The intrinsic superposition-model parameters and spin-lattice strain coefficients were determined. Partial substitution of V^{5+} for Ti^{4+} in $SrTiO_3$ yields $Sr_{(1-x/2)}\square_{x/2}Ti^{4+}_{(1-x)}V^{5+}_xO_3$ ($x \leq 0.5$). The effect of the cation vacancies thus created on the polarity of the substrate bonds was investigated, and the optical and electrical properties of the product studied. It was suggested [194] that an increase in covalency of the M-O bond (M = small cation) in the perovskite is due to the incorporation of V^{5+}. Thermogravimetric measurements as a function of oxygen activity at 1473-1673K on a series of lanthanum-doped $SrTiO_3$ prompted Flandermeyer et al.

[195] to postulate a model that assumes the absroption of excess oxygen in the structure which compensates the donors *via* cationic defect formation. A comparison of this model with the experimental results revealed reasonable agreement. Gulya and Gyori [196] have examined the performances of photoelectrochemical cells with $SrTiO_3$, $BaTiO_3$ and $KTaO_3$ electrodes. The voltammetric characteristics, the response to conductance, nonconductance and UV solar radiation, and the external electrical potential required to prime the electrolytic process have been reported for polycrystalline $SrTiO_3$ photoelectrodes [197].

The mineral srilankite $(Zr_{0.33}Ti_{5.67})O_2$ is orthorhombic (space group *Pbcn*), with Zr and Ti distributed at random among the sites of the α-lead dioxide structure. Each metal ion is bonded to six oxygen atoms forming distorted $(Ti,Zr)O_6$ octahedra [198]. Ti and Nb are not randomly distributed in monoclinic (space group C2/m) $TiNb_2O_7$, for which there is preferential occupation of one type of site by the Ti atoms [199]. Greeger and coworkers [200] have employed EXAFS and XANES (x-ray absorption near edge structure spectroscopy) to evaluate the effect of alpha-recoil damage in metamict, annealed and synthetic complex titanium-niobium-tantalum oxides. A comparison of results obtained for the metamict *vs* annealed and crystalline samples indicates minor changes in the first coordination sphere (Ti-O) and major disruption of the second coordination sphere (Ti-Ti) for the metamict state. The data were interpreted in terms of a mechanism in which tilting of cation coordination polyhedra is the principal effect of any damage resulting from alpha-recoil events.

The organic interculates $H_{0.5}(LH)_{0.5}TiNbO_5$ [L = NH_3, $MeNH_2$, $EtNH_2$, $BuNH_2$, $PrNH_2$] have been prepared *via* reaction between $HTiNbO_5$ and L [201]. The rutile-type $Ru_xTi_{1-x}O_2$ coatings are metastable solutions wherein chloride ions are likely to replace the oxide ions on the sublattice O^{2-} sites [202].

The luminescence of $Bi_4Ti_3O_{12}$ crystals results from the interaction of the domain boundaries with crystal lattice defects. An electroluminescence

examination of $Bi_4Ti_3O_{12}$ shows that during pulsed polarization reversal only the final stage of polarization reversal, corresponding to a side movement of domain boundaries, is accompanied by the luminescence [203]. Room-temperature Raman spectra of single-crystal $Bi_{12}TiO_{20}$ exhibit relatively narrow and sharp low-frequency Raman lines, with increasing linewidth as the frequency increases to 318 cm^{-1} followed by a decrease for the highest frequency modes [203]. The frequencies of the normal vibrations of F-symmetry in the room-temperature infrared reflection spectrum (10-50 μm) of single-crystal $Bi_{12}TiO_{20}$ were obtained for the center of the Brillouin zone of the sample. The results were compared with previously published data from Raman and infrared transmission spectra of $Bi_{12}TiO_{20}$, and to refine the data for $Bi_{12}SiO_{20}$ and $Bi_{12}GeO_{20}$ [204]. At 80-300K, the photochromic effect in $Bi_{12}MO_{20}$ crystals (M = Ti, Si, Ge) depends on the absorption coefficient in the absorption shoulder spectral region and on the concentration of trapping sites with E_T = 0.5 - 1.2 eV [205].

Senuliene et al. [206] have investigated the existence of a complete range of solid solutions between $Bi_{12}SiO_{20}$ and $Bi_{12}TiO_{20}$ and their optical properties. The optical spectra revealed (a) absorption in the vicinity of the fundamental edge, (b) infrared absorption and reflection, and (c) specific rotation of plane polarized light for $Bi_{12}Si_{1-x}Ti_xO_{20}$. Intergrowth compounds [X1][YM] are yielded upon interaction of $LiBi_3O_4Cl_2$-type compounds (X1) with members of the bismuth titanate series $\{[M_2O_2][M_{m-1}R_mO_{3m+1}]$, m = 1-4$\}$. The ideal space groups for the intergrowth compounds are reportedly P4/mmm or Cmmm; however, all [X1][YM] compounds are distorted, thus possessing symmetry lower than P4/mmm or Cmmm. A trial, ideal structure $[PbBiO_2Cl][Bi_4Ti_3O_{12}]$ (space group Cmmm) was given; as well, a possible model of the true unknown structure was discussed and compared to the orthorhombic structure of $Bi_4Ti_3O_{12}$ (see Figure 4) [207].

The preparation of $BaTiO_3$ from $Ba(NO_3)_2$, $BaCO_3$, $Ba(OH)_2$ or BaC_2O_4 and $TiO_2 \cdot xH_2O$, anatase or rutile has been examined by thermogravimetry and x-ray diffractometry. $BaTiO_3$ forms in the reaction of $Ba(NO_3)_2$ with TiO_2, while other titanates result from reaction of other reactant combinations. The

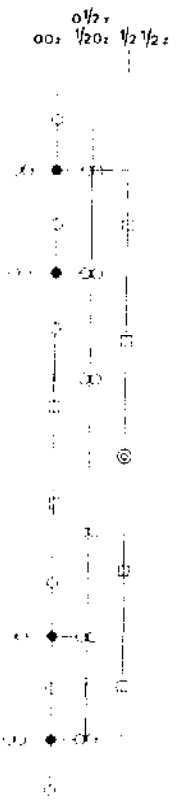

FIGURE 4: A schematic picture of the ideal crystal structure of $[PbBiO_2Cl][Bi_4Ti_3O_{12}]$ in space group P4/nmm. The heavy atom parameters are from a refinement in Cmmm. Empty, black and double circles indicate O, Ti and Cl, squares (Pb, Bi).

reactivity of reactants is of the order $Ba(NO_3)_2$ > $BaCO_3$ ≳ $Ba(OH)_2$ and anatase > $TiO_2 \cdot xH_2O$ ≳ rutile; BaC_2O_4 is converted to the carbonate prior to reaction with TiO_2 [208]. Beauger and coworkers [209] propose a mechanism to account for the macroscopic reproduction of the various solid-solid interfaces expected in the preparation of $BaTiO_3$ from $BaCO_3$ and TiO_2. The mechanism entails (a) the formation of $BaTiO_3$ at the expense of TiO_2 by Ba diffusion from $BaCO_3$, (b) the formation of Ba_2TiO_4 at the expense of the $BaTiO_3$ layer via Ba diffusion, and (c) the conversion of Ba_2TiO_4 to $BaTiO_3$, with release of an unidentified species of BaO stoichiometry which diffuses towards TiO_2 through $BaTiO_3$ to form $BaTiO_3$.

Active hydrated TiO_2 reportedly [210] reacts with aqueous ammonia solutions of $BaCl_2$ to yield amorphous barium polytitanates, containing ≤ 4.1×10^{-3} moles

of barium per gram of TiO_2. At 1173-1273K, crystallization of $BaTi_4O_9$ occurs. SEM and AES methods were utilized to study the epitaxial growth mechanism for the vacuum condensation of $BaTiO_3$ films by thermal evaporation onto $SrTiO_3$, TiO_2(rutile) and Al_2O_3(ruby) substrates. Faceting and lateral growth of islands of small lattice misfit and parallel orientation suggest a Frank-van der Merve mechanism [211]. The crystal structure of $BaTiO_3CeO_2$ has been examined using the EPR spectrum of Fe^{3+}, contaminating pure $BaTiO_3$, at 113-433K. The observed powder spectra were classified according to pure $BaTiO_3$, lightly doped $BaTiO_3$ (0,05-0.5 mole % CeO_2), and heavily doped $BaTiO_3$ (1-3 mole % CeO_2). The possibility of observing crystallographic phase changes in ferroelectric polycrystalline $BaTiO_3$ with various CeO_2 concentrations was confirmed by observing the EPR spectra of high-spin (Fe^{3+}) in polycrystalline $BaTiO_3$ at various temperatures [212]. Guenter and Jameson [213] obtained the structure of orthorhombic α'-Ba_2TiO_4, and related it to that of monoclinic β-Ba_2TiO_4 (see Figure 5). The TiO_4 tetrahedra are discrete, and three Ba atoms possess

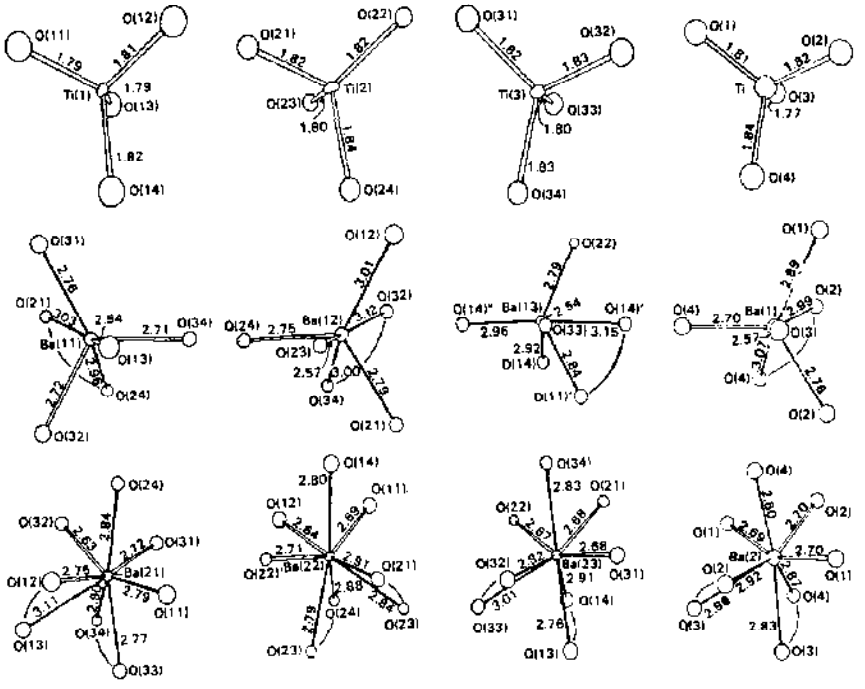

FIGURE 5: The coordination polyhedra for orthorhombic α'-Ba_2TiO_4 (first three columns) and monoclinic β-Ba_2TiO_4 (last column) [213].

irregular eight-fold coordination while the other three Ba atoms have irregular six-fold coordination. Structural refinements have been performed on the isostructural (space groups $P6_3/mmc$) six-layer, R-type hexagonal ferrites $BaTi_2Fe_4O_{11}$ and $BaSn_2Fe_4O_{11}$. The structure consists of h-stacked BaO_3 and O_4 layers in a 1:2 ratio. Three octahedral sites are occupied between O_4 layers, and an octahedral site and a tetrahedral site are occupied between the BaO_3 and O_4 layers. The octahedral sites are occupied by Ti (or Sn) and Fe, while the pair of tetrahedral sites is occupied by one Fe atom (see Figure 6) [214].

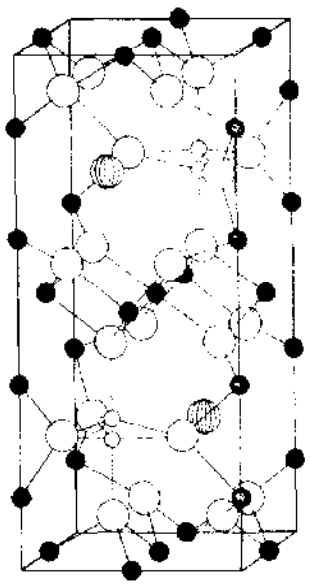

FIGURE 6: Unit cell structure of $BaSn_2Fe_4O_{11}$, which is isostructural with $BaTi_2Fe_4O_{11}$. Shaded circles, Ba; open circles, O; solid circles, octahedral sites occupied by (Sn, Ti) and Fe; small open circles, tetrahedral site occupied by Fe with an occupation rate of 50% [214].

The composition and crystal structure of orthorhombic (space group Pba 2) $Ba_{5.75}Pr_{9.5}Ti_{18}O_{54}$ have been refined. The structure reportedly [215] consists of TiO_6 octahedra joined into an infinite chain via common vertices along [001]

and to two other TiO_6 groups ($[Ti_9O_{27}]_o$) with BaPr lying between the channels.

A modified relaxation method has been employed to determine the specific heat of a single crystal of pure $BaTiO_3$ [216]. The results reveal a pure T^3 dependence of the specific heat in the 3-10K temperature range with no anomalous extra contribution, contrary to the general $T^{3/2}$ term expected for the specific heat of ferroelectrics at 2-10K. The experimentally observed polariton spectral features of NH_4Cl and $BaTiO_3$ crystals have been analysed on the basis of theoretical calculations, taking into account polariton Fermi resonance [217]. The room-temperature high frequency edge Raman spectra have been recorded for tetragonal $BaTiO_3$. Two new narrow width lines, not previously cited, are reported [218]. Sharon and Sinha [219] have determined some of the photoelectrochemical properties of n-$BaTiO_3$ doped with La, prepared by the alkoxy method. The bandgap (3.19 eV), donor level and space charge region were obtained. Furthermore, the flatband potential does not depend on the nature of the electrolyte, except for KI and $Fe(CN)_6^{4-}$, while the conduction band-edge position depends on the nature of the electrolyte. This suggests that the metal-semiconductor model of Mott-Schottky is not strictly applicable to the semiconductor-electrolyte system.

Valley and Klein [220, 221] have utilized the charge-transport model of photorefractivity to evaluate four figures of merit that can be used to characterize the performance of photorefractive materials. The figures of merit include (a) the steady-state index change, (b) the response time, (c) the energy per area to write a grating with 1% diffraction efficiency, and (d) the index change per absorbed energy per unit volume (photorefractive sensitivity). The indices are evaluated as a function of grating period and applied external electrical field for $Ba_{12}SiO_{20}$ (a fast material with a relatively small electrooptic coefficient) and $BaTiO_3$ (a slower material with a larger electrooptic coefficient).

The synthesis and analysis of lanthanum titanate has been cited in the Russian literature [222]. The phase relations at 1473-1623K for the sections

$La_4Ti_3O_{12}/MTiO_3$ (M = Ca, Sr, Ba), $La_2TiO_5/MTi/O_5$ (M = Ca, Sr), and $La_4Ti_3O_{12}/La_2MgTiO_6$ have been istablished by x-ray phase analysis. The formation of $MLa_4Ti_4O_{15}$ (M = Ca, Sr, Ba), $La_5Ti_{3.5}Mg_{0.5}O_{15}$, $Ca_2La_4Ti_5O_{18}$ and $La_6Ti_4MgO_{18}$, having hexagonal perovskite structures, was identified [223]. The crystallization temperatures of $La_{2/3-x}M_{3x}TiO_3$ (M = Li, Na, K) were determined by x-ray phase analysis and DTA. The addition of M leads to a decrease in the crystallization temperature in the sequence Li > K > Na [224].

The effect of initial pressure on the overall kinetics of the decomposition of N_2O over the double perovskite La_2TiCoO_6 at 673-733K has been established. As well, the catalytic activity of La_2TiCoO_6 has been compared to that of other La_2TiMO_6 compounds (M = divalent transition metal ions) [225].

Van Dijk et al. [226,227] have investigated the electrical and catalytic properties of some oxides with the fluoride or pyrochlore structure, including lanthanide titanates doped with cerium. The bulk magnetization and magnetic susceptibilities of $HoTiO_3$ and $ErTiO_3$ single crystals have been determined [228]. For $HoTiO_3$ and $ErTiO_3$, easy direction of magnetization is along the b- and c-axes, respectively, with respect to the 'Pbnm' chemical cell. The saturation magnetic moments along the easy axes are 7.5(2) μB per formula unit for $HoTiO_3$ and 6.9(2) μB for $ErTiO_3$ at 4.2K [228].

c. TiO_2

(i) Preparative Methods

A radio-frequency glow discharge promotes the reaction between $TiCl_4$ and oxygen to deposit TiO_2 thin films at low temperatures (298-973K) [229]. Ultra-fine (120-1500 Å) TiO_2(rutile) particles have been prepared from $TiCl_4$ at <373K and have been calcined. The effect of particle size on the photocatalytic activity in aqueous methanol has been reported [230]. Electrolysis of a $TiCl_4$ solution in the presence of 5 mole % $ZrOCl_2$ in a diaphragmless electrolytic cell yields the sol of hydrated TiO_2 [231]. TiO_2 thin films have been prepared at 403-523K by chemical vapor deposition involving $TiCl_4$ hydrolysis on a heated disk that rotates a silicon substrate [232]. Rutile-

type TiO_2 needles are produced upon chemical-vapor deposition from the TiF_4/H_2O system at elevated temperatures. Employing a flow method from a $Na_2TiF_6/TiO_2/H_2O$ system under controlled conditions, the TiO_2 needles grow preferentially in the [001] direction [233]. Ultrafine amorphous TiO_2 particles ($\leq 300\ m^2 \cdot g^{-1}$) have also been prepared by chemical vapor deposition of $Ti(OPr^i)_4$ (reaction 3).

$$Ti(OPr^i)_4 \longrightarrow TiO_2 + 4\ C_3H_6 + 2\ H_2O \qquad (3)$$

The reaction is catalysed by the TiO_2 deposit on the reactor wall [234]. The photocatalytic activity of Pt/TiO_2, for which the TiO_2 was prepared from $Ti(OCH(CH_3)_2)_4$, depends on the calcination temperature of TiO_2 [235].

TiO_2 optical coatings were obtained by ion-sputtering techniques, for use as multilayered interference mirrors and filters on glass substrates. The coatings were characterized by their absorption coefficients, film thickness and transmission spectra [236]. The utilization of argon and oxygen ions to bombard a film during deposition was studied as a potential technique for controlling the optical and mechanical properties of TiO_2 films [237, 238]. Thin films of TiO_2 formed by sputtering techniques were found to be mechanically stable, nearly amorphous and very adherent [239]. Nb_2O_5-doped n-TiO_2 has been prepared by vacuum annealing; the conductivity changes have been measured as a function of doping [240].

A thin-film polycrystalline TiO_2(rutile) photoanode obtains by the oxidation of a titanium sheet in air at 873K for 3 hr, followed by activation in hydrogen at 873K for 1 hr. The photoanode's optical-to-electrical conversion behavior was determined from flatband potentials, current-voltage curves, and spectral response [241]. The structure and electrochemical properties of TiO_2 photoanode films, prepared via reactive evaporation of titanium in 10^{-4} torr oxygen, have also been investigated [242].

(ii) Structure and Characterization

The equilibrium geometrical parameters of TiO_2 (also ScO_2^-, VO_2^+, FScO, $FTiO^+$ and FCuO) have been calculated by the Hartree-Fock method utilizing

valence double-exponential Roos-Veillard-Vinot basis sets for 3d metals and double-exponential Oors-Siegbahn basis sets for oxygen and fluorine. The calculations favor an angular structure with a valence angle (OTiO) equal to 115° for TiO_2 [243]. Munnix and Schmeits [244] have calculated wave-vector-resolved and -integrated surface densities of electronic states for defect-free TiO_2 [110] and TiO_2 [001] using the scattering theoretical method. The creation of these surfaces leads essentially to oxygen p-derived resonances in the valence-band region and to titanium d-derived resonances in the conduction band region. In agreement with available UV-photoelectron spectroscopic results, the gap for both faces is free of occupied surface states. New structural models were derived for oxygen vacancy defects which occur in impurity and dopant-controlled regimes of slightly substoichiometric rutiles. An analysis of the electrostatic valencies of the oxygen ions led to a suggestion that the oxygen vacancies should readily trap H^+ ions. These new small defect models offer an explanation for the many conflicting interpretations of physical property measurements of reduced and doped rutiles [245]. Computer simulations have shown that small defects should yield observable contrast for bright-field phase contrast images of rutile. The calculations provide a basis for reliable interpretation of observed images, if artifact contrasts can be excluded or controlled by the preparative method [246]. High-resolution electron microscopy and controlled preparative methods have allowed examination of the nature and structure of small defects existing within the nonstoichiometric rutile phase TiO_{2-x} ($0 \leq x \leq 0.01$). Using new linear cationic interstitial defect structural models, the atomic mechanisms involved in crystallographic shear plane nucleation and growth and the eventual evolution to an ordered crystallographic shear structure have been elucidated [247]. Calculations have been performed for the energetics of reduced TiO_2(rutile) crystals containing (i) an isolated {132} crystallographic shear plane, (ii) an ordered array of {132} crystallographic shear planes corresponding to an oxide of composition $Ti_{20}O_{39}$, (iii) a vacancy disk lying on {132} planes, and (iv) an ordered array of vacancy disk lying on {132} planes,

which yields the crystal composition $Ti_{20}O_{39}$. The calculations employed the polarizable point ion shell model and account for the electronic polarizabilities of ions involved. The results suggest that vacancy disks will be converted into crystallographic shear planes in real crystals, and will not exist as discrete defects. Also, a change in dielectric constant does not appear to have a significant effect on the stability of vacancy disks, but does have an effect on the energetics of crystallographic shear planes. The latter observation suggests that crystallographic shear planes are only favored in crystals of high dielectric constant [248]. Woning and Van Santen [249] have predicted greater reducibility of the coordinatively unsaturated Ti^{4+} ions at the rutile surface than at the anatase surface, based on calculations of the electrostatic potential at the most densely pack rutile (110) and anatase (001) crystal faces. As a consequence, the intrinsic Lewis acidity of coordinatively unsaturated Ti^{4+} ions at the rutile (110) face is larger than that of the Ti^{4+} ions at the anatase face.

X-ray diffraction line broadening studies of shock-loaded TiO_2(rutile) have been performed to determine residual lattice strain and coherent crystallite sizes. Rutile exhibits residual strain values near 2×10^{-3} at peak shock-loading pressures of 20-27 GPa. Coherent crystallite size reduction with decreasing pressure, and a gradual strain decrease and crystallite size increase with temperature were observed [250]. The high-temperature single-crystal x-ray diffraction analysis of TiO_2(rutile) at 300-1280K reveals an increase in the oxygen positional parameter with increasing temperature [251]. Ovchinnikov and Luk [252] have published a paper on the structural transformations in hydrolytic titanium dioxide films in the Russian literature. The effect of mechanical grinding on the structural transition of TiO_2 has been studied using several anatase samples prepared from different starting materials and with varying particle size. It was observed that the rate process of the anatase→rutile transition depends on the initial particle size and is independent of the difference in starting materials or of surface adsorbents

[253].

The Raman spectra of two natural (from the Ural-polar region) brookite TiO_2 samples have confirmed x-ray phase analytical data which show that one sample is free of large amounts of impurities while the second sample contains rutile. The Raman spectra exhibited 36 active vibrations, significantly more than the number observed for anatase or rutile [254]. Electron energy-loss spectroscopy (ELS) has been employed to study the electronic, localized and delocalized vibrational losses of TiO_2 (110). Band-gap defect states are indicated by electronic loss features at defect surfaces at approximately 8 eV; while in the higher loss-energy region above 3 eV, well-known interband transitions have been detected. Vibronic loss structures were characterized by three different delocalized Fuchs-Kliewer surface phonons as well as multiple and combination losses thereof [255]. The measured Stark effect induced in the infrared lattice bands of the Ti-O oscillator in TiO_2 has demonstrated that the intensity of reflection from the electrically polarized oscillators depends on induced polarization effects. Estimates of the degree of polarization and the dipole moment were made [256].

The atomic bonding in TiO_2 films deposited by ion beam sputtering of metal targets has been examined by x-ray photoelectron spectroscopy (XPS). The results show a single bonding state and no evidence of suboxides above a 5% level. Sputter-deposited TiO_2 exhibits a relatively narrow (1.7 eV) 1s line [257]. The intrinsic data of the XPS and x-ray-induced Auger electron (XAES) spectra of TiO_2 has been reported, along with spectral data for Sc_2O_3, V_2O_5 and NiO [258]. AES and electron stimulated desorption (ESD) studies reveal a marked increase in the O:Ti ratio on a TiO_2 sample at 575-975K. This observation is anomalous inasmuch as the oxygen-rich surface is observed under conditions for bulk reduction of TiO_2. The ESD lowers the O:Ti surface ratios by removing positive ions such as O^+ [259]. Surface defects produced in TiO_2 (110) by thermal treatment and ion bombardment have been studied by XPS, XAES and ELS techniques. High-temperature low-oxygen pressure treatment leads to

the formation of point defects with characteristic shifts in the cation core levels (Ti 2p and Ti 3p) of 1.7 eV towards lower binding energies and in the anion core level (O 1s) towards higher binding energy. Simultaneously, attenuation of non-bonding oxygen 2p valence band states, an additional Auger peak at 5.3 eV higher energy than the $L_3M_{23}V$ transition of ideal surfaces without point defects, and a pronounced electron loss feature at 0.8 eV were observed. The results suggest a defect-related gap state with mainly Ti 3d contribution 0.3 eV below the conduction band edge [260].

The annealing behavior of shock modified TiO_2(rutile) powder has been studied by TEM, x-ray, line-broadening, and ESR. Dislocations generated by shock treatment persist essentially unaltered through the 748K annealing, while substantial recovery is observed after the 1273K annealing [261]. An x-ray absorption fine structure (EXAFS) examination of crystalline TiO_2(anatase) and highly dispersed TiO_2 prepared via hydrolysis of $Ti(BuO)_4$ indicate that the latter sample has a mean particle radius of R_g = 35 Å in which 30% of the TiO_2 octahedra lie on the surface. An analysis of the EXAFS data indicates that the dispersed material is of the anatase form with coordination distances identical to those of the crystalline sample for all coordinations involving the coupling of three octahedra. The results were explained on the basis of increased compliance of the surface over that of the bulk [262].

Photoconductivity in crystalline TiO_2(rutile) is produced by competing single- and two-photon events; the first-order and second-order photoconductimetric cross sections are 3.6×10^{-26} cm^2 and 1.54×10^{-50} cm^4-sec, respectively. A thermoluminescence study of TiO_2(rutile) reports traps with thermal ionization energies between 0.4 and 0.9 eV below the conduction band. Traps with photoionization energies of 1 and 2 eV below the conduction band are believed responsible for the observed results, and may or may not be due to impurities (alumina) known to be present [263]. Kinetic energy distributions of various ionic species from a TiO_2 film have been obtained using the energy cut-off property of an ion reflector in a laser microprobe mass spectrometer.

The energy distributions were attributed predominantly to the locus of ion formation in the accelerating electrostatic field [264]. In situ multiple-beam interferometry (MBI) reflection has been employed to observe titanium thin-film high-temperature oxidation and to determine the extinction coefficient of TiO_2 thin films. The extinction coefficient of TiO_2 is $\beta = 3.6 \times 10^{-4}$ cm^{-1} for the He-Ne laser wavelength $\lambda = 632.8$ nm [265].

The effects of x-ray and γ-ray previous-irradiation on the viscosity and the aggregative stability of TiO_2 powder suspensions have been examined. When the powder is irradiated at a 10-100 Hz dose, the stability of the suspension in polar organic liquids increases significantly. This is due to the formation of additional positively charged centers on the surface of the particles [266]. Walther and Schirmer [267] have investigated the effect of stochastic interface roughness as well as of film thickness 'd' on light scattering from sputtered TiO_2 layers on a quartz glass substrate. The study shows dominating interface scattering and a 'd'-dependent interference of scattered light. Calculations reveal the importance of microroughness autocorrelation functions for describing the scattering.

Flash photolysis (347 nm) of a TiO_2 sol containing an adsorbed electron scavenger (e.g., platinum, methyl viologen) gives rise to an immediate broad absroption with $\lambda_{max} = 475$ nm. The absorption decays within milliseconds in acidic solution; and within microseconds in alkaline solution depending on $[OH^-]$. The absorption spectrum is the result [268] of excess positive holes trapped at the surface of the colloidal particles. Upon flash photolysing a TiO_2 sol containing an adsorbed scavenger for positive holes (e.g., polyvinyl alcohol, SCN^-), a broad absorption ($\lambda_{max} = 650$ nm) is observed, which decays in the presence of an electron scavenger. The absorption spectrum has been attributed to excess electrons trapped close to the surface of the colloidal particles [268].

Rakhmanov and coworkers [269] have found that the efficiency of spectral sensitization of TiO_2 photoimaging layers depends on the method of sensitization

of the dye into the layer. The highest sensitization efficiency is achieved when dye absorption on the TiO_2 layer surface is performed prior to the addition of a protective coating on the layer. It was observed that moisture adsorption and desorption in TiO_2 optical filters can be retarded via bombardment with 3 keV oxygen ions. The retardation is presumed to be due primarily to a swelling of the TiO_2 surface as the material is converted from crystalline to amorphous [270].

Yolou and Nadjo [271] report direct observation of surface states at n-TiO_2 by the impedence technique using acetonitrile, a solvent not expected to strongly solvate the surface. A layer of TiO_2(rutile) has been investigated to determine the quantum yield of the primary charge separation and the role of surface states [272]. A qualitative model of the photoeffect in rutile layers was presented. The modification of a TiO_2 film surface with malonic acid (4×10^{-3} to 4×10^{-4} M, for 5-60 min) leads to an increase in film sensitivity by a factor of 20-100, to an increase in the absolute value of the photopotential, to an increase in the rates of reduction processes on TiO_2 electrodes, and to a cathodic shift of potential [273]. The treatment of TiO_2 films on Ti or on a dielectric support by $H_2C_2O_4$ solutions at 368-370K leads to an increase in the film's photosensitivity by a factor of 3-5 and 10-50, respectively. The surface modification results in increased absorbance values of the photopotential and decreased relaxation rate, decreased dark anodic current in the potential range 0 to +1.8 eV, a shift in the cathodic direction of the stationary potential, and a decreased concentration of ionized donor levels [274]. A study of Ti/TiO_2 growth in 5M NaCl at 363K (pH = 2.5) gives rise to a linear log i vs log t plot with the well-known slope of -0.94. For potentials lower than 1.4V, growth follows the inverse log law from which various parameters were calculated [275].

The E-pH dependence of TiO_2 electrodes has a linear nature with higher angular coefficients than theory predicts. The effect of the semiconductor nature of electrodes on the pH-function was investigated by determining the

E-pH dependence for samples of Ti/TiO_2 (doped with 1 and 5 mole fraction ruthenium) exposed and not exposed to UV light [276].

Voltammetric experiments have given evidence that H_2O_2 is photogenerated in an intermediate step of the water splitting reaction on an n-TiO_2 polycrystalline electrode. It was suggested [277] that the photo- and electroluminescence properties of n-TiO_2 in contact with aqueous solution could result from the inelastic electron transfer from the semiconductor conduction band to bandgap surface states associated to chemisorbed H_2O_2 molecules. The preparation of TiO_2 electrodes by plasma spraying and their photoelectrochemical behavior in 0.1N NaOH have been reported [278]. This plasma spraying technique shows promise for the praparation of large area TiO_2 electrodes for the photoelectrolysis of water. o-xylene, p-xylene and toluene are oxidized on irradiated n-TiO_2 electrodes to the corresponding aldehydes and alcohols in acetonitrile containing Et_4NClO_4 and Et_4NBr. Under irradiation, anodically and photochemically generated bromine radicals catalysed the oxidation by dissolved oxygen [279]. The semiconductor $TiO_2(B)$, obtained by hydrolysis of $K_2Ti_4O_9$ and subsequent heating, possesses a crystal structure which can accomodate the insertion of guest atoms. Photoelectrochemical experiments have characterized the polycrystalline material as n-type with an energy gap of 3 eV. Electrochemical reduction of protons at $TiO_2(B)$ electrodes results in the appearance of new electronic states within the energy gap, thus rendering the semiconductor sensitive to visible light. These states presumably originate from intercalated hydrogen which diffuses through the sample. An anodic photocurrent is observed upon optical excitation of these states, and has been interpreted as light-induced deintercalation of hydrogen from $TiO_2(B)$ to yield protons [280]. Model calculations have been performed to estimate the catalytic influence of electrochemical diodes on the rate of electron transfer reactions [281]. A distribution function of the current density i(E) independence on the electronic energy E was obtained. The predictions from this model seem to be in reasonable agreement with

experimental results recently obtained for passive Ti and Ti.TiO_2/Au-diodes [281].

Photoelectrochemical conversion with a polycrystalline TiO_2 electrode, prepared by flame oxidation of titanium metal, reveals the processes to be sensitive to applied voltage, oxidized TiO_2 thickness, and to the concentration of the solution in the photoelectrochemical cell [282]. The anodic current begins at -0.8V in 1N NaOH, while the photocurrent appears at approx. 420 nm and increases with light intensity. The emf of the cell drops at a rate of 58.5 mV/pH. Photoelectrochemical properties of photoanodes prepared from TiO_2 films deposited onto Ti substrates by plasma-enhanced chemical vapor deposition have been determined [283]. The plasma-deposited photoanodes display quantum efficiencies higher than those for thermally grown films and comparable to those reported for single-crystal rutile. Presumably, the microstructure of the plasma-deposited films is primarily responsible for the high quantum efficiencies [283]. A thin-film polycrystalline n-TiO_2 photoanode was obtained by thermal oxidation (at 873K) of a Ti sheet in air [284]. Doping with Y-Cr or La-Cr simultaneously creates the possibility of enhanced quantum efficiency and spectral response to visible light [284].

Abdullin [285] has reported preliminary results on a study of the nature of inclusion of TiO_2 particles (0.5- 2 μm in size) during the electrodeposition of zinc on the (0001) and ($10\bar{1}0$) faces of a zinc single crystal. An electrodeposited TiO_2-polyacrylate-nickel composite electrode has been prepared for a photoelectrocatalytic reaction [286]. Fornarini and coworkers [287] have further examined the energetics of p/n photoelectrochemical cells containing simultaneously illuminated p-type photocathodes and n-type photoanodes, using appropriate combinations of n-TiO_2, n-WSe_2, n-$MoSe_2$, n-WS_2, p-InP, p-GaP and p-Si electrodes.

(iii) Reactions Of and On TiO_2

Infrared spectroscopy is an interesting tool to study the disproportionation of NO on TiO_2. During UV irradiation, TiO_2 catalyses the

oxidation of CO, CH_4, and MeOH by nitrogen oxide [288]. TPD studies of the formation of ethane, ethylene, and propylene in the irradiated CH_4/TiO_2 system indicate that the process is most effective under x-ray or long-wavelength light irradiation behind the edge of the fundamental absorption band of the TiO_2 [289]. Upon UV irradiation of an aqueous solution of $K_4Fe(CN)_6$ in the presence of HCHO and metallic oxides (TiO_2, MgO, U_2O_3), several amino acids (glycine, α-alanine, aspartic acid) are catalytically formed [290].

The nature of surface species formed during the thermal decomposition of $[Fe(CO)_5]$ on clean TiO_2 powder has been investigated using Moessbauer spectroscopy and volumetric gas-phase analyses. On all TiO_2 samples, low-temperature decomposition (383K) leads to the formation of an Fe^{2+} species and an Fe^0 species, both of which are likely associated with surface OH groups. High-temperature decomposition (673K) yields a nearly complete conversion of the metal to the Fe^{2+} species [291]. The photoassisted heterogeneous decompositions of 1,2-dibromomethane, 1,1-dibromomethane [292], $ClCH_2CH_2Cl$, $Cl_2C=CCl_2$, $ClCH_2CO_2H$, and Cl_2CHCO_2H [293], $ClCH=CCl_2$ and $CHCl_3$ [294] are catalysed by TiO_2. 1,2-dibromomethane and 1,1-dibromomethane are degraded to HBr and CO_2 in dilute aqueous suspensions of near-UV-illuminated TiO_2 [292], while the decomposition of $ClCH=CCl_2$ and $CHCl_3$ give HCl and CO_2 in the presence of solar-illuminated TiO_2(anatase) [294], as does the decomposition of $Cl_2C=CCl_2$, $ClCH_2CH_2Cl$, $ClCH_2CO_2H$ and Cl_2CHCO_2H in the presence of near-UV-illuminated TiO_2 [293].

The reduction of TiO_2 and $TiCl_4$ in a hydrogen plasma jet has been studied by Kikukawa et al. [295]. For TiO_2, the highest reduced product is TiO; titanium metal is not obtained. Colloidal TiO_2 sensitizes the photoreduction of Methyl Orange to a hydrazine derivative, for which a maximum rate is achieved at pH 4.7 in an oxygen-free system and at pH 3.0 in the presence of oxygen. Similar behavior was observed for Methyl Red. Flash photolysis experiments showed that electron transfer from TiO_2 to Methyl Orange depends on the protonated dye concentration and on the potential of an electron in the TiO_2

conduction band [296]. The rates of $Cr_2O_7^{2-}$ reduction and HCO_2H decarboxylation on TiO_2 photocatalysts were examined as a function of temperature. While no appreciable temperature dependence was observed for the reduction of $Cr_2O_7^{2-}$, the logarithmic rate for HCO_2H decarboxylation seems to depend linearly on the reciprocal temperature up to ca. 333K whereupon a tendency of saturation occurs [297].

The effect of γ-irradiation on the catalytic activity of TiO_2 and ZrO_2 in the reduction of CO_2 has been examined by Shishkina and coworkers [298]. A review by Malati and Wong [299] discusses doping TiO_2 for use in solar energy applications. Also included is a section on the photocatalysed reduction of CO_2.

The rate of hydrogen oxidation on TiO_2(rutile) is one order of magnitude higher than that on TiO_2(anatase), owing to the different bond strength of the surface oxygen [300]. Infrared spectroscopy and product analysis have been used to determine the influence of preadsorbed pyridine on the adsorption, dehydration, and dehydrogenation of EtCHMeOH on TiO_2 [301]. In the presence of oxygen, the major products from the butoxide are butenes with EtCOMe being a minor product; in the absence of oxygen, only butenes are formed. Preadsorbed pyridine inhibits butene formation and enhances that of EtCOMe [301]. The effect of added TiO_2 on the oxidation of Cr_2O_3 in highly disperse mixtures with Al_2O_3 during calcination in air at 875K has been investigated by chemical analysis and magnetochemical techniques [302].

The photocatalytic oxidation of SO_2 and/or cis-2-butene in oxygen over TiO_2(anatase) yields SO_3 from SO_2 and CO_2 from cis-2-butene. The presence of SO_2 reduces the photocatalytic activity of TiO_2 on the oxidation of cis-2-butene [303]. The TiO_2-sensitized photooxidation of sulfides yields sulfoxides and sulfones, with sulfide radical cations as the proposed reaction intermediates [304]. The roles of oxygen and water in the photocatalysed oxidation of aromatic hydrocarbons (benzene, toluene) on TiO_2 were investigated in order to determine the mechanism for the formation of radicals [305]. Electron

transfers from H_2O and toluene to the photogenerated positive holes, synchronized with electron transfer from the photoexcited TiO_2 to oxygen, result, respectively, in aromatic nuclear hydroxylation to yield phenolic products and in the oxidation of the side chain of toluene to give $PhCH_2OH$ and PhCHO [305]. Several substituted naphthalenes react with oxygen to yield ring-cleaved products upon long-wavelength UV irradiation of TiO_2 powders suspended in oxygen-saturated acetonitrile solutions. A mechanism involving sensitized formation of the substituted naphthalene cation radical is proposed [306]. Unsupported TiO_2 colloids catalyse the photooxidation of Methyl Orange and concomitant reduction of oxygen. The presence of H_2O_2 inhibits oxidation, while the presence of cationic surfactants and cationic polymers increases the rate of oxidation [307].

The TiO_2-photocatalysed hydroxylation of C_6H_5OH and C_6H_5ONa has been studied under a variety of experimental conditions. In the presence of oxygen, o-, m- and p-hydroxybenzoic acids were formed in the same isomeric distribution observed for ·OH attack on C_6H_5OH. In the absence of oxygen, the yield of hydroxy compound is quite low, though high yields are found on addition of Fe(III). The effects of oxygenated slurries and added H_2O_2 have also been determined. The results appear consistent with the generation of ·OH *via* the positive holes of the TiO_2 particles, followed by ·OH attack on the aromatic ring and subsequent oxidation of the hydroxy adduct with oxygen or Fe(III) to yield the corresponding phenol [308]. The TiO_2-photocatalysed hydrogenation of alkenes and alkynes with water to produce major hydrogenation products accompanied by C=C and C≡C bond fission products were studied by Anpo *et al.* [309]. Water molecules, and not surface OH^- groups, are thought to be responsible for the reaction. The C=C and C≡C bond fission that accompanies hydrogenation is likely due to the interaction of the alkenes or alkynes with the trapped electron (Ti^{3+}) and hole (·OH) pairs [309].

Santacesaria *et al.* [310] have studied the kinetics of hydrated TiO_2 precipitation by thermal hydrolysis from sulfuric acid solutions. The rate-

determining steps are kinetic-controlled, rather than diffusion-controlled, and an increase in H_2SO_4 concentration affords a decrease in nucleation and growth rates. Zirconium stabilizes nitric acid solutions which contain titanium; the stabilization apparently is the result of interaction between hydrolysed zirconium and titanium compounds. The precipitates of TiO_2 and ZrO_2 from the nitric acid solutions are hydrated polymeric species [311]. The reaction of H_3PO_4 with $TiO_2 \cdot xH_2O$ was examined as a function of temperature, H_3PO_4 concentration, and reaction time. The maximum degree of H_3PO_4 conversion is achieved in 40 min at 373K, and a conversion of less than 50% was attained. The reaction is accelerated in the presence of other acids (e.g., H_2SO_4) [312].

Thin TiO_2 films prepared by thermal oxidation, vapor deposition, and anodic oxidation have been examined for their composition, surface structure, and film thickness [313]. Additionally, their electrical and photoelectrochemical properties were also determined [313]. The efficiency of differently prepared TiO_2 particles in the photochemical water splitting reaction through band gap irradiation of aqueous suspensions has been examined by Borgarello and Pelizzetti [314]. The effects of pH and loading with noble metals and RuO_2 are reported. RuL_2^{2+}-derivatized (L = diisopropyl-2,2'-bipyridine-4,4'-dicarboxylate) TiO_2 particles loaded with Pt and RuO_2 were shown to be active in producing hydrogen from water by visible light in the absence of a sacrificial organic donor [315]. Muraki and coworkers [316] have reported that the photocatalytic oxidation of H_2O on TiO_2 particles yields initially only the formation of H_2O_2, in contrast to the commonly accepted supposition of oxygen generation. Freshly precipitated polycrystalline amorphous and colloidal TiO_2(anatase) were deemed inefficient photocatalysts for hydrogen production from water and propan-2-ol and for methane and hydrogen production from acetic acid. Their reactivity is attributed to the formation of titanium(III) species rather than electron-hole pairs [317]. In the presence of redox catalysts (TiO_2, Pt, Pd, ZnO, Ni) and an aqueous solution of proflavin and methylviologen (MV^{2+}), the reduction of H_2O by MV^+ is accompanied by

hydrogen evolution. A temperature dependence study shows enhanced hydrogen evolution at higher temperatures (339K) and hindered MV^+ reduction. At 339K, hydrogen yields increase with a decrease in pressure [318].

d. M/TiO_2

Group IIA

Isothermal sections of the $CuO/Y_2O_3/TiO_2$ system were examined by x-ray diffraction at 1273 and 1473K. No ternary oxide formation occurs. At the temperatures cited, the $Y_2O_3/Ca_3Ti_2O_7(CaTiO_3, Ca_4Ti_3O_{10})$ and $CaTiO_3/Y_2TiO_5(Y_2Ti_2O_7)$ sections are quasibinary [319].

Group VB

A high-resolution electron microscopic study of the disorder in two types of rutile-related crystallographic-shear phases reveals variations in orientation of the crystallographic-shear planes [320]. The samples tested include rutile that was melted in an argon-arc furnace, and a V_2O_3-doped TiO_2 quenched from 1873K [320]. Electron microscopy and electron diffraction, coupled with EPR, have been employed to detect substitutional and/or interstitial V^{4+} ions and isolated extended defects at low V_2O_3 concentrations. At higher V_2O_3 concentrations, the extended defects become ordered, giving rise to the homologous series (M_nO_{2n-1}) for which M = Ti + V [321]. An x-ray absorption fine structure study of V_2O_5/TiO_2 catalysts shows that the catalytically active surface phase supported on anatase does not possess a structure characteristic of V_2O_5 [322]. When supported on anatase, the basic structural unit possesses two terminal (r = 1.65 Å) and two bridging (r = 1.90Å) bonds. The catalytic activities of unsupported and supported V_2O_5 catalysts were examined for the oxidation of H_2 [323]. The active oxygen species is believed to be the surface V=O species. The turnover frequency for V_2O_5/TiO_2 and V_2O_5/Al_2O_3 remains constant and independent of the kind of support or V_2O_5 content [325]. A similar study was carried out for the oxidation of carbon monoxide, for which the turnover frequency of V_2O_5/TiO_2 samples increases with

increasing V_2O_5 content [324]. The results indicate that the oxidation of CO on V_2O_5 catalysts is a structure-sensitive reaction, and that the activity of surface defects is much higher than that of the surface V-O species in the smooth (010) face of V_2O_5.

The effects of V_2O_5 deposition on TiO_2 (anatase, rutile) has been examined under conditions in which TiO_2 acts solely as a support [325]. The catalysts were characterized with respect to their activities and selectivities in the oxidation of o-xylene, toluene, p-methoxytoluene and p-tert-butyltoluene. Higher selectivities to partial oxidation products and lower selectivities to total oxidation products (except for p-tert-butyltoluene) were observed with V_2O_5-TiO_2(anatase) catalysts compared with V_2O_5-TiO_2(rutile) catalysts. The results were rationalized in terms of lower acidity and lower degrees of V_2O_5 reduction of the anatase catalysts [325]. ESR studies of V_2O_5 deposited in different quantities on the surface of rutile and anatase reveal that reduced V_2O_5 is present on both TiO_2 surfaces as dispersed $(V{=}O)^{2+}$ groups and V^{4+} ions in the V_2O_5 phase [326]. In the anatase-containing samples, the $(V{=}O)^{2+}$ groups are densely placed and resistant to oxidation in an oxygen atmosphere, while the $(V{=}O)^{2+}$ groups on rutile are more scarcely dispersed and more easily oxidized. Of several supported metal oxide catalysts investigated for the selective gas phase oxidation of toluene, the V_2O_5/TiO_2 catalyst system appears to be most effective [327]. The different catalytic behavior observed for V_2O_5 supported on Degussa TiO_2 and Tioxide TiO_2 was attributed to the presence of phosphorus and potassium impurities in the Tioxide sample; for the latter, a large negative effect on the catalytic properties has been observed. These impurity effects were studied in detail for the oxidation of toluene to benzoic acid and of o-xylene to phthalic anhydride [328].

Infrared spectroscopy [329-331] and x-ray diffractometry [330, 331] were employed to study the oxidation of alcohols catalysed by V_2O_5/TiO_2. Vorob'ev and coworkers [332] report kinetic data for the oxidative ammonolysis of toluene on a V_2O_5/TiO_2 catalyst; the redox mechanism of Mars and van Krevelen seemed

applicable [332].

The kinetics of the reduction of nitric oxide by ammonia on supported V_2O_5 catalysts have been investigated by several groups [333-335]. A study of this reaction at 433-573K on V_2O_5 supported on TiO_2, Al_2O_3, ZrO_2, SiO_2 and MgO shows that the surface V=O groups are catalytically-active centers and the rate constants are proportional to the surface V=O group concentration [333]. Wong and Nobe [334] have looked at this reaction in the presence of oxygen on TiO_2 (anatase)- and TiO_2(rutile)-supported V_2O_5 catalysts prepared by the chemical mixing technique and the impregnation method. The following observations were made: i) the intrinsic rates of the $NO-NH_3-O_2$ reaction are first order with respect to NO and zero order with respect to NH_3 for all catalysts; ii) the intrinsic activity of the V_2O_5/TiO_2 catalysts, prepared by the chemical mixing technique, is greater than that for catalysts prepared by the impregnation method; and iii) the TiO_2(rutile)-supported catalysts have the lowest activities owing mainly to their low surface areas. Another investigation [335] has focussed on the deactivation of a V_2O_5/TiO_2 catalyst with deposited alkali metal salts, and on catalyst regeneration. In the reduction of NO with NH_3 in the absence of SO_x, the degree of deactivation is significantly affected by the type of salt deposited; the order is $KCl \geq K_2CO_3 > NaCl > Na_2CO_3 \geq KNO_3 \geq K_2SO_4 > NaNO_3 > Na_2SO_4$. The effect of the salts (transformed into sulfates) on the degree of deactivation decrease in the presence of SO_x. The deactivation is caused mainly by the reaction of alkali metal salts with V_2O_5, leading to the formation of an inactive oxide complex. The catalysts can almost be completely regenerated by washing with water [335].

Kiwi and coworkers [336] have examined niobium-doped TiO_2 with respect to its inclusion in water photocleavage processes. EPR spectra of Nb-doped TiO_2 have indicated that niobium occupies substitutional Ti^{4+} sites in the form of $Nb^{4+}(4d^1)$.

Group VIB

The temperature dependence of the solubility limit of Cr_2O_3 in

TiO_2(rutile) has been investigated by electron microscopy. The following observations are reported: i) $(Ti,Cr)O_{2-x}$ is a true nonstoichiometric phase, containing small defects effectively randomized homogeneously throughout the rutile lattice; ii) the approximate temperatures for small/extended defect equilibrium in $(Ti,Cr)O_{2-x}$ ($0 \leq x \leq 0.05$) were determined. The results have been interpreted in terms of linear cationic interstitial small defect models [337]. The amplified susceptibility effect was used to determine the presence and relaxation of the spin-spin temperature in magnetically diluted $TiO_2:Cr^{3+}$ crystals [338]. The observed behavior was rationalized as a manifestation of spectral diffusion in the EPR line which is broadened as a result of spin-spin interactions between paramagnetic centers distributed randomly within the sample. The broadening in such a system is essentially nonuniform, and the spectral diffusion is a process of formation of a quasi-nonequilibrium spin-spin reservoir [338].

A finely dispersed titanium-molybdenum catalytic system was successfully prepared thermally upon precipitation of $(NH_4)_6Mo_7O_{24}\cdot 4H_2O$ from solutions on TiO_2 followed by baking at 773K [339]. A variety of surface spectroscopic techniques were used and chemical activity measurements made to characterize several supported metal catalysts, that included Mo on TiO_2 and Al_2O_3. The reaction of the catalysts with H_2 and H_2S/H_2 diagnosed different species [340]. The direct synthesis of hydrazine over $MoO_3/TiO_2/Mg(OH)_2$ and amorphous TiO_2 (among other catalyst systems) has been performed, along with activation of (H + N) by silent discharge at room temperature [341]. Molybdenum/titanium oxide catalysts catalyze the oxidation of ethanol [342] and propylene [342, 343]. An infrared and x-ray diffraction study of the MoO_3/TiO_2 catalyst shows that at low Mo content, MoO_3 is highly dispersed on TiO_2 with the formation of an amorphous phase associated with the weakening of the Mo=O bond [342]. TiO_2 promotion is associated with the rate acceleration of the reduction step [342]. In the propylene oxidation reaction, the catalytic activity depends on the phases present, and an increase in Mo content stabilizes the anatase form of

TiO_2 [343].

Group VIII

Well-dispersed, supported oxidic catalysts have been synthesized *via* reaction (adsorption) of [Fe(acac)$_3$] (acac = acetylacetonato) with the surface OH groups of a TiO_2 support [344]. An almost complete monolayer of Fe_2O_3 can be formed on TiO_2 by continuous adsorption of [Fe(acac)$_3$]. X-ray diffraction, Moessbauer spectroscopy and magnetic susceptibility measurements were employed to characterize the $TiO_2/FeNb_2O_6/NbO_2$ system [345]. The study shows the following: i) isolation of a wide domain of rutile solid solution; ii) Fe is divalent in the whole domain; iii) a second type of Fe(II) is observed in the limit $Ti^{IV}_{1-x}Fe^{II}_{x/3}Nb^{V}_{2x/3}O_2$, presumably a consequence of a small loss of oxygen involving the formation of Ti^{3+}. A study of the conductivity and thermoelectrical power in this system established the presence of two domains, in which the π^* bands involve the Ti-3*d* and Nb-4*d* orbitals. The first domain is characterized by the simultaneous presence of Ti^{IV}, Ti^{III} and Nb^{V}, and corresponds to the triangle $Ti^{IV}O_2$--$Fe^{II}Nb^{V}_2O_6$--$Ti^{III}_{0.5}Nb^{V}_{0.5}O_2$. The second domain, in which all titanium ions are trivalent, is characterized by the simultaneous presence of Ti^{III}, Nb^{IV}, and Nb^{V} and corresponds to the triangle $Nb^{IV}O_2$--$Fe^{II}_2Nb^{V}_2O_6$--$Ti^{III}_{0.5}Nb^{V}_{0.5}O_2$ [345]. The carbon monoxide/hydrogen reactions over iron/titanium dioxide catalysts have been examined [346, 347], as has been the TiO_2/Fe_2O_3 system for use as a heterojunction anode [348].

The photoelectronic properties of a $Ti_{0.97}Ru_{0.03}O_2$ biphasic crystal in an aqueous electrolyte have been examined [349] to determine the effect of Ti^{4+} substitution by Ru^{4+} on the electrochemical and photoelectrochemical properties. Ruthenium ions in the TiO_2 lattice form a narrow cationic impurity band, between the oxygen-2*p* valence band and the titanium-3*d* conduction band. Several groups [350-356] have investigated the use of RuO_2/TiO_2 anodes in the chlorine evolution reaction. Janssen [350] has reviewed the mechanisms and the kinetic data for this reaction on various types of RuO_2/TiO_2 electrodes, and has presented new experimental results. The chlorine evolution on this

type of electrode occurs according to the Volmer-Heyrowsky mechanism, where the Volmer reaction is in quasi-equilibrium, and the Heyrowsky reaction and eventually the diffusion of molecular chlorine away from the electrode surface into the bulk solution determines the potential-current density relationship. On RuO_2/TiO_2 anodes, the rate of evolution-ionization of chlorine increases with increasing pH. Additionally, the order of the reaction with respect to H^+ depends on pH and on the electrode potential; the order with respect to Cl^- does not depend on pH and is equal to one. To account for these results, a stepwise reaction mechanism was proposed in which the slow electrochemical stage of Cl^- discharge precedes the fast electrochemical stage occurring with the detachment of H^+ [351]. Spasojevic and coworkers [352] report an anodic electrocatalyst, having a titanium substrate with a catalyst of RuO_2/TiO_2, for use in chlor-alkali cells, chlorate cells, seawater electrolysis and similar applications. The performance of the catalyst was characterized by determining the anodic potential at constant current versus time, by Tafel curves, and by its durability, along with charging currents, electrode charge and crystal structure. The properties of a RuO_2/TiO_2 anode in which the active material is deposited on an intermediate layer (30-60 μm) of porous titanium have been studied for the electrolytic manufacture of chlorine, chlorates and other chlorine-containing compounds [353]. The change in composition of the active coating of a RuO_2/TiO_2 anode during operation in strongly acidic solutions was studied by Auger electron spectroscopic and x-ray microanalytical methods [354, 355]. A substantial enrichment of the coating in ruthenium is observed, along with the introduction of a significant amount of chlorine into it. The low corrosion resistance of these anodes in strongly acidic chloride solutions is presumed due to the instability of the titanium component of the coating under these conditions [354,355]. Computer programs have been developed to analyse electrochemical reaction schemes with application to the evolution of chlorine [356].

The RuO_2/TiO_2 system is known to catalyze the Fischer-Tropsch synthesis of

hydrocarbons [357, 358], CO_2 reduction [359], and the oxidation of SO_2 [360], of benzene, chlorobenzene and dichlorobenzene [361]. In the Fischer-Tropsch reaction, the catalytic activity of RuO_2/TiO_2(anatase, rutile) depends on the calcination temperature of the support, the crystal structure (anatase or rutile), and the reduction temperature [357]. A comparison of the activities of RuO_2/TiO_2 and RuO_2/Al_2O_3 catalyst systems in the Fischer-Tropsch reaction reveals that RuO_2/TiO_2 has the higher activity for the Fischer-Tropsch synthesis and lower selectivity for methanation. These trends were elucidated by the reduced chemisorption of CO and H, likely caused by a strong metal-support interaction [358]. The reduction of CO_2 to HCO_2H, HCHO and MeOH was performed by illuminating aqueous suspensions of TiO_2 with a high-pressure mercury lamp [359]. The rate of product appearance is enhanced by doping TiO_2 with RuO_2. Inasmuch as the efficiency declines under prolonged illumination, it was suggested that the observed photoreduction is not a truly photocatalytic reaction [359]. The effect of a transfer-agent catalyst (iodide ion) on the anodic oxidation of SO_2 in H_2SO_4 solutions has been investigated in connection with the possibility of obtaining hydrogen in the H_2SO_4 thermodynamic cycle [360]. The iodide ion catalyses the electrooxidation of SO_2, and results in higher reaction rates. On RuO_2/TiO_2 anodes and on graphite electrodes, benzene, chlorobenzene and dichlorobenzene are electrochemically inert [361].

The electrolysis of NaCl/HCl solutions can take place with titanium anodes coated by thermal decomposition of $RuCl_3$ or $RuCl_3/TiCl_3$. Polarization curves were determined for the oxygen evolution process, the rate of which was used to assess the activity and selectivity of the electrode [362]. The photoelectrochemical properties of TiO_2 single-crystal electrodes on which small amounts of RuO_2 were deposited have been investigated by Sakata et al. [363]. The RuO_2 on n-type semiconductors serves as a reduction catalyst for the water-splitting reaction and other hydrogen-evolution reactions. In the presence of strong electron acceptors such as Ag^+ or Fe^{3+}, the RuO_2 on TiO_2 functions as a reduction site for photocatalytic oxygen evolution. The kinetics of reduction

of aqueous solutions of Ce^{IV} and $[Ru(bpy)_3]^{3+}$ (bpy = 2,2'-bipyridine), in the presence of catalytic amounts of RuO_2 colloids stabilized with polybrene and colloidal TiO_2 particles loaded with RuO_2, have been examined by stopped-flow spectrophotometric techniques. The TiO_2/RuO_2 colloidal particles are very active catalysts [364]. The preparation of rhodium- and ruthenium-loaded TiO_2 particles from cluster precursors ($[Rh_6(CO)_{16}]$, $[Ru_3(CO)_{12}]$) has been reported, and their activity in mediating water decomposition *via* band-gap excitation determined. Bifunctional Rh/RuO_2-loaded TiO_2 exhibits optimal performance, with an overall light-to-chemical energy conversion efficiency of 0.13% [365].

Experiments performed by Takasaki *et al.* [366] have shown that the particle size of cobalt in a Co/TiO_2 catalyst increases with increasing reduction temperature up to 873K. At 973K, where the TiO_2 anatase → rutile transformation occurs, the cobalt particles redisperse to individual crystallites. The redispersion was confirmed by measuring the specific activity of the cobalt catalyst for propene hydrogenation. High-temperature x-ray diffraction spectroscopy was employed to determine the relationship between the TiO_2 phase transformation and the cobalt redispersion. The specific activities and selectivities of unsupported cobalt and cobalt supported on TiO_2, Al_2O_3, SiO_2, C and MgO have been measured for the CO hydrogenation reaction. The specific activity varies with support, dispersion, metal loading and preparation method. The order of decreasing CO hydrogenation activity at 1 atm and 498K for catalysts containing 3 wt. % Co is Co/TiO_2, Co/SiO_2, Co/Al_2O_3, Co/C and Co/MgO. Product selectivity was best correlated with dispersion and extent of reduction [367]. EXAFS studies have established the formation of tiny clusters of Co_3O_4 in a TiO_2 support after calcination of Co/TiO_2 catalysts prepared by an alkoxide technique. That the Co metal particles in the catalyst can be controlled to an even size level after reduction by hydrogen is due to the high dispersion of the Co_3O_4 clusters [368].

The temperature-programmed reduction (TPR) of Rh/TiO_2 catalysts reveals two reduction peaks, ascribed to the reduction of small, well-dispersed Rh_2O_3

particles and of large, bulk-like Rh_2O_3 particles. Reduction of Rh_2O_3 is complete at >450K, while TiO_2 is reduced partly by a metal-catalysed process at >500K [369]. ESR and nmr spectroscopy were used to study a Rh/TiO_2(rutile) catalyst reduced at 773K after contact with air and subsequent hydrogen treatment of the passivated sample at T_H = 295 - 773K [370]. The results indicate that, at T_H < 573K, hydrogen is strongly bonded to the Rh particles, and reversible generation of Ti^{3+} ions and hydrogen species weakly adsorbed on to the metal occur. A mechanism was proposed that implicates heterolytic splitting of H_2 at the metal-support interface, followed by proton stabilization on the support. At T_H > 573K, further H_2 adsorption on the metal and on the support occurs, leading to a deeper reduction of the support [370]. An electron spin echo study of Ti^{3+} in Rh/TiO_2 formed by the reaction with D_2 at room temperature shows that no deuterium exists within 0.6 nm of Ti^{3+} [371]. The formation of Ti^{3+} is presumably due to electron transfer from D atoms to Ti^{4+} at the boundary between Rh metal and TiO_2, and subsequent stabilization of D atoms by OH anions on the TiO_2 surface. A study of the thin film model using several surface science techniques provided evidence for the role of both encapsulation and electronic effects in Rh/TiO_2 catalysts [372]. An indirect effect of the support on the kind of bimetallic interaction has been observed on Rh-Ag catalysts supported on TiO_2 compared to SiO_2. The effect occurs at significantly lower temperatures than the direct strong metal-support interaction between Rh and TiO_2. The main feature of the indirect effect is the pronounced decay in the H_2 chemisorption capability and activity for ethane hydrogenolysis with time when the catalysts are left in flowing H_2 at 523K. The behavior was rationalized in terms of a modification of the energetics of the metal-metal interaction, which may cause the Ag to spread over the Rh particles [373]. The effect of various supports (TiO_2, Al_2O_3, SiO_2, MgO) for rhodium catalysts has been investigated with respect to the adsorption, desorption, and dissociation of CO [374]. The reactivity of surface carbon produced by CO disproportionation was also examined. CO adsorption at 300K on

the various supported Rh samples yields almost identical infrared spectra, while the desorption temperature of CO (463-473K) is nearly the same for all the samples. The efficiency of the various supports in promoting CO dissociation over the rhodium catalysts decreases in the order TiO_2 > Al_2O_3 > SiO_2 > MgO [374]. The addition of alkali metal cations to TiO_2-supported rhodium catalysts results in an improved selectivity for C_2-oxygenated compounds in the CO-H_2 reaction under atmospheric pressure. The dependences of the reaction rates on pretreatment conditions and reaction temperatures are also reported [375]. Mechanisms of ethanol formation *via* CO insertion in a methyl-metal bond or in a methoxy group have been described by Deluzarche *et al.* [376] with regard to the results of Takeuchi and Katzer (1982) concerning the isotopic repartition of ^{13}C and ^{18}O in the ethanol formed from a mixture of $^{13}C^{16}O$ and $^{12}C^{18}O$. The reaction was carried out on a Rh/TiO_2 catalyst.

High-resolution transmission electron microscopy, *in situ* ferromagnetic resonance studies, and a scanning Auger surface analysis have afforded an insight into the intimate details of the Ni-TiO_2 interaction. The combined results of these studies have led to the development of a model that involves the migration of Ti-O moieties onto the surface of the Ni particles during reduction in hydrogen [377]. Pejryd [378] has carried out a solid state emf study of the equilibria (4) and (5) at 1020-1520K by measuring the equilibrium

$$Ni(s) + TiO_2(s) + 1/2\ O_2(g) \longleftrightarrow NiTiO_3(s) \qquad (4)$$

$$Ni(s) + 1/2\ O_2(g) \longleftrightarrow NiO(s) \qquad (5)$$

oxygen partial pressures with an oxygen concentration cell. The dependence of room-temperature hydrogen production from liquid methanol or propanol on the degree of reduction of Ni and the Ni content of UV-illuminated (≥ 297 nm) Ni/TiO_2 catalysts was recently examined [379]. The optimum rate of hydrogen production from methanol occurs at approx. 5% Ni content. The Fischer-Tropsch synthesis over nickel supported on TiO_2, Al_2O_3 or SiO_2 yields CH_4 regardless of the H/CO ratio. For Ni-Ti on the same supports, C_1-C_5 hydrocarbons are

produced [380]. Raupp and Dumesic [381] have suggested that the apparent suppression of CO and H_2 adsorption typically observed at 300K for TiO_2-supported Group VIII catalysts (e.g., Ni/TiO_2) may be due to the existence of TiO_2 species on the surfaces of the metal particles. For the catalyst prepared *via* deposition of a submonolayer amount of titanium and subsequent oxidation *in situ* on a polycrystalline Ni foil in ultrahigh vacuum, the activation energy for CO desorption is significantly reduced by the presence of TiO_2 surface species. Kao [382] has reviewed the surface properties and carbon monoxide hdyrogenation activities of Ni/TiO_2. The adsorption and catalytic behavior of mixtures of 7.0% Ni/TiO_2 and 0.6% Pt/TiO_2 have been investigated [383]. Turnover frequencies based on oxygen adsorption remain constant, while activity per gram of metal and turnover frequencies based on hydrogen adsorption are 1.5 - 2.5 times greater in the mixtures. The results are thought to be consistent with a model that attributes the higher activity to a strong metal-support interaction effect which changes the intrinsic properties of the nickel crystallites [383]. Chung and coworkers [384, 385] have studied the catalytic CO hydrogenation reaction over several differently prepared $Ni/TiO_2(100)$ and $Ni/TiO_2(111)$ model catalysts at 463K, P_H = 60 Torr and P_{CO} = 20 Torr. On the basis of their results, a model was proposed for strong metal-support interaction in which the presence of TiO_2 on the metal surface, induced by high-temperature treatment, and the possible incorporation of surface or subsurface hydrogen act synergistically to modify and maintain the activity of TiO_2-supported catalysts [384]. Auger and vibrational spectroscopy provided evidence for the segregation of TiO_x ($x \approx 1$) on nickel and its effects on carbon monoxide chemisorption. Both physical coverage of the Ni surface by TiO_x and the chemical interaction between Ni and TiO_x on the surface are involved in the strong metal-support interaction [385].

An XPS study of palladium particles dispersed on TiO_2 substrates indicates a positive shift of the Pd $3d_{5/2}$ core level binding energy, reaching approx. 0.8 eV at high dispersion. Possible mechanisms for the observed

energy shifts were discussed [386]. High-resolution transmission electron microscopy and hydrogen chemisorption measurements elucidated the sintering behavior of Pd supported on TiO_2 and on Al_2O_3 following reduction at ≤1073K. The anomalous behavior of Pd/TiO_2 was rationalized in terms of a model in which reduction of TiO_2 to Ti_4O_7 leads to the simultaneous formation of mobile titanium suboxides; these are free to migrate onto the metal particle surface [387]. The surface of amorphous TiO_2 is capable of stabilizing a high concentration of O_2^- when annealed at <823K. When Pd is supported on porous TiO_2 glass, reaction with H_2 at room temperature and low pressures produces paramagnetic Ti^{3+} centers, with concomitant destruction of O_2^- [388]. Carturan and coworkers [389] have prepared supports for glass-titania-palladium catalysts in the hydrogenation of olefins. Glass beads (38- 75 μ in diameter) were contacted with a degassed $Ti(OBu)_4$ solution in ethanol, air-dried, and heated to 673K. Addition of Pd was made by immersing the TiO_2-coated beads in a pentane solution of $Pd(C_3H_5)_2$, reducing with hydrogen, and drying at reduced pressure. The TiO_2 layer contains surface OH groups and promotes Pd dispersion.

SCF-X_α-SW molecular orbital calculations indicate that the Pt metal-TiO_2 support interaction is such that no metal-metal bonding occurs. The calculations showed that the $(TiO_6)^{8-}$ configuration reproduces acceptably the electronic properties of TiO_2. Calculations for the $(Pt/TiO_6)^{8-}$ model show a strong repulsion between the Pt atom and the adjacent oxygen ions, thus making it improbable that Pt is able to approach sufficiently near the $(TiO_6)^{8-}$ configuration for metal-metal bonding to occur, even though there is some bonding between the Ti-3d and Pt-5d orbitals [390]. Henrick [391] has published a polemic to show that the cluster calculations of J.A. Horsley [392] do not represent the interaction of Pt atoms with Ti^{3+} species at oxygen ion vacancy sites on the TiO_2 surface, and thus cannot explain localized charge transfer in strong metal-support interaction. A subsequent reply by Horsley [393] has also appeared.

A thermal desorption spectroscopic study of the adsorption of D_2 on

Pt/TiO_2 powders reveals two thermally activated states in addition to chemisorption on Pt. The activated states were attributed to spillover states on the oxide. One state was ascribed to spillover on a special oxide site, possibly TiO_x associated with the Pt metal [394]. Sequential dosing of H_2 and D_2 on Pt/TiO_2 followed by thermal desorption into vacuum yields incomplete isotope mixing of the desorbing products and provides evidence for the spillover of hydrogen and/or deuterium from the Pt onto the oxide [395]. High-temperature oxidation confirms the presence of an intermediate state in the spillover mechanism. Oxygen titration experiments, coupled with the desorption of sequentially dosed isotopes, indicate that desorption of spillover deuterium proceeds by a mechanism involving surface migration back to Pt sites rather than recombination and desorption directly from the oxide [396]. Oxygen isotope exchange experiments on neat TiO_2 and on Pt/TiO_2 containing 0.5, 5 or 10 wt. % Pt gave the following results: i) on increasing the Pt content, the isotope exchange rate decreases for pre-oxidized samples; ii) homogeneity of surface oxygen is decreased by the Pt deposits for oxide surfaces with a slightly reduced stoichiometry, but remains unaffected for pre-oxidized surfaces [397].

The reducibility of Pt on TiO_2 and γ-Al_2O_3 has been examined by temperature-programmed reduction. Reduction of Pt/TiO_2 leads to metal-assisted reduction of the support. Below 500K only a small part of the support is reversibly reduced in the near vicinity of the metal particles; above 500K further metal-assisted reduction of the TiO_2 support occurs, likely promoted by increased ion mobility [398]. Catalysts consisting of Pt films on oxidized titanium have been studied by secondary ion mass spectroscopic methods to determine their temperature-dependent structural characteristics. Encapsulation of the metal overlayers by the support material was observed and correlated with thermal desorption spectra. The encapsulation and electronic interactions occur simultaneously to alter the behavior of these catalysts [399]. For TiO_2 supported metal catalysts which are reduced at temperatures

greater than 1015K, a shielding of the metal particles from gases is observed and attributed to a phase transformation of anatase to rutile with a concurrent encapsulation of the metal particles [400]. An x-ray photoelectron spectral (XPS) investigation of Pt and Rh supported on TiO_2 and γ-Al_2O_3 shows that: i) for Pt/TiO_2 pre-reduced at less than 1015K, slightly higher binding energies occur than for Pt/Al_2O_3; ii) for M/TiO_2 samples pre-reduced at greater than 1015K, an increase in binding energy of the metal core levels occurs in combination with a decrease in the dispersion of the metal. The behavior was explained [401] by encapsulation and spalling of the metal particles during an observed anatase → rutile phase transformation. Sungbom and coworkers [402] have performed an XPS study of the platinum species photodeposited on TiO_2 from aqueous H_2PtCl_6 in the presence and absence of an acetic acid/sodium acetate buffer. Two Pt/TiO_2(anatase) catalysts prepared by different methods have been characterized by XPS, electron microscopy and cyclic voltammetry [403]. Various samples of TiO_2 and Pt/TiO_2 were investigated by x-ray diffraction before and after hydrogen or vacuum treatment at elevated temperatures. The appearance of a Pt_3Ti x-ray diffraction pattern seemed relevant to the strong metal-support interaction on the Pt/TiO_2 catalyst [404].

The chemisorption of hydrogen, carbon monoxide, and oxygen on Pt/TiO_2 was studied in order to develop a technique for measuring Pt dispersion on TiO_2. Hydrogen adsorption was found to be the most satisfactory technique to measure dispersion subsequent to the destruction of the metal-support interaction [405]. The extent of isothermal chemisorption of hydrogen, carbon monoxide and oxygen on the surfaces of Pt crystallites supported on TiO_2, SiO_2, Al_2O_3, MoO_3 and sodium tungsten bronzes has been measured at 77-523K and 0-5 kPa. Under these conditions, the extent of adsorption (q, in μmole per gram) rarely reaches a saturation value (q_{max}) and in general the gradient dq/dp is affected by Pt dispersion, surface area, nature of the support and of the adsorbate, pressure, and temperature [406]. Surface area measurements have been made for titanium deposited on ultra-high purity Pt particles which were subsequently oxidized

and reduced. The results from BET and H_2- and CO-adsorption measurements argue against morphological changes and alteration of the Pt Fermi level by electron transfer to explain the behavior, but do support a model of special active sites existing at the Pt-TiO_2 interface [407]. Hong and Chen [408] have determined the effect of Nb_2O_5 dopant on the electrical conductivity of a Pt/TiO_2 metal-semiconductor catalyst under H_2 and CO atmospheres. The effect was attributed to the impurity level of the donor impurity Nb_2O_5. A strong interaction between Pt and the TiO_2 support has been observed in a reductive high-temperature treatment, that produces an increase in the catalytic activity as a result of a decrease in CO coverage of the active Pt surface [409]. The frequency shift of the infrared absorption band of adsorbed CO was the probe used to monitor the oxidation state of platinized TiO_2(anatase) photocatalysts [410].

The electrochemical reduction of CO_2 at platinized and non-platinized TiO_2 film electrodes has been examined by cyclic voltammetry. CO_2 undergoes strong, irreversible adsorption on the Pt/TiO_2 surface and results in the formation of an electrochemically detectable species. The reduction of adsorbed CO_2 at the Pt/TiO_2 electrode produces two kinds of reduced species, whose existence was explained in terms of surface diffusion of the reaction intermediates and/or products between adsorption sites at Pt and at TiO_2 [411]. An AES and XPS study of the adsorption of CO_2 on TiO_2 and Pt/TiO_2 was carried out by Tanaka et al. [412]. The C 1s XP spectrum exhibits six different species, assigned to graphite C, HCO_3^-, CO_3^{2-}, adsorbed CO_2, TiC on TiO_2, and adsorbed CO on Pt.

The preparation of a photocatalyst from TiO_2 particles loaded with 0.7% Pt and coated with a film of poly(vinylpyridine) supporting zinc tetraphenylporphyrin has been reported; the use of this photocatalyst for the oxidation of SO_2 has been described [413]. The low efficiency (0.07%) of conversion of light to oxidizing power was attributed to light scattering effects in the system.

The photocatalytic hydrogenation of alkynes and alkenes with water over

TiO_2 yields photoproducts formed by hydrogenation accompanied by fission of the reactant C≡C or C=C bond as the major products. Over Pt/TiO_2, a significant enhancement of hydrogenation without bond fission is observed, along with the formation of oxidation products (CO, CO_2). With Pt/TiO_2, a photoelectrochemical process predominates, with the reduction of H^+ on Pt particles and the oxidation by $OH^\cdot$ on TiO_2 bringing about photohydrogenation without bond fission and the formation of oxidation products, respectively [414]. The effect of lignite on the photocatalytic dissociation of water vapor was studied in the presence of platinized TiO_2(rutile) under UV light. In the presence of lignite, H_2/CO_2 mixtures were produced, indicating lignite gasification [415]. The quantum efficiency for the photolysis of water vapor over NaOH-coated Pt/TiO_2 catalysts is reported. The photocatalytic activity depends on the crystal structure and the source of TiO_2, though not on the catalyst preparation method. Various observations were made: i) the activity of anatase is greater than that of rutile irrespective of its source; ii) the activity of anatase is affected by impurities, the degree of crystal growth, and grain size; iii) the activity of rutile is affected only by grain size. A maximum quantum efficiency of 19% was achieved using MCB anatase [416]. There is a hydrogen/deuterium isotope effect for the hydrogen evolution site in photocatalytic processes on Pt/TiO_2. The observed separation factor (5.3 ± 0.5) is similar to that reported for a Pt electrode, but different from that for a TiO_2 electrode. The Pt sites are the reduction site on the catalyst [417].

Group IB

A double-coated TiO_2/Ag/stainless steel (SS) semitextured substrate has been developed for incorporation in an amorphous silicon solar cell. The surface irregularity of the TiO_2/Ag/SS back surface reflector yields an increased short-circuit current density which corresponds to an increase in the solar cell collection efficiency in the longer wavelength region of visible light [418]. X-ray diffraction, TEM, chemisorption of N_2O, H_2 and O_2, and

H_2-titration of adsorbed oxygen have been employed to characterize a catalyst of very small silver crystallites supported on TiO_2 [419]. The influence of the concentration of ionized donors in a TiO_2 electrode on the energy conformity of the Ag^+/Ag redox potential in solution and of the surface states formed in TiO_2 by fine silver particles have been investigated by Strel'tsov et al. [420]. The $TiO_2/Ag/TiO_2$ multilayer configuration forms an optically transparent infrared reflective coating. The deposition of the TiO_2 films from liquid polymer solutions gives substantial advantages over the rf sputtering desorption method [421]. Adsorption of Ag^+ at 10^{-9} to 10^{-8} mol-ion per cm^2 on a TiO_2 film does not cause changes in the spectral distribution of film sensitivity; however, changes are observed for $[Ag^+] > 10^{-8}$ mol-ion per cm^2. The Ag^+ in TiO_2 films containing hexamethylindocarbocyanine iodide serves to create localized electronic states in a forbidden gap of TiO_2 which leads to an increased efficiency of dye spectral sensitization. The Ag^+ ion and dye molecules interact on the TiO_2 surface to form a complex which undergoes a photoinitiated decomposition to form Ag^0 latent image centers [422]. Similar results were obtained by Fujimoto and coworkers [423].

Group IIB

The electrodeposition of Zn/TiO_2 coatings, carried out in a $ZnSO_4/Na_2SO_4/KAl(SO_4)_2$/dextrin bath, was studied with respect to the effects of cathode current density, bath temperature, and agitation intensity in the bath on the properties and composition of the electroplates [424]. The composition and structure of the interface layer between polycrystalline CdSe films and oxidized titanium substrates, used as photoelectrodes, have been examined by transmission electron microscopy and electron diffraction techniques. In samples exhibiting good adhesion of layers, Cd-Ti intermetallic compounds and oxides are found; such compounds are absent in samples with poor adhesion [425].

Group IIIA

Okazaki and coworkers [426] have shown that a ternary oxide having

the atomic ratio Ti/Si/Al = 47.5/47.5/5 exhibits a high catalytic activity for cumene cracking after a surface fluorination using 1 wt. % HF. While the $TiO_2/SiO_2/Al_2O_3$ catalyst slightly promotes methanol conversion (to olefins) when the mixed oxide is prepared by coprecipitation, surface treatment (using CF_3Cl) yields enhanced catalytic activity. The binary oxide catalyst TiO_2/Al_2O_3 is inactive for olefin formation, though TiO_2/Al_2O_3 prepared by coprecipitation and surface-treated with CF_3Cl is active. XPS measurements reveal that fluorine atoms, introduced into mixed metal oxides by fluorination using CF_3Cl, selectively combines with aluminum atoms on the mixed oxides prepared by coprecipitation. The addition of 0.3% TiO_2 to 0.3% Pd/Al_2O_3 yields increased thermal stability and stabilizes the catalytic activity of Pd/Al_2O_3 in the hydrogenation of benzene [427]. The crystallization thermal expansion coefficient, chemical stability toward distilled water, density, and infrared reflection spectra have been determined for MO_2-$Al(PO_3)_3$ (M = Ti, Si, Ge) as a function of MO_2 content ($\leq$ 25 mol %).. The results were discussed in terms of association and degree of polymerization of PO_4 tetrahedra in the glass structure, which depend on the coordination states of Al^{3+} and M^{4+} [428].

Group IVA

Schwiecker [429] has discussed the fabrication of optical multilayers from the dielectric materials TiO_2 and SiO_2 by electron bombardment or by thermal methods. Reflection and transmission curves determined the quality of the multilayers. A study of the interaction between Ti and SiO_2 films at 673-1243K shows that the reaction proceeds in a layer-by-layer manner, and consists of reduction of SiO_2 as a result of the formation of a titanium-rich silicide at the interface. At high temperatures, a titanium-rich oxide forms near the surface [430]. The stability of silane monolayers, synthesized on TiO_2 electrodes during the photoelectrolysis of water at various pH values, has been determined by XPS [431]. In general, silane layers suffer noticeable losses after a Coulomb/cm^2 of charge was passed. Crosslinking the silane layer during synthesis and reacting the electrode a second time effected a

significant improvement in the stability. The most stable silane layer was prepared from $SiCl_4$ capped with Me_2SiCl_2 [431]. Clear, homogeneous, monolithic gels were obtained in the $M_2O/M'O_2/SiO_2/P_2O_5$ system (M = Li, Na, K; M' = Ti, Zr) by a low-temperature chemical polymerization from metal or non-metal alkoxide hydrolysis [432]. The rutile/anatase phase composition of TiO_2 layers in all dielectric multilayer SiO_2/TiO_2 optical coatings has been characterized by Raman spectroscopy [433]. By contrast, XPS was employed to characterize the surface chemical composition of various SiO_2-coated TiO_2 powders [434]. Electrochemical and photoelectrochemical processes occurring in 0.5N K_2SO_4 at the TiO_2/Si heterojunction have been reported by Kulak and Poznyak [435].

Rutherford back scattering, nuclear reaction analysis and x-ray diffraction methods have ascertained the behavior and effect of oxygen on titanium silicide formation in the TiO_2/Si and $Ti/TiO_2/Si$ systems [436]. Diffusion of oxygen toward the surface region occurs during the growth of the silicide layer. When the oxygen concentration in the surface layer exceeds the solubility limit, titanium oxide precipitates and the silicide growth nearly ceases [436]. The same authors [437] have examined the oxygen behavior and its effect on the annealing properties of these two systems. Min'ko and Trunaev [438] have determined the solubility of TiO_2 in silicate melts by an electromotive force method.

The electrochemical characteristics of glasses of the system $Na_2O/K_2O/TiO_2(Ti_2O_3)/SiO_2$ have been investigated using galvanic cells of the type Ag/AgCl/KCl(sat'd)‖solution A/glass/solution/reference electrode [439]. Ichikawa et al. [440] have shown that ethanol yields from the CO/H_2 reaction over Rh/SiO_2 catalysts increase significantly when SiO_2 supports containing Ti, Zr, Hf, Th, V, Nb and Ta oxides are employed. Additionally, increased rates of C_2H_4 hydroformylation to yield EtCHO and PrOH were noted upon addition of zirconium and titanium oxide precursors to the Rh/SiO_2 catalyst. TiO_2 and ZrO_2 promote CO association and CO insertion to form acyl precursors

for the formation of C_2-oxygenated compounds.

The preparation of an improved PbO_2 anode on a titanium substrate (instead of graphite) has been reported by Hine and Yasuda [441]. Titanium was treated in hot 15% oxalic acid, coated with a $RuCl_3/Ti(OBu)_4$/acidified butanol solution and fired in air at 773K for 5 minutes. Some oxidation of the interlayer and/or titanium was observed during the electrodeposition of PbO_2.

Group VA

Homogeneously mixed fine powders of the TiO_2-P_2O_3 system have been prepared by wet chemistry from titanium alkoxides and H_3PO_4 in an ethanol solution, and by rapid drying with the Heiss Petroleum Trocknung (HPT) method [442]. The reaction between the components and the homogeneity of chemical compositions in the powder and its sintering were characterized by infrared absorption spectroscopy, thermogravimetry-DTA, dilatometry, x-ray diffraction and SEM imagry after heat treatment (523-1273K) [442]. DTA, chemical analysis, infrared spectroscopy, and x-ray phase analysis were used to characterize phases in the TiO_2-H_3PO_4 system at 463-523K, from which the compound TiP_2O_7 was identified [443]. PCl_5 reacts with γ-Al_2O_3 at 373K to yield $AlCl_3$ and $POCl_3$, while TiO_2 reacts with PCl_5 in $POCl_3$ in a 2:1 and 6:1 ratio to give $TiCl_4$ and $[PCl_4][TiCl_5]$, respectively [444]. Also, TiO_2 reacts with S_2Cl_2 and chlorine to produce $TiCl_4$ and $[SCl_3][TiCl_5]$.

Lanthanum Series

The hydrothermal preparation and characterization (x-ray diffraction, infrared spectra, thermal analysis) of 1.5 $Na_2O/Ln_2O_3/5$ TiO_2 (Ln = La, Nd, Sm, Gd, Tb, Dy, Er, Yb) have been reported by Zaginaichenko and coworkers [445]. The compounds for which Ln = La, Nd, Sm amd Gd possess a cubic perovskite-type structure, while the other compounds are less symmetrical. A series of phases has been synthesized by ceramic methods in the M_2O_3-TiO_2 systems (M = Nd, Pr, La) at 1473-1623K. The most probable composition is believed to be

$M_4Ti_9O_{24}$, as obtained from composition analysis and density determinations. An x-ray diffraction study of the compounds $M_4Ti_9O_{24}$ shows they are orthorhombic, space group 'Fddd' [446]. TiO_2/Nd_2O_3 (0.25 mol%) systems have been prepared *via* thermal decomposition of the coprecipitated hydroxides, followed by annealing at 673, 873 and 1013K. The effect of Nd_2O_3 on the structure change in TiO_2 has also been examined. The anatase → rutile transition is inhibited by Nd_2O_3 [447]. Phase equilibria in the Eu_2O_3/TiO_2 system have been studied at 1670-2600K in air by DTA and x-ray phase analysis [448]. The compound Eu_2TiO_5 incongruently melts at 2090 ± 15K and undergoes a polymorphic transition at 1970 ± 15K; while the compound $Eu_2Ti_2O_7$ congruently melts at 2110 ± 25K.

4.8 INTERMETALLIC COMPOUNDS

Results obtained from specific heat determinations of several alloys with $TiAl_3$-type structures have been discussed in terms of theoretical calculations of band structure and stability of the ordered alloys [449]. Interactions between titanium films and boron-implanted silicon substrates at 923K reveal the formation of significant amounts of intermediate silicide phases (TiSi and Ti_5Si_3), and thus a higher sheet resistance. Annealing at ≥ 973K results in conversion of the titanium film into predominantly $TiSi_2$, with a lower sheet resistance. Boron accumulates on the surface as a consequence of redistribution into the silicide layer during annealing [450]. Profound ambient gas effects have been observed [451] on the reaction of titanium with silicon. After the start of reduction of interfacial oxides, the initial stage proceeds rapidly, the extent of which depends on the nature of the titanium-gas interaction. The final stage commences upon interference of the silicide phase and the ambient species, with the rate depending on the nature of the latter.

The effect of thermal activation for hydrogen absorption on the surface of FeTi has been investigated employing i) transmission and reflection

electron diffraction to study structural changes, and ii) magnetization to re-examine the magnetic evidence for surface segregation of elemental iron [452]. Several oxides of iron and titanium were observed on the FeTi surface following activation. The role of these surface oxides is important in the activation and inhibition of hydrogen absorption in FeTi [452]. The hydriding kinetics of FeTi were studied before and after complete activation. Those specimens exposed to the air could be reactivated at 291K without heat treatment. The kinetics reveal an initial slow reaction rate due to the presence of an oxide film on the FeTi surface. Reaction rate enhancement was observed upon compacting the FeTi powder with aluminum or manganese powders, which react with the oxide adsorbed on the FeTi surface. During the activation heat treatment, the oxide film is broken down and new catalytic FeTi surface sites are exposed [453]. Laboratory-scale experiments with granulated FeTi show that fluidized bed reactors are superior to stationary bed reactors for hydrogen absorption-desorption cycles. This conclusion was based on observations i) of easier cooling of fluidized bed during hydrogen absorption, ii) of a faster rate of hydrogen absorption in the fluidized bed, and iii) of the absence of FeTi sintering and reactor deformation due to hot spots with the fluidized bed [454].

A three-terminal capacitance method has been used to measure the temperature dependence of forced volumetric magnetostriction $\delta\omega/\delta H$ for $Ni_{1-x}Ti_x$ ($x \leq 0.1$). At ~8 at. % Ti-Ni, the value of $\delta\omega/\delta H$ changes from positive to negative with increasing temperature. Thermodynamic and Kornetzki-Kouvel relationships were used to determine the pressure coefficients $\delta \ln\mu/\delta p$ and $\delta \ln T_c/\delta p$ [455]. NiTi and $NiTi_2$ have been prepared by a coprecipitation, reduction, and diffusion treatment, and the electrode potential-time relations determined [456]. Electrical resistivities, lattice parameters, Curie temperatures and spin-disorder resistivities were reported for Co_2Ti_{1-x} ($x = 0, +0.25, -0.25$) [457]. Bardi and coworkers [458] have studied the surface properties of the ordered Pt_3Ti because of the changes in

the catalytic behavior of Pt in the presence of Ti in the reduction of oxygen to H_2O in acid fuel cells. Common electroless plating and electroplating baths have been used in the plating of titanium and its alloys, with particular attention paid to surface activation prior to plating. With titanium alloys, the laser phase is dissolved and the surface topography generated by activation depends on the alloy and on its heat treatment condition [459].

A rotating disk anode of titanium alloy VT 1-0 (2.6 mm in diameter) was used to investigate the effect of the anode potential on the electrical resistance and capacitance of the surface film on titanium and on the current density. Based on increasing the localization of the titanium machining process, the recommended electrolytes include i) NaCl 50 g/L + $Na_2Cr_2O_7 \cdot 2H_2O$ 35 g/L and ii) NaCl 50 g/L + $Na_2Cr_2O_7 \cdot 2H_2O$ 35 g/L + LiCl 10 g/L. Under these conditions, a sharp change in surface film properties (resistance and capacitance) is observed, resulting in changes in current densities and current efficiencies as well [460]. Corrosion properties of Ti (VT 1-0) have been studied by several groups. Sedenkov and coworkers [461] have investigated the corrosion resistance of technically pure Ti (VT 1-0) in a system composed of HNO_3/chloride/fluoride, and found that after 200 hours the samples are covered with pits. The pitting corrosion potentials of Ti (VT 1-0) alloys were determined in hot (≤ 413K) concentrated chloride solutions (25% KCl, 40% LiCl, 25% NH_4Cl, 40% $CaCl_2$, 30% $MgCl_2$, 30% $NiCl_2$) [462]. Several corrosion inhibitors (e.g., benzotriazole, 2-mercaptobenzotriazole, citric acid, sodium hexametaphosphate, sulfosalicylic acid, dicyclohexylammonium nitrate, lithium chromate, ferrous oxalate, lithium molybdate, lithium hydroxide) were tested for various metal alloys, including Ti (VT 1-0) which was observed to be the most resistant alloy [463].

4.9 TITANIUM ELECTRODES

Koyanagi [464] has briefly reviewed the properties and applications of noble metal-electroplated titanium electrodes. The influence of the manganese ion (0.1-0.5 ppm) on the current efficiency has been investigated in the direct

electrolysis of seawater on titanium electrodes coated with noble metals and their oxides. The anodes studied include Ti coated with Pt, Pt black, IrO_2/Pt, IrO_2, and PdO/Pt. The coated anodes were subsequently coated with various thicknesses of MnO_2 by electrodeposition, and the active chlorine concentration in seawater was measured following electrolysis. The PdO/Pt-coated electrode exhibits a high initial current efficiency and is minimally influenced by manganese [465]. The electrode reaction 6 has been studied on Ti, Nb and Ta

$$MnO_4^- + 3e^- + 4\,H^+ \rightleftharpoons MnO_2 + 2\,H_2O \qquad (6)$$

planar electrodes. During the reduction of MnO_4^-, control of the process alters from electrochemical to limitations mixed with diffusion in the solid phase [466].

The behavior of mechanically-polished and/or anodically polarized Ti electrodes at low positive potentials at pH 0.3 and 11.0 was investigated. The oxide electroformation potential on a mechanically-polished electrode exhibits a complex dependence on bulk solution pH, possibly due to hydroxy complex formation on the titanium oxide surface [467]. The addition of a second, more inert oxide (ZrO_2) to an active RuO_2 layer on a Ti anode substantially increases the service life of the anode with respect to oxygen evolution in 6M NaOH. Optimum service life (approx. 200 Hrs.) obtains for an 80/20 (RuO_2/ZrO_2) mol% oxide mixture. The increased stability was attributed [468] to better protection of the base metal attack on the ZrO_2.

A study of the kinetics of evolution and ionization of chlorine on a Ti electrode coated with nickel cobaltite has been carried out by constructing steady-state polarization curves. On the spinel $NiCo_2O_4$, a three-stage mechanism of discharge and ionization of chlorine occurs with the first fast electrochemical step occurring with the detachment of a proton [469]. The effect of Cl^-, Br^- and I^- on the hydrogen evolution overvoltage on Ti (VT 1-00) in 0.5M H_2SO_4 has been studied for various electrode surface treatments (electrochemical polishing, HF + HNO_3 etching, HF etching followed by rinsing

with water). The magnitude of the change in hydrogen overvoltage on a Ti electrode during halide ion adsorption depends significantly on the conditions of electrode surface preparation [470]. The behavior of activated Ti electrodes in mercury electrolytic cells were investigated with respect to mode of activation: etching, and coating with ruthenium and titanium chloride solutions and annealing in air to yield a RuO_2 and TiO_2 surface layer. The good quality of these activated anodes were characterized by industrial studies at various current density values, with protection against short-circuiting and various thicknesses of the active layer [471].

4.10 CORROSION

The weight loss method was employed to determine corrosion losses of the titanium alloy VT 1-0 at 293 and 313K in 2M H_2SO_4 with F^- addition. The VT 1-0 alloy is very corrosion-resistant upon addition of 0.070M Fe(III) and 0.20M Al(III) [472]. Gravimetric and electrochemical techniques have been used to study the corrosion behavior of titanium in air at 593-813K in a molten system composed of 55 wt.% $ZnSO_4$, 25 wt.% KCl and 20 wt.% NaCl. The corrosion in a sulfate-chloride melt occurs with mixed anodic-cathodic control [473]. A study of the corrosion of Ti, Mo, and W in a fused sulfate-chloride electrolyte has also been reported [474]. Krapivkina [475] has found that Ti (VT 1-0) possesses a high corrosion resistance in media containing NH_4SCN and thiourea at 293-533K, when compared to various stainless steel samples. Polarization curves have been obtained for Ti (VT 1-0) in $ZrOCl_2$ solutions at 291-343K [476]. In this medium, Ti has a high corrosion resistance, and a corrosion potential of -175 mV (vs -500 mV in HCl).

The corrosion characteristics of the local dissolution of titanium in concentrated chloride solutions has been studied by Ruskol [477], who has also determined the pitting corrosion of Ti in $CaCl_2$ solutions [478]. Titanium is commonly employed in chloride-saturated NaCl solutions. The corrosion failure mechanism, conditions for inhibition of hydrogen absorption, and the corrosion of Ti due to oxygen-chlorine compound build-up in such media have been

elucidated *via* cathodic polarization methods [479]. The steady-state potential of Ti has been determined in $CaCl_2$, $SrCl_2$ and $BaCl_2$ melts (*vs* a chlorine reference electrode) at 1073-1373K in an argon atmosphere to explain the effect of the nature of the cation (Ca, Sr, Ba) on the corrosion behavior of Ti. With increasing temperature and decreasing cation radius, the steady-state potentials became more positive [480]. The corrosion behavior of Ti coupled to stainless AISI 304, Monel and Inconel materials in methanol containing 0.4% HCl has been elucidated. In the absence of coupling to these materials, the Ti corrosion rate is very low. Upon coupling, the corrosion rate increases dramatically [481].

Tungusova and coworkers [482] have elucidated the characteristics of corrosion and the electrochemical behavior of titanium in solutions of ammonium and potassium fluorides. Similar studies were performed on the behavior of Ti in NH_4HF_2 and KHF_2 solutions ($\leq$ 5M) at 293K. In KHF_2 media containing Na^+, the corrosion of Ti decreases monotonically with increasing salt concentration. In concentrated NH_4HF_2 solutions, the addition of NaF activates the corrosion process, apparently caused by the formation of a mixed-salt film on the metal surface [483]. Gerasyutina *et al.* [484] have determined the influence of tropeolins O, OO and OOO indicators on the corrosion rate and polarization of Ti (VT 1-1) in 5N H_2SO_4 and 5N HCl. The tropeolins apparently provide a 94-99.8% protective effect for Ti at 293-353K at comparatively low concentrations (0.5-10 mmol/L). The application of an external current in electrochemical production processes has been investigated as a means of protecting titanium from corrosion [485]. Also, the corrosion resistance of titanium parts of a membrane bipolar electrolytic cell has been studied by Balitskii and coworkers [486].

4.11 TITANIUM MELTS

The electrode reaction mechanisms and diffusion rates of metal ions deposited on a cathode are important factors in metal electrowinning and electrorefining in order to determine the maximum allowable values of electrode

current density, the electrocrystallization nature of the cathodic deposits and the purity of the resulting metal. Makarov and Balikhin [487] have investigated the behavior of Ti ions in low melting salt mixtures based on chlorides of potassium, magnesium and lithium, which enables one to perform electrolytic refining of titanium at 773K. The same authors utilized a method of continuous plotting of polarization curves with linear scanning of potential to elucidate the cathodic process during electrorefining and production of titanium in KCl-NaCl, KCl-LiCl and KCl-$MgCl_2$ electrolytes [488]. Chronopotentiometry and linear sweep voltammetry were used to study the electrode reaction steps of Ti(III) and Ti(II) in NaCl-KCl and LiCl-KCl eutectic melts. Diffusion activation energies have been determined from diffusion coefficient data at various temperatures; and the effects of temperature on Ti electrocrystallization was discussed [489]. The effect of decreasing the strength of the chlorotitanate complexes formed in melts on the diffusion coefficient of titanium has been examined by chronogalvanometric methods. The optimum electrolytic conditions for this study consist of a mixture containing 38-42 mol% $MgCl_2$/KCl, which melts at a sufficiently low temperature and yields a high limiting diffusion current value at low temperatures [490].

A study of the potential dependence of graphite and some metal anodes on the current density in different melts containing titanium chloride (NaCl/KCl/$MgCl_2$/$TiCl_3$/$TiCl_2$) has been carried out by Voleinik and coworkers [491], and the electrochemical corrosion of titanium in alkaline earth chloride melts has been investigated [492].

The discharge of titanium and zirconium from chloride-fluoride melts at 983K has been characterized by chronovoltammetry. The ratio of Ti and Zr in the cathodic deposits depends on the concentrations of K_2ZrF_6 and of K_2TiF_6 in the melt; as well, this ratio can be altered by using F^- to control the basicity of the melt [493]. Barannik and coworkers [494, 495] have studied the reaction of air with $TiCl_2$ and $TiCl_3$ dissolved in NaCl-KCl melts containing

varying amounts of $MgCl_2$ and Mg. The Ti concentration in the melt decreases more rapidly when the melt is in contact with air, in contrast to contact with argon or an air/argon mixture, and when $MgCl_2$ is present.

Claims have been made regarding the desirability of molten salt anodizing in anhydrous media. However, recent results on the anodization of Ti, Al, Nb, W and Mo samples in a low-melting urea-NH_4NO_3 eutectic at 318-358K reveals that H_2O seems to be a necessary electrolyte component, by influencing the oxide growth process and breakdown voltage [496].

4.12 COORDINATION COMPLEXES OF TITANIUM

a. CYCLOPENTADIENYL COMPLEXES

The crystal and molecular structure of the bimetallic complex $[(\eta^5\text{-}C_5H_5)_2Ti(\mu\text{-}H)_2Al(H)_2]_2(CH_3)_2NCH_2CH_2N(CH_3)_2 \cdot C_6H_6$ is illustrated in Figure 7. The complex is triclinic, space group $P\bar{1}$, wherein the two $Cp_2TiH_2AlH_2$

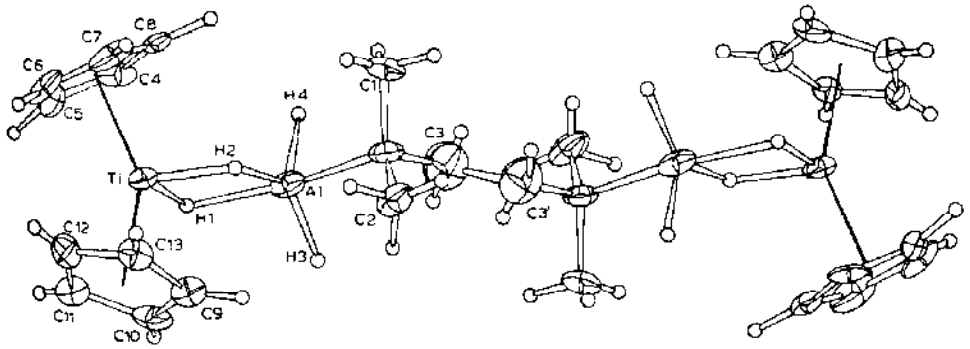

FIGURE 7: General view of $(Cp_2TiAlH_4)_2(CH_3)_2NCH_2CH_2N(CH_3)_2$. Thermal ellipsoids are shown for P = 0.3 [497].

moieties are linked by a tetramethylethylenediamine molecule. The Al atom is bonded to the Ti atom by a double hydrogen bridge, and has trigonal bipyramidal stereochemistry [497]. Aromatic aldehydes are known to be coupled by $[Ti(Cp)_2(CO)_2]$ to produce pinacols and olefins in good yield. In contrast, aliphatic aldehydes react to give primarily the corresponding alcohols, while aromatic ketones produce a mixture of products.. Scheme I depicts a reasonable reaction course which can account for the observed products [498]. The

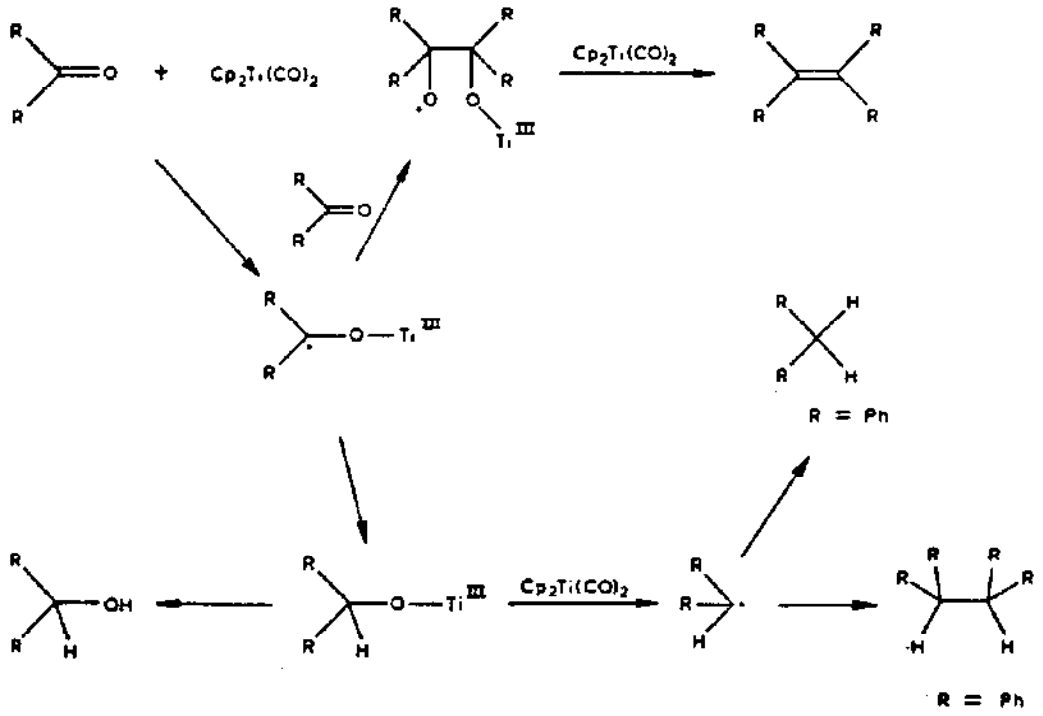

SCHEME I

Grignard reaction of BuMgBr, n-$C_{11}H_{23}COCl$ (lauroyl chloride) and $[Ti(Cp)_2(Cl)_2]$ in diethyl ether at room temperature produces lauryl alcohol in 58% yield. A similar reaction with ethyl laurate at 273K yields 60% lauryl alcohol, while reaction in refluxing diethyl ether gives 72% lauryl alcohol [499]. The titanium complex prepared from $[Ti(Cp)_2(Cl)_2]$ and $NaBH_4$ in THF in the presence of crown ethers efficiently promotes the catalytic hydroboration of alkenes, styrenes and alkynes with $NaBH_4$ to yield sodium alkyl- and alkenyl-borohydrides; these are converted into alcohols, phenylalkanols and alkenes, respectively [500].

b. OTHER COMPLEXES

Krasochka and coworkers [501] have elucidated the structure of bis(benzene)titanium(0), BBT, and bis(toluene)titanium(0), BTT, via x-ray diffractometry. BBT is triclinic, space group $P\bar{1}$, while BTT is rhombohedral, space group Pbca. Both complexes possess a sandwich structure. The Extended Huckel MO method was employed to determine the electronic structures of BBT and BTT, for which the calculated metal-ligand and ligand-metal charge transfer transitions agree well with experimental absorption spectral data. The electronic spectra of the distorted octahedral complexes $[Ti(Cl)_3(THF)_3]$, $[Ti(Cl)_3(THF)_2(CH_3CN)]$ and $[Ti(Cl)_3(CH_3CN)_3]$ have been interpreted employing the angular overlap model using the transferability assumption for the single ligand parameters. A determination of the σ and π bonding parameters e_λ for the Ti(III)-ligand bonds has led to a two dimensional spectrochemical series; e_σ: Cl < C_4H_8O (THF) < CH_3CN and e_π: CH_3CN < C_4H_8O < Cl [502]. The heterogeneous catalyst $[Ti(PhCH_2)_4]/TiCl_4$ has been developed for the polymerization of ethylene. Other main group and transition metal chlorides were substituted for $TiCl_4$; excess $AlCl_3$ or $MgCl_2$ and $[Ti(PhCH_2)_4]$ also yield polymerization catalysts [503].

Reaction between $TiCl_4$ and the N-benzylidene-N',N'-dimethylethylene-diamines, L = $RC_6H_4CH{=}NCH_2CH_2NMe_2$ (R = H, 2-Cl, 4-Cl, 2-MeO, 4-MeO, 4-Me), gives $TiCl_4L$ complexes which have been characterized by elemental analysis,

electrical conductivity, and infrared and proton nmr spectroscopy. The ligand L is bidentate towards titanium [504]. An XPS investigation of the titatrane complexes LTiR (H_3L = triethanolamine; R = O-COR'-type substituents, R' = various substituents), using the direct comparison method, has verified the existence of the N→Ti dative bonds. The N_{1s} binding energy of the titatrane complexes are 0.4 to 0.9 eV higher than that of H_3L, and the $Ti_{2p^{3/2}}$ binding energies are lower than that of the corresponding composite materials. In agreement with dative bond formation, there is an increase in the coordination number and a decrease in the inner shell binding energy in the acceptor atom [505]. $TiCl_4$ reacts with $KNPh_2$ in a 1:3 molar ratio in benzene to yield $Ti(NPh_2)_3Cl$. Other N-organyl substituted metal amides have also been prepared, including $Ti(NHPh)_4$ and $Ti(NHPh)_3Cl$ from $TiCl_4$ and NaNHPh, and $Ti(NPh_2)_3CH_2C_6H_5$ from $TiCl_4$ and $C_6H_5CH_2MgCl$ [506].

The photoexcited triplet state of oxotitanium(IV) tetraphenylporphyrin, (TPP)Ti=O, has been investigated by ESR and laser photolysis [507]. At room temperature in ethanol, (TPP)Ti=O is in equilibrium with (TPP)Ti=O(EtOH) in which EtOH is coordinated in an axial position (reaction 7). Laser photolysis

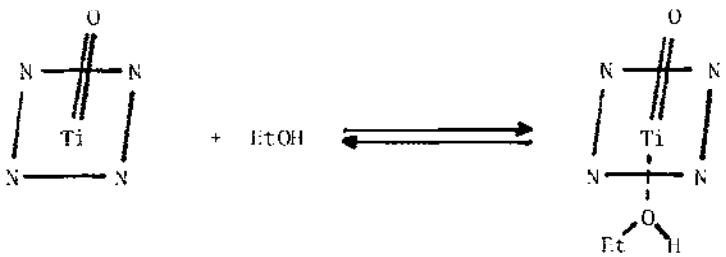

(7)

experiments of (TPP)Ti=O in acidic EtOH solutions at room temperature reveal that the triplet state, $(TPP)Ti=O^{3*}$, is efficiently quenched by protons via a diffusion-controlled process. The quenching mechanism is presumably due to electrophilic protonation (reactions 8-10), where the lifetime of $(TPP)Ti^{+}\text{-}OH^{3*}$ was assumed to be very short as no transient ascribable to this species was observed during proton-induced decay of $(TPP)Ti=O^{3*}$ [507]. Treating $(TPP)Ti^{IV}=O$ with catechol (H_2cat) or 3,4-toluenedithiol (H_2tdt) yields

$$(TPP)Ti{=}O^{3*} + EtOH_2^{+} \longrightarrow (TPP)Ti^{+}\text{-}OH^{3*} + EtOH \quad (8)$$

$$(TPP)Ti^{+}\text{-}OH^{3*} \longrightarrow (TPP)Ti^{+}\text{-}OH \quad (9)$$

$$(TPP)Ti^{+}\text{-}OH + EtOH \longrightarrow (TPP)Ti{=}O + EtOH_2^{+} \quad (10)$$

$(TPP)Ti^{IV}(cat)$ and $(TPP)Ti^{IV}(tdt)$, respectively [508]. Electrochemical reduction of the products results in the formation of the anion radicals $[(TPP)Ti^{IV}(cat)]^{-}$ and $[(TPP)Ti^{IV}(tdt)]^{-}$. The unstable titanium(III) complexes $[(TPP)Ti^{III}(cat)]^{-}$ and $[(TPP)Ti(tdt)]^{-}$ form upon reaction of $(TPP)Ti^{III}F$ with the sodium salt of the chelates. Both reduced catecholato derivatives are transformed into $[(TPP)Ti^{IV}{=}O]^{-}$. A mechanism has been proposed to account for the auto-oxidation of $[(TPP)Ti^{III}(tdt)]^{-}$ to $(TPP)Ti^{IV}{=}O$ and $(TPP)Ti^{IV}(tdt)$ [508]. Chang [509] has recently reviewed some electrochemical and spectroelectrochemical studies of metalloporphyrins containing Ti, Mo, Ni, Fe, and Ru.

The preparation and characterization (x-ray diffraction, magnetic measurements, infrared and electronic spectra, XPS) of $Ti[M(CN)_6]$ (M = Co, Rh, Ir) have been reported. All complexes form a three-dimensional framework of two octahedral coordination units MC_6 and TiN_6. Upon formation of $Ti[M(CN)_6]$ from the corresponding potassium salt, the π back-donation in the $[M(CN)_6]^{3-}$ moiety is enhanced by the bridge formation through the cyanide ligand. The complex is depicted in Figure 8 [510]. $M'Cl_4$ (M' = Ti, Te, Sn, Si) reportedly reacts with $M(H_2L)$ (M = Cu, Ni; H_4L = 3-HO_2C-2-$HOC_6H_3CH{=}NCH_2CH_2N{=}CHC_6H_3$-2-OH-3-$CO_2H$) to yield $MM'Cl_2$; these complexes have been characterized by elemental analysis, electrical conductivity, magnetic measurements, and infrared and electronic spectroscopy. The carboxylate groups coordinate to M' and the nitrogen and phenolic oxygen atoms coordinate to M [511].

Malhotra and coworkers [512] reported the preparation of $Ti(ONp)_nCl_{4-n}$ (NpOH = 2-naphthol; n = 1-4) and $Ti(ONp)_4 \cdot NpOH$ by the reaction of $TiCl_4$ with NpOH in the appropriate molar ratio in benzene under various experimental conditions. Molecular weight and infrared spectroscopic studies of these

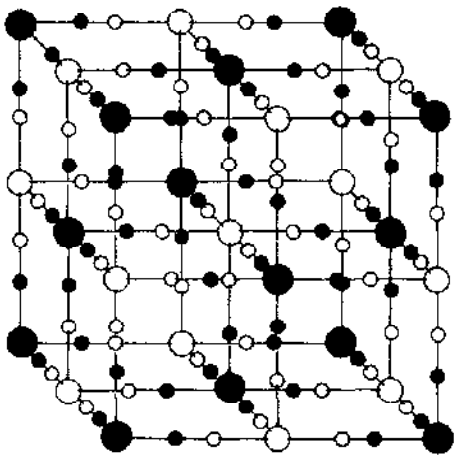

FIGURE 8: Structure of $Ti[M(CN)_6]$. Solid circles, M; large open circles, Ti; small solid circles, C; small open circles, N [511].

titanium(IV) naphthoxide complexes suggest they are dimeric with MpO bridges. Monomeric, nonelectrolytic $TiCl_nL_{4-n}L'_2$ (HL = naphthol; n = 2,3; L' = acetophenone, benzophenone, $CH_3C(O)C_2H_5$) were prepared via reaction of $TiCl_nL_{4-n}$ and L'. The dimeric complexes TiL_4L' result from the reaction between $TiL_4 \cdot HL$ and L' [514]. $TiCl_{4-n}L_n$ (HL = naphthol; n = 1-3) react with various α-hydroxyaldehydes and ketones (HQ = benzoin, 2-hydroxyacetophenone, salicylaldehyde) in the appropriate molar ratio to produce TiL_3Q, TiL_2QCl, TiL_2Q_2, $TiCl_2LQ$, and $TiClLQ_2$. Possible structures for these complexes were presented, based on elemental analyses, conductance, cryoscopic and infrared spectral measurements [514]. Additionally, $TiCl_nL_{4-n}$ (L = 2-naphthol; n = 1-3) react with amine N-oxides to give $TiCl_nL_{4-n}A_2$ (A = pyridine N-oxide, α-, β- and γ-picoline N-oxide) and $TiCl_nL_{4-n}A'$ (A' = 1,10-phenanthrolineN,N'-dioxide, 2,2'-bipyridineN,N'-dioxide). On the other hand, $TiL_4 \cdot HL$ reacts with these amine N-oxides to form $TiL \cdot A_2$ (or $TiL \cdot A'_2$) [515].

The alkoxy chlorotitanium(III) complexes $M(OR)_nCl_{3-n}$ (M = Ti, V; R = Me,

Et, Bu; n = 1,2) have been prepared via reaction of MCl_3 and $HC(OR)_3$ (reaction 11). The reaction mechanism postulated [516] likely involves the six-member

$$TiCl_3 + n\ HC(OR)_3 \longrightarrow Ti(OR)_nCl_{3-n} + n\ RCl + n\ HC(O)OR \quad (n = 1,2) \qquad (11)$$

cyclic intermediate (4). The $Ti(OR)_nCl_{3-n}$ complexes are polymeric probably the

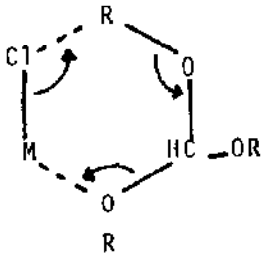

(4)

result of the presence of alkoxide bridges, although chlorine bridges and partial direct metal-metal interaction cannot be ruled out [516]. Chadha and Gupta [517] have demonstrated the strong Lewis acid behavior of $Ti(OR)Cl_3$ and $Ti(OR)_2Cl_2$ (R = Me, Et, C_2H_4Cl, $C_2H_2F_3$) by their formation of 1:2 complexes with DMSO and pyridine, and 1:1 complexes with naphthaldehyde. Whereas the 1:2 complexes have six-coordinate titanium(IV), the corresponding 1:1 complexes are dimeric. Reaction between $Ti(OR)_4$ (R = Et, Pr^i) and AcNCS yields $Ti(OR)_{4-n}(NCS)_n \cdot xAcOEt$ (R = Et, n = 1-3, x = 0; n = 4, x = 1; R = Pr^i, n = 1,2, x = 0). The $Ti(OEt)_{4-n}(NCS)_n$ complexes, for which n = 1 and 2, are dimeric in benzene with bridging ethoxide. In acetone, all of the products are monomeric [518]. $Ti(OR)_4$ (R = Et, Pr^i) reacts with HL (HL = $C_2H_5CH(OH)CH{=}CHCH_3$) in the appropriate molar ratio to give TiL_4. The product was characterized by elemental analysis, molecular weight determination and infrared and nmr spectral studies [519]. Reaction of the $Ti(OPr^i)_4$-NaNp-N_2 system (NaNp = sodium naphthylide) with trans-$Pt(H)Cl(PPh_3)_2$ produces considerable yields of free ammonia. Hydrogen promotes the formation of ammonia [520]. The reduction

of titanium in $Ti(OBu)_4$ by treating it with Et_3Al, Et_2AlCl or $Et_{1.5}AlCl_{1.5}$ has been examined with respect to the effect of temperature, Al:Ti ratio, and duration of the reaction on the kinetics of Ti^{3+} formation [521]. Pilati and coworkers [522] have studied the mechanism of the polycondensation formation of poly(butylene terephthalate) catalysed by $Ti(OBu)_4$. Kinetic equations were derived and discussed employing model molecules, and compared to experimental results obtained at various temperatures and reactant molar ratios. $Ti(OBu)_4$ and aniline serve as catalysts for the esterification of adipic acid and tetrabromophthalic anhydride by 2-ethyl-1-hexanol and 1-octanol. A kinetic study has shown that i) adipic acid is more reactive than tetrabromophthalic anhydride, ii) 2-ethyl-1-hexanol is more reactive than 1-octanol, and iii) $Ti(OBu)_4$ is a more effective catalyst than aniline [523].

The kinetics of styrene polymerization, catalysed by $Ti(OBu)Cl_3$ and $AlEt_3/AlBu^i_3$ cocatalysts in heptane, have been examined. Maximum steady-state rates were achieved at an Al:Ti ratio of 1.5:1, and were first-order in monomer and catalyst. The overall polymerization activation energy (44-46 kJ/mole) is in good agreement with a coordinated anionic mechanism, for which an alkylated $TiBuCl_3$ is thought to be the species affecting the polymerization [524]. The reaction of enol silyl ethers $ROSiMe_3$ [R = CEt=CHMe, $C(C_6H_2Me_3$-2,4,6)=CHMe, cyclohexenyl, methyl-substituted cyclohexenyl] with $TiCl_4$ has produced the trichlorotitanium enolates $ROTiCl_3$, which are unique owing to their relatively electron deficient double bonds. The enolate structure of the products was deduced from ^1H nmr spectra [525].

Chaudhuri and Diebler [526] have employed spectrophotometric and temperature-jump relaxation techniques to study the equilibrium and the kinetics of complex formation of titanium with acetate (Ac^-), monochloroacetate ($ClAc^-$), and dichloroacetate (Cl_2Ac^-) in aqueous media. The kinetic data indicate that at least two reaction pathways contribute to the formation of $TiAc^{2+}$, $Ti(ClAc)^{2+}$ and $Ti(Cl_2Ac)^{2+}$. A strong associative character for the substitution processes at $Ti(H_2O)_6^{3+}$ ions is indicated by increasing second-

order rate constants with ligand basicity. Cation exchange and spectroscopic studies of the complexation of titanium(IV) with oxalic acid as a function of pH and titanium concentration have shown the formation of protonated and polynuclear titanium oxalate complexes. The equilibrium constant for the formation of $Ti(OH)_2(C_2O_4)$ is 34 ± 5, and the stability constant is (1.8 ± 0.3) x 10^6 [527].

A gray-black film forms on the nickel cathode in an electrolysis cell with a platinum anode and a 0.18M $K_2TiO(C_2O_4)_2$ bath. The film is amorphous and contains 50% titanium, though detailed identification was not performed [528]. $PbTiO(C_2O_4)_2 \cdot 4H_2O$ and $Pb(Ti_{1-x}Zr_x)O(C_2O_4)_2 \cdot nH_2O$ (x = 0.5, 0.25) have been prepared and characterized by x-ray diffraction, infrared spectroscopy and thermal analysis. In air or oxygen, the decomposition occurs in three stages: i) dehydration, ii) decomposition of the oxalate to a carbonate, and iii) decomposition of the carbonate to $PbZrO_3$ [529].

The transesterification kinetics of the carboxylic acids RCO_2Bu (R = H, Me, Bu, Me_3C, $CHCl_2$, CCl_3, CH_2Br, CH_2OPh, CH_2CH_2Cl, $CHPh_2$) by sec-butyl orthotitanate have been determined in heptane [530]. The kinetics of the reaction between a titanium(IV) peroxo complex and Fe(II) were examined by spectrophotometric methods at 408 nm and by ESR spectroscopy. The postulated mechanism involves intrasphere electron transfer between Fe(II) and Ti(IV) in a binuclear peroxo bridged intermediate [531].

The synthesis and spectral properties of $TiCl_3(glyH)_3$ (glyH = glycine) have been reported. The complex was characterized by potentiometric curves, chemical analysis, magnetic properties, and infrared and electronic spectroscopy [532]. A green complex with λ_{max} at 710 nm forms upon reaction of a solution (pH = 2) composed of Alizarine S, Ti^{4+} and Ti^{3+} (4:1:10). Neither of the two titanium species alone has an effect on the absorption spectrum of the dye (λ_{max} = 420 nm), although at pH 4 Ti^{4+} forms a 1:2 complex with the dye have λ_{max} at 510 nm. A mechanism in which the Ti^{3+} reduces the dye to its leuco form, catalysed by Ti^{4+}, and the leuco compound forms a complex with Ti^{4+}

and Ti^{3+}, was proposed [533]. Jabs and Gauhe [534] have characterized the titanyl ascorbate complexes $TiOL_2 \cdot 2H_2O$ and $TiO(OH)L$ (HL = L-ascorbic acid) by electronic, infrared and ^1H nmr spectra. Measurements of the H_3O^+ concentration of aqueous solutions of both complexes led to a simple model for describing their protolytic behavior. An analysis and comparison have been made of the exact (Koutecky theory) and approximate (reaction layer theory) equations for describing kinetic polarographic currents. The electroreductions of a Ti(IV) citrate complex and a Ni thiocyanate complex revealed that the exact and approximate solutions lead to similar constants for the rate of formation of the electroactive complex of the metal [535].

Spectrophotometric methods have been employed to study the formation of monocomplexes of Ti(III), Cr(III) and Al(III) with mannose at pH 1.5 and ionic strength 1.0 (NH_4Cl) at 293 ± 1K [536]. Titanium(III) and vanadium(III) acrylate complexes have been cited in the Russian literature [537].

The new titanium(IV) chloroacetate complexes $TiL_2L'_2$ and $Ti(O_2CCCl_3)_4$ [HL = $ClCH_2CO_2H$, HL' = cyclopentadiene, acetylacetone; HL = Cl_2CHCO_2H, HL' = cyclopentadiene, acetylacetone, salicylaldehyde, 2-hydroxyacetophenone, 8-hydroxyquinoline; HL = Cl_3CCO_2H, HL' = cyclopentadiene, salicylaldehyde] were prepared from TiL'_2Cl_2 and NaL. In the $TiL_2L'_2$ complexes (HL' ≠ cyclopentadiene), the acetate groups are monodentate, forming octahedral complexes; in $TiCp_2L_2$, the acetate groups are bidentate [538].

Electrode reaction parameters (k_s, α) have been determined at 298K for Ti(IV) systems (Ti-oxalic acid, Ti-EDTA, Ti-N-(2-hydroxymethyl)EDTA, Ti-CyDTA) and the uranyl ion in acidic solutions. The parameters were determined using approximate equations of current-potential curves derived by Nishihara for the d.c. polarographic catalytic wave. The presence of a large excess of oxidizing agent and a maximum wave on the catalytic waves were found to interfere with the experiments [539].

The preparation and characterization (ESR, nmr and infrared spectra) of the titanium(III) complexes $Ti_2L_2Cl_2$ (H_2L = mandelic acid) have been reported.

These dimeric complexes are formed by the bridging carboxylato groups with the coordination of the deprotonated alcohol group [540]. The semi-synthetic antibiotic organometallic derivatives of 6-aminopenicillanic acid (5) (M = Ti(IV), Zr(IV), Hf(IV), R = Cp, η^5-indenyl) have been prepared and claimed to possess in vitro bactericide activity. Substituents into the penicillin

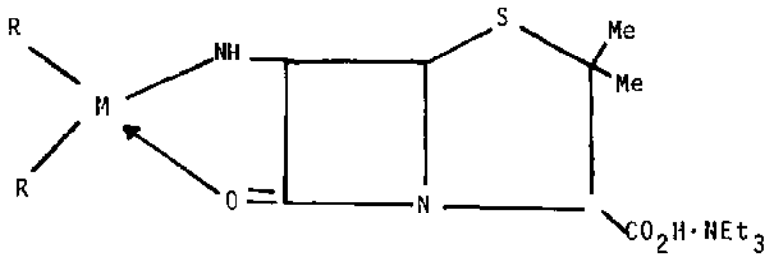

(5)

nucleus effects changes in the antibiotic activity and β-lactamase susceptibility. Infrared, UV and ^1H nmr spectra for the Ti(IV) complex are reported; the complex is biologically active against various drug-resistant bacteria [541].

The solvolysis of $TiCl_n(MeSO_3)_{4-n}$ (n = 1-3) with $Cl_mH_{3-m}CCO_2H$ (m = 1-3) yields $TiL_n(MeSO_3)_{4-n}$ (n = 1-3; HL = $Cl_mH_{3-m}CCO_2H$). Most of these complexes have bridging $MeSO_3$ groups and $Ti[O_6]$ chromophores. $TiL_n(MeSO_3)_{4-n}$ form 1:1 and 1:2 complexes with 2,2'-bipyridine and pyridine, respectively [542].

A spectrophotometric study (190-350 nm) at 298K and ionic strength 3 (NaCl) has revealed the formation of titanium(IV) complexes with protonated pyrophosphate ions, specifically $TiO(H_2P_2O_7)_2^{2-}$ and $TiO(H_2P_2O_7)$. Protonation constants for $H_2P_2O_7^{2-}$ (pH-titration method) are 22.4 M^{-1} and 5.0 M^{-1} for $H_3P_2O_7^-$ and $H_4P_2O_7$, respectively [543]. While Nb and Ta are extracted as $HNbF_6$ and $HTaF_6$ with bis(2-ethylhexyl)phosphate [HDEHP] serving as a neutral

extractant, Ti is extracted in complex form, such as $TiOF(HA_2)$ where HA is HDEHP [544].

The titanium(III) complex $[TiL_2(H_2O)_2]Cl$ (6) {HL = 3-(4-pyridyl)triazoline-5-thione} has been prepared and characterized by infrared and electronic spectra and magnetic moment measurements. The synthesis of (6) involves mixing

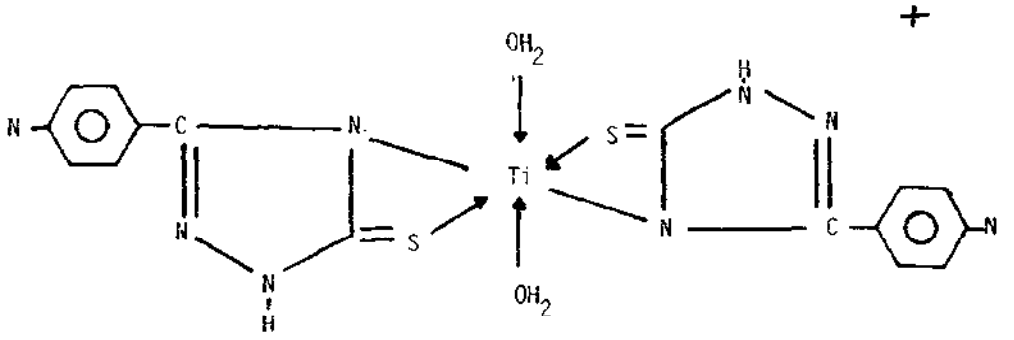

(6)

$TiCl_3$ with the ligand in a 3:1 (Ti:L) molar ratio. The spectral and magnetic moment results have been interpreted in terms of an octahedral structure in which the two H_2O molecules are at trans positions [545].

4.13 ACKNOWLEDGEMENTS

Our work is generously supported by the Natural Sciences and Engineering Research Council of Canada (to NS) and by the Consiglio Nationale delle Ricerche (Roma) through its "Progetto Finalizzato Chimica Fine e Secondaria" (to EP). We are also grateful to NATO for support through Grant No. 543/84.

4.14 REFERENCES

1. To whom correspondence should be addressed at Concordia University.
2. M.A. Jamieson, N. Serpone and E. Pelizzetti, Coord. Chem. Rev., 73 (1986) 175.
3. J.R. Ufford and N. Serpone, Coord. Chem. Rev., 57 (1984) 301.
4. N. Serpone, M.A. Jamieson, F. Disalvio, P.A. Takats, L. Yeretsian and J.R. Ufford, Coord. Chem. Rev., 58 (1984) 87.
5. L.I. Johansson, C.G. Larsson and A. Callenas, Ann. Isr. Phys. Soc., 6 (1984) 321.
6. S. Matsuda and A. Kato, Appl. Catal., 8 (1983) 149.

7. L.I. Krishtalik, Indo-Sov. Jt. Symp. Recent Trends Electrochem. Sci. Technol., 1st 1979 (Pub. 1983), 25.
8. A.A. Berdyshev, Deposited Doc., (1983) VINITI 389-83, 42pp.
9. Y. Fujiki and T. Mitsuhashi, Seramikkusu 19 (1984) 200.
10. J.J. Legendre, R. Moret, E. Tronc and M. Huber, Prog. Cryst. Growth Charact.,(1983) 7(Cryst. Growth Charact. Polytype Struct.) 309.
11. B. Palosz, Phys. Status Solidi A, 80 (1983) 11.
12. Z.A. Foroulis, Acta Cient. Venez., 33 (1982) 351.
13. H.F. Franzen, At. Energy Rev., Spec. Issue, 9 (1983) 371.
14. J.E. Newberry, Annu. Rep. Prog. Chem., Sect. A: Inorg. Chem., 79 (1983) 173.
15. H. Takahashi, Hoshi Yakka Daigaku Kiyo, (1983) 13.
16. P.S. Wang, W.E Moddeman and W.C. Bowling, J. Hazard. Mater., 9 (1984) 103.
17. E. Brauer, B. Streb, H. Baumann, F. Rauch and H. Schwenk, Hydrogene Mater., Congre. Int., 3rd 1 (1982) 155.
18. N.G. Alexandropoulos, G. Boulakis, D. Papadimitriou and I. Theodoridou, Phys. Status Solidi B, 120 (1983) K19.
19. B.I. Bennett, from Energy Research Abstracts, 9 (1984) Abstr. No. 14248.
20. D.G. Musaev and A.I. Boldyrev, Koord. Khim., 10 (1984) 309.
21. D.G. Westlake, Mater. Res. Bull., 18 (1983) 1409.
22. A.K. Filonenko, V.A. Bunin and V.I. Vershinnikov, Khim. Fiz., (1982) 260.
23. V.K. Smolyakov, E.A. Nekrasov and Yu.M. Maksimov, Fiz. Goreniya Vzyva, 20 (1984) 63.
24. B. Champagne, S. Dallaire, A. Adnot, J. Less-Common Met., 98 (1984) L21.
25. Yu.M. Maksimov, A.T. Pak, L.G. Raskolenko and A.A. Zenin, Fiz. Goreniya Vzryva, 20 (1984) 74.
26. A.S. Nechepurenko, B.M. Lepinskikh and E.A. Knyshev, Izv. Akad. Nauk SSSR, Neorg. Mater., 19 (1983) 1837.
27. M.M. Sychev, L.B. Svatovskaya, T.A. Korneeva, A.P. Sizonenko and M.G. Efros, Antikorroz. Pokrytiya, Tr. Vses. Soveshch. Zharostoikim Pokrytiyam, 10th, (1981) Pub. 1983, 18.
28. G.V. Samsonov, T.V. Dubovik, G.V. Trunov, A.N. Toropov and E.V. Sokhovich, Tugoplavkie Nitridy, (1983) 110.
29. J. Bouteillon and A. Marguier, Surf. Technol., 22 (1984) 205.
30. V.M. Danilenko, L.V. Strashinskaya and T.I. Shaposhnikova, Karbidy i Materialy na ikh Osnove, Kiev, (1983) 54.
31. G. Schadler, P. Weinberger, J. Klima and A. Neckel, Solid State Commun., 51 (1984) 35.
32. S.A. Kutolin, S.N. Komarova, Z.G. Alieva and Yu.A. Frolov, Zh. Fiz. Khim., 58 (1984) 139.
33. H. Xiong, Zhongnan Kuangye Xueyuan Xuebao, (1984) 74.
34. R. Konishi and S. Kato, Jpn. J. Appl. Phys., Part 1, 23 (1984) 975.
35. A.M. Chaplanov, Izv. Akad. Nauk SSSR, Ser. Fiz., 48 (1984) 269.
36. M. Schuhmacher and P. Eveno, Solid State Ionics, 12 (1984) 263.
37. A.V. Yuzhanina, G.V. Naumova, L.A. Mashkovich and A.F. Kuteinikov, Konstr. Mater. Osn. Ugleroda, 17 (1983) 79.
38. M. Eizenberg, R. Brener and S.P. Murarka, J. Appl. Phys., 55 (1984) 3799.
39. I.E. Pavlov, Fiz. Khim. Obrab. Mater., (1984) 47.
40. N.V. Alekseev, A.V. Kolesnikov and M.N. Fol'kov, Latv. PSR Zinat. Akad. Vestis, Kim. Ser., (1984) 56.
41. F. Teyssandier, M. Ducarroir and C. Bernard, J. Mater. Sci. Lett., 3 (1984) 355.
42. F. Teyssandier, M. Ducarroir and C. Bernard, CALPHAD: Comput. Coupling Phase Diagrams Thermochem., 8 (1984) 233.
43. I.I. Timofeeva, A.A. Rogozinskaya and A.A. Adamovskii, Tugoplavkie Nitridy, (1983) 154.
44. E.G. Pavlyuk, L.G. Maskhuliya, S.A. Persinin, T.V. Boikova and N.V. Val'yanova, Deposited Doc., (1983) VINITI 2540-83, 11 pp.
45. M. Uda and S. Ohno, Nippon Kagaku Kaishi, (1984) 862.

46. O. Matsumoto, T. Shibutami and Y. Kanzaki, Proc. Int. Ion Eng. Congr., 3 (1983) 1391.
47. V.T. Kosolapov, A.F. Levashov, Yu.M. Markov and G.V. Bichurov, Tugoplavkie Nitridy, (1983) 27.
48. V.S. Sinel'nikova, A.N. Pilyankevich, L.V. Strashinskaya and T.I. Shaposhnikova, Tugoplavkie Nitridy, (1983) 25.
49. O.V. Pshenichnaya and P.S. Kislyi, Tugoplavkie Nitridy, (1983) 54.
50. L.M. Kirilyuk, O.V. Roman and G.N. Dubrovskaya, Tugoplavkie Nitridy, (1983) 31.
51. G. Benedek, M. Miura, W. Kress and H. Bilz, Phys. Rev. Lett., 52 (1984) 1907.
52. D.W. Field, Phys. Status Solidi B, 123 (1984) 479.
53. M.K. Hibbs, J.E. Sundgren, B.E. Jacobson and B.O. Johansson, Thin Solid Films, 107 (1983) 149.
54. H. Hoechst, R.D. Bringans and R.L. Johnson, Ann. Isr. Phys. Soc., 6 (1984) 336.
55. A. Armigliato, G. Celotti, A. Garulli, S. Guerri, P. Ostoja and C. Summonte, Vide, Couches Minces, 38 (1983) 401.
56. E. Valkonen, T. Karlsson, B. Karlsson, B.O. Johansson, Proc. SPIE-Int. Soc. Opt. Eng., 401(Thin Film Technol.) (1983) 375.
57. S.P. Kogel, R.G. Avarbe, T.N. Chizhik and N.V. Barteneva, Izv. Akad. Nauk SSSR, Neorg. Mater., 19 (1983) 1665.
58. M. Valeskalne, L. Cera and T. Millers, Latv. PSR Zinat. Akad. Vestis, Kim. Ser., (1983) 687.
59. A.I. Kharlamov, A.N. Rafal, L.K. Shvedova and O.P. Kulik, Tugoplavkie Nitridy, (1983) 62.
60. J.C. Schuster and J. Bauer, J. Solid State Chem., 53 (1984) 260.
61. S. Hayashi and T. Hirai, J. Mater. Sci., 18 (1983) 3259.
62. K. Nobugai and F. Kanamaru, Mem. Inst. Sci. Ind. Res., Osaka Univ., 41 (1984) 27.
63. T. Yamamoto, S. Kikkawa and M. Koizumi, Mater. Res. Bull., 18 (1983) 1451.
64. S.P. Freidman, V.R. Galakhov, V.M. Cherkashenko, V.A. Gubanov and E.Z. Kurmaev, Zh. Strukt. Khim., 25 (1984) 42.
65. M. Ishii, M. Saeki and I. Kawada, Phys. Status Solidi B, 124 (1984) K109.
66. B. Palosz, Mater. Sci., 8 (1982) 29.
67. A. Caille, Y. Lepine, M.H. Jericho and A.M. Simpson, Phys. Rev. B: Cons. Matter, 28 (1983) 5454.
68. G.L. Holleck, K.M. Abraham, P.B. Harris, J.L. Goldman, J. Avery, M.W. Rupich and S.B. Brummer, Proc. Power Sources Symp., 30th, (1982) 68.
69. Y. Matsuda, M. Morita, K. Takata, J. Electrochem. Soc., 131 (1984) 1991.
70. T. Yamamoto, S. Kikkawa and M. Koizumi, J. Electrochem. Soc., 131 (1984) 1343.
71. Anon., (USA), Res. Discl., 236 (1983) 373.
72. S. Kikkawa and M. Koizumi, Mem. Inst. Sci. Ind. Res., Osaka Univ., 41 (1984) 101.
73. S.P.S. Yen, D.H. Shen, R.P. Vasquez, B.J. Carter and R.B. Somoano, Proc.-Electrochem. Soc., 84-1(Lithium Batteries) (1984) 403.
74. D.H. Yen, S.P.S. Yen, B.J. Carter and R.B. Somoano, Proc.-Electrochem. Soc., 84-1(Lithium Batteries) (1984) 395.
75. M. Sasaki, H. Negishi, M. Inoue and T. Yasunaga, J. Phys. Chem., 88 (1984) 3082.
76. A.V. Kozinkin, A.T. Shuvaev, A.S. Golub, Yu.N. Novikov and M.E. Vol'pin, Izv. Akad. Nauk SSSR, Ser. Khim., (1984) 1429.
77. S.N. Patel and A.A. Balchin, Z. Kristallogr, 164 (1983) 273.
78. D. Cherns and G.P. Ngo, J. Solid State Chem., 50 (1983) 7.
79. D. Cherns, D.R. Johnson and G.P. Ngo, Conf. Ser.-Inst. Phys., 68(Electron Microsc. Anal., 1983) (1984) 413.
80. G.A. Wiegers, R.J. Haange and C.F. Van Bruggen, Synth. Met., 9 (1984) 9.
81. O. Abou Ghaloun, P. Chevalier, P. Molinie and L. Trichet, Rev. Chim. Miner., 21 (1984) 1.

82. M.A. Ulibarri Cormenzana, F. Gonzalez Garcia, P.S. Valerga Jimenez and F. Gonzalez Vilchez, An. Quim., Ser. B, 80 (1984) 23.
83. K. Sieber, B. Fotouhi and O. Gorochov, Mater. Res. Bull., 18 (1983) 1477.
84. M. Schaerli and H.P. Waldvogel, J. Phys. C, 17 (1984) 2427.
85. M. Inoue and H. Negishi, J. Phys. Soc. Jpn., 53 (1984) 943.
86. J.M. Tarascon, F.J. DiSalvo, M. Eibschutz, D.W. Murphy and J.V. Waszczak, Phys. Rev. B: Condens. Matter, 28 (1983) 6397.
87. A.V. Kozinkin, A.T. Shuvaev, S.V. Kozorezov, A.S. Golub, Yu.N. Novikov and M.E. Vol'pin, Fiz. Tverd. Tela (Leningrad), 26 (1984) 697.
88. A.V. Kozinkin, A.T. Shuvaev, S.V. Kozorezov, Yu.N. Novikov, A.S. Golub, M. E. Vol'pin, E.S. Blokhina and A.A. Tutchenko, Deposited Doc., (1982), VINITI 944-83, 16 pp.
89. R.L. Barinskii, E.P. Shevchenko, I.M. Kulikova, A.S. Golub, Yu.N. Novikov and M.E. Vol'pin, Dokl. Akad. Nauk SSSR, 274 (1984) 1381.
90. G.A. Scholz and R.F. Frindt, J. Electrochem. Soc., 131 (1984) 1763.
91. G.A. Scholz, from Diss. Abstr. Int. B, 44 (1984) 2477.
92. E.A. Ukshe, N.G. Bukun, A.E. Ukshe, L.V. Sherstnova and V.I. Kovalenko, Elektrokhimiya, 20 (1984) 1246.
93. A. Honders, A.J. Hintzen, J.M. Der Kinderen, J.H.W. De Wit and G.H.J. Broers, Solid State Ionics 9-10(Pt. 2) (1983) 1205.
94. Y. Nishio, N. Kobayashi and Y. Muto, Solid State Commun., 50 (1984) 781.
95. K.O. Klepp and G. Eulenberger, Z. Naturforsch., B: Anorg. Chem., Org. Chem. 39B (1984) 705.
96. D.J. Huntley, from Diss. Abstr. Int. B, 44(12, Pt. 1) (1984) 3773.
97. L.A. Kamenskaya and A.M. Matveev, Zh. Neorg. Khim., 29 (1984) 1614.
98. Yu.K. Noga and Yu.K. Delimarskii, Ukr. Khim. Zh. (Russ. Ed.), 50 (1984) 237.
99. R.L. Lichti, Chem. Phys. Lett., 105 (1984) 228.
100. R.M. Suter, M. Karnezos and S.A. Friedberg, J. Appl. Phys., 55(6, Pt. 2B) (1984) 2444.
101. R.M. Lobkovskaya, A.V. Kolesnikov, V.F. Kaminskii, G.E. Sukhanova, L.G. Shcherbakova and R.P. Shibaeva, Izv. Akad. Nauk SSSR, Neorg. Mater., 20 (1984) 873.
102. I. Kanesaka, K. Kawai, T. Miyatake and M. Kakugo, Spectrochim. Acta, Part A, 40A (1984) 705.
103. B.H. Lipshutz and M.C. Morey, Tetrahedron Lett., 25 (1984) 1319.
104. G. Lunn, E.B. Sansone and L.K. Keffer, J. Org. Chem., 49 (1984) 3470.
105. J. Mejzlik, M. Lesna, O. Hamrik, L. Pololanik, J. Blatny and V. Reinohl, Chem. Prum., 33 (1983) 505.
106. S.L. Saratovskikh, A.D. Pomogailo, O.N. Babkina and F.S. D'yachkovskii, Kinet. Katal., 25 (1984) 464.
107. P. Corradini, V. Barone, R. Fusco and G. Guerra, Gazz. Chim. Ital., 113 (1983) 601.
108. E.A. Shishkina, I.S. Kolomnikov, T.V. Lysyak, A.V. Rudnev, E.P. Kalyazin and Yu.Ya. Kharitonov, Dokl. Akad. Nauk SSSR, 277 (1984) 650.
109. A.I. Kryukov, A.V. Korzhak, S. Ya. Kuchmii, Teor. Eksp. Khim., 20 (1984) 36.
110. A.V. Korzhak, S. Ya. Kuchmii and A.I. Kryukov, Zh. Neorg. Khim., 29 (1984) 938.
111. A.I. Kryukov, A.V. Korzhak and S. Ya. Kuchmii, Teor. Eksp. Khim., 20 (1984) 169.
112. S. Ya. Kuchmii and A.I. Kryukov, Teor. Eksp. Khim., 20 (1984) 421.
113. V.A. Kazakov, N.V. Petrova and V.N. Titova, Int. Wiss. Kolloq.- Tech. Hochsch. Ilmenau, 28 (1983) 257.
114. V.L. Solozhenko, I.V. Arkhangel'skii, A.M. Gas'kov, Ya.A. Kalashnikov and M.V. Pletneva, Zh. Fiz. Khim., 57 (1983) 2265.
115. S. Wu, Lanzhou Dazue Xuebao, Ziran Kexueban, 20 (1984) 83.
116. T.K. Klindukhova, G.N. Suvorova, L.B. Koroleva and M.I. Komendantov, Zh. Org. Khim., 20 (1984) 529.
117. D.S. Aspandiyarova, Geterogen. Khim. Reaktsii, Alma-Ata, (1983) 20.

118. R.V. Vizgert, E.V. Polyakova, T.M. Pekhterova and S.A. Khrapko, Zh. Org. Khim., 19 (1983) 1608.
119. R.V. Vizgert, E.V. Polyakova, A. Yu. Chervinskii, Zh. Obshch. Khim., 54 (1984) 905.
120. V. Kh. Dubruskin and S.E. Kurashvili, Izv. Akad. Nauk SSSR, Neorg. Mater., 20 (1984) 498.
121. V. Kh. Dobruskin and S.E. Kurashvili, Izv. Akad. Nauk SSSR, Neorg. Mater., 20 (1984) 502.
122. T.C. DeVore and T.N. Gallaher, High Temp. Sci., 16 (1983) 269.
123. S.P. Narula, R. Shankar and S. Kumar, Indian J. Chem., Sect. A, 23A (1984) 661.
124. R. Singh and V.D. Gupta, Spectrochim. Acta, Part A, 40A (1984) 407.
125. J.C. Jochims, R. Abu-El-Halawa, L. Zsolnai and G. Huttner, Chem. Ber., 117 (1984) 1161.
126. G. Guo, Y. Xie and Y. Tang, Sci. Sin., Ser. B (Engl. Ed.), 27 (1984) 1.
127. J.C.W. Chien, J.C. Wu and C.I. Kuo, Polym. Prepr. (Am. Chem. Soc., Div. Polym. Chem.) 24 (1983) 109.
128. V.A. Zakharov, Indian J. Technol., 21 (1983) 353.
129. S. Lin, Z. Liu, J. Chen and Y. Lu, Zhongshan Daxue Xuebao, Ziran Kexueban, (1983) 1.
130. V.P. Mardykin and R.K. Morozova, Izv. Vyssh. Uchebn. Zaved., Khim. Khim. Tekhnol., 27 (1984) 357.
131. L.S. Bresler, K.V. Kisin, A.V. Lubnin and N.N. Marassanova, Vysokomol. Soedin., Ser. A, 25 (1983) 2103.
132. F.W. Schultz, G.S. Ferguson and D.W. Thompson, J. Org. Chem., 29 (1984) 1736.
133. F.P. DeHaan, W.D. Covey, R.L. Ezelle, J.E. Margetan, S.A. Pace, M.J. Sollenberger and D.S. Wolf, J. Org. Chem., 49 (1984) 3954.
134. Yu.V. Pozdnyakovich, R.P. Savyak and S.M. Shein, Zh. Org. Khim., 19 (1983) 1674.
135. G.N. Mazo and S.I. Troyanov, Zh. Neorg. Khim., 28 (1983) 2986.
136. M.K. Chikanova and E.S. Vorontsov, Fiz. Khimiya i Elektrokhimiya Redk. Met. v Solev. Rasplavakh, Apatity, (1983) 51.
137. A.A. Malygin and S.I. Kol'tsov, Napravlennyi Sint. Tverd. Veshchestv, 1 (1983) 17.
138. P.I. Stepanov, E.N. Moskvitina, Yu.Ya. Kuzyakov, E.A. Sviridenkov and A.N. Savchenko, Vestn. Mosk. Univ., Ser. 2: Khim., 24 (1983) 442.
139. Yu. A. Lysenko, A.A. Kuropatova, E.A. Troshina and N.V. Golofast, Deposited Doc., (1982) VINITI 785 Khp-D82, 9pp.
140. G.I. Kadyrova and E.A. Ivanova, Fiz.-Khim. Osn. Redkomet. Syr'ya, (1983) 9.
141. D. Michalska-Fong, P.J. McCarthy and K. Nakamoto, Spectrochim. Acta, Part A, 39A (1983) 835.
142. V.L. Solozhenko, A.M. Gas'kov and Ya.A. Kalashinkov, Kokl. Akad. Nauk SSSR, 273 (1983) 1143.
143. A.V. Kozinkin, A.T. Shuvaev, R.N. Lyubovskaya, M.Z. Aldoshina, M.L. Khidekel and S.V. Zubkov, Deposited Doc., (1982) VINITI 5327-82, 15pp.
144. G.I. Kadyrova and E.A. Ivanova, Fiz.-Khim. Osn. Redkomet. Syr'ya, (1983) 3.
145. J.K. Gillie and T.C. DeVore, High Temp. Sci., 16 (1983) 387.
146. B. Leuenberger and H.U. Guedel, Mol. Phys., 51 (1984) 1.
147. S. Mohan and S. Durai, Indian J. Phys., B, 57B (1983) 420.
148. K. Takiguchi, S. Ogawa and Y. Takahashi, Proc. Int. Ion Eng. Congr., 2 (1983) 1337.
149. P. Roche, E. Pelletier and G. Albrand, J. Opt. Soc. Am. A, 1 (1984) 1052.
150. S.E. Tomberg and A.L. Rogatskii, Taboty po Fiz. Khimii, L., (1983) 11.
151. V.A. Tskhai, N.N. Lutin, P.V. Gel'd and L.P. Mokhracheva, Izv. Akad. Nauk SSSR, Neorg. Mater., 20 (1984) 1169.
152. M.G. Blanchin, L.A. Bursill, D.J. Smith and G.J. Wood, Lawrence Berkeley Lab., [Rep.] LBL (1983) LBL-16031, Proc. Int. Conf. High Voltage Electron

Microsc., 7th, 381.
153. L.A. Bursill and D.J. Smith, Nature (London), 309 (1984) 319.
154. N. Ait-Younes, F. Millot and P. Gerdanian, Solid State Ionics, 12 (1984) 437.
155. L. Bursill, M.G. Blanchin and D.J. Smith, Proc. R. Soc. London, [Ser.] A, 391 (1984) 373.
156. Y. Yamada, K. Yoshida, H. Ota, S.G. Jun, L.A. Bursill and A.E.C. Spargo, Mater. Res. Soc. Symp. Proc., 21(Phase Transform. Solids) (1984) 155.
157. V.A. Perelyaev, N.I. Kadyrova, Yu.G. Zainulin and S.T. Alyamovskii, Izv. Akad. Nauk SSSR, Neorg. Mater., 19 (1983) 1501.
158. F.W. Kutzler and D.E. Ellis, Phys. Rev. B: Condens. Matter, 29 (1984) 6890.
159. E. Michiels and R. Gijbels, Spectrochim. Acta, Part B, 38B (1983) 1347.
160. Y. LePage and M. Marezio, J. Solid State Chem., 53 (1984) 13.
161. F.J. Sciwert and R. Gruehn, Z. Anorg. Allg. Chem., 503 (1983) 151.
162. F.J. Sciwert and R. Gruehn, Z. Anorg. Allg. Chem., 510 (1984) 93.
163. C. Canali, A. Carnera, G. Celotti, G. Della Mea and P. Mazzoldi, Mater. Res. Soc. Symp. Proc., 24(Defect Prop. Process. High-Technol. Nonmet. Mater.) (1984) 459.
164. D.W. Murphy, R.J. Cava, S.M. Zahurak and A. Santoro, Solid State Ionics, 9-10(Pt. 1) (1983) 413.
165. R.J. Cava, D.W. Murphy, S. Zahurak, A. Santoro and R.S. Roth, J. Solid State Chem., 53 (1984) 64.
166. P.P. Edwards, R.G. Egdell, I. Fragala, J.B. Goodenough, M.R. Harrison, A. F. Orchard and E.G. Scott, J. Solid State Chem., 54 (1984) 127.
167. M.R. Harrison, P.P. Edwards and J.B. Goodenough, J. Solid State Chem., 54 (1984) 136.
168. N.V. Porotnikov, N.G. Chaban and K.I. Petrov, Zh. Neorg. Khim., 28 (1983) 2466.
169. R. Werthmann and R. Hoppe, Z. Anorg. Allg. Chem., 509 (1984) 7.
170. I.G. Shekhtman, E.I. Burmakin and G.K. Stepanov, Izv. Akad. Nauk SSSR, Neorg. Mater., 20 (1984) 697.
171. E.A. Belinskaya and L.P. Filina, Vestn. Leningr. Univ., Fiz. Khim., (1984) 52.
172. P.A.M. Berdowski and G. Blasse, Chem. Phys. Lett., 107 (1984) 351.
173. T. Ishii, Solid State Ionics, 9-10(Pt. 2) (1983) 1333.
174. K.P. Belov, A.N. Goryaga and A.I. Kokorev, Vestn. Mosk. Univ., Ser. 3: Fiz., Astron., 24 (1983) 48.
175. A.N. Gubkin and A.G. Tochenaya, Fiz. Khim. Tverd. Tela, (1982) 68.
176. P.E.D. Morgan, Mater. Res. Bull., 19 (1984) 369.
177. S.A. Azimov, D.D. Gulamova, N.N. Mel'nik, M. Kh. Sarkisova, S.Kh. Suleimanov and L.M. Tsapenko, Izv. Akad. Nauk SSSR, Neorg. Mater., 20 (1984) 469.
178. H. Mayata, Y. Nakagawa, T. Ono and Y. Kubokawa, Sov.-Yaponskii Semin. Katal., Sb. Kokl., 7th, (1983) 84.
179. L. Carlos Otero-Diaz and M.A. Alario-Franco, An. Quim., Ser. B, 80 (1984) 69.
180. K. Kidoh, K. Tanaka, F. Marumo and H. Takei, Acta Crystallogr., Sect. B, B40 (1984) 329.
181. A. Andriamanana, M. Lamache and D. Bauer, Electrochim. Acta, 29 (1984) 1051.
182. B. Danzfuss and U. Stimming, J. Electroanal. Chem. Interfacial Electrochem., 164 (1984) 89.
183. M.V. Astakhov, B.S. Bokshtein, V.V. D'yachuk and A.A. Lykasov, Izv. Vyssh. Uchebn. Zaved., Chern. Metall., (1984) 1.
184. M. Shiojiri, S. Sekimoto, T. Maeda, Y. Ikeda and K. Iwauchi, Phys. Status Solidi A, 84 (1984) 55.
185. S.V. Koshcheev and A.E. Cherkashin, Izv. Akad. Nauk SSSR, Neorg. Mater., 19 (1983) 1875.

186. O.N. Kovalenko, P.G. Tsyrul'nikov, V.V. Popovskii, E.M. Moroz and N.N. Boldyreva, Zh. Prikl. Khim. (Leningrad), 57 (1984) 795.
187. K. Kidoh, K. Tanaka, F. Marumo and H. Takei, Acta Crystallogr., Sect. B: Struct. Sci., B40 (1984) 92.
188. G. Balducci, G. Gigli, M.M.F. Goldenberg and M. Guido, J. Chem. Thermodyn., 16 (1984) 207.
189. J.K. Srivastava, S.M. Rao and R. Vijayaraghavan, Proc. Nucl. Phys. Solid State Phys. Symp. 1980, (Pub. 1983) 23(C), 689.
190. V.B. Reddy, S.P. Goel and P.N. Mehrota, Mater. Chem. Phys., 10 (1984) 365.
191. H. Tagawa, K. Kimura, T. Fujino and K. Ouchi, Denki Kagaku oyobi Kogyo Butsuri Kagaku, 52 (1984) 154.
192. S. Tsunekawa, H.F.J. Watanabe and H. Takei, Phys. Status Solidi A, 85 (1984) 467.
193. K.A. Mueller and W. Berlinger, J. Phys. C, 16 (1983) 6861.
194. M.R. Balasubramanian, J. Mater. Sci., 19 (1984) 1890.
195. B.F. Flandermeyer, A.K. Agarwal and H.U. Anderson, J. Mater. Sci., 19 (1984) 2593.
196. I. Gulya and L. Gyori, Energ. Atomtech., 37 (1984) 16.
197. E. Neaugu, I. Jemna and A. Bufor, An. Stiint. Univ. "Al. I. Cuza" Iasi, Sect. Ib, 29 (1983) 95.
198. A. Willgallis and H. Hartl, Z. Kristallogr., 164 (1983) 59.
199. M. Gasperin, J. Solid State Chem., 53 (1984) 144.
200. R.B. Greegor, F.W. Lytle, R.C. Ewing and R.F. Haaker, Nucl. Instrum. Methods Phys. Res., Sect. B, 229 (1984) 587.
201. S. Kikkawa, F. Kanamaru and M. Koizumi, Inorg. Synth., 22 (1983) 86.
202. P.H. Duvigneaud and A. Coussement, J. Solid State Chem., 52 (1984) 22.
203. O.E. Bochkov, V.A. Podol'skii, S.A. Popov and S.A. Plerova, Kristallografiya, 29 (1984) 805.
204. Yu.G. Zaretskii, M.V. Krasin'kova, G.A. Kurbatov, Yu.I. Ukhanov and Yu.V. Shmartsev, Fiz. Tverd. Tela (Leningrad), 26 (1984) 2233.
205. V.A. Gusev, V.A. Detinenko and A.P. Sokolov, Avtometriya, (1983) 34.
206. D. Senuliene, G. Babonas, F.I. Leonov, I. Muminov and V.M. Orlov, Phys. Status Solidi A, 84 (1984) 113.
207. B. Aurivillius, Chem. Scr., 23 (1984) 145.
208. H. Tagawa and J. Ohashi, Denki Kagaku oyobi Kogyo Butsuri Kagaku, 52 (1984) 485.
209. A. Beauger, J.C. Mutin and J.C. Niepce, J. Mater. Sci., 18 (1983) 3543.
210. T.V. Tuz, I.P. Alekseeva and V.N. Pak, Izv. Vyssh. Uchebn. Zaved., Khim. Khim. Tekhnol., 27 (1984) 631.
211. V.I. Kukuev, M.A. Sevostianov and Yu.Ya. Tomashpol'skii, Poverkhnost, (8) (1984) 54.
212. M.A.A. Issa, A.M. Hassib and Z.H. Dughaish, J. Phys. D, 17 (1984) 2057.
213. J.R. Guenter and G.B. Jameson, Acta Crystallogr., Sect. C:Cryst. Struct. Commun., C40 (1984) 207.
214. M.C. Cadee and D.J.W. Ijdo, J. Solid State Chem., 52 (1984) 302.
215. R.G. Matveeva, M.B. Varfolomeev and L.S. Ilyushchenko, Zh. Neorg. Khim., 29 (1984) 31.
216. M. Hortal, S. Vieira and R. Villar, Ferroelectrics, 54 (1984) 653.
217. M.P. Lisitsa, A.M. Yaremko and A. Yu. Tkhorik, Kvantovaya Elektron. (Kiev), 24 (1983) 56.
218. A.A. Kukharskii, Elem. Vozbuzhdeniya Segnetoelektr., (1983) 60.
219. M. Sharon and A. Sinhar, Sol. Energy Mater., 9 (1984) 391.
220. G.C. Valley and M.B. Klein, Proc. SPIE-Int. Soc. Opt. Eng., 388(Adv. Opt. Inf. Process.) (1983) 112.
221. G.C. Valley and M.B. Klein, Opt. Eng., 22 (1983) 704.
222. O.V. Meshkova, T.G. Deineka, L.T. Bazhenova and A.K. Timchenko, Sb. Nauch. Tr. VNII Monokristallov, Stsintillyatsion. Materialov i Osobo Chist. Veshchestv., (10) (1983) 142.
223. M. Herman and L.M. Kovba, Zh. Neorg. Khim., 28 (1983) 2377.

224. A.G. Belous, L.G. Gavrilova, S.V. Polyanetskaya, E.Ya. Makarova and V.P. Chalyi, Ukr. Khim. Zh. (Russ. Ed.), 50 (1984) 460.
225. K.V. Ramanujachary, N. Kameswari and C.S. Swamy, J. Bangladesh Acad. Sci., 8 (1984) 55.
226. M.P. Van Kijk, J.H.H. Ter Maat, G. Roelofs, H. Bosch, G.M.H. Van de Velde, P.J. Gellings and A.J. Burggraaf, Recl.: J.R. Neth. Chem. Soc., 103 (1984) 38.
227. M.P. Van Dijk, J.H.H. Ter Maat, G. Roelofs, H. Bosch, G.M.H. Van de Velde, P.J. Gellings and A.J. Burggraaf, Mater. Res. Bull., 19 (1984) 1149.
228. J.E. Greedan, C.W. Turner and D.A. Goodings, J. Magn. Magn. Mater., 42 (1984) 255.
229. L.M. Williams and D.W. Hess, J. Vac. Sci. Technol., A, 1 (1983) 1810.
230. H. Harada and T. Ueda, Chem. Phys. Lett., 106 (1984) 229.
231. L.M. Sharygin, S.M. Vovk and T.G. Malykh, Kolloidn. Zh., 46 (1984) 607.
232. K.S. Yeung and Y.W. Lam, Thin Solid Films, 109 (1983) 169.
233. T. Oota, I. Yamai and M. Yokoyama, J. Cryst. Growth, 66 (1984) 262.
234. H. Komiyama, T. Kanai and H. Inoue, Chem. Lett., (1984) 1283.
235. H. Harada, H. Hidaka and T. Ueda, Res. Bull. Meisei Univ., Phys. Sci. Eng., 20 (1984) 45.
236. L.R. Bitner, D.V. Gunbin and T.I. Danilina, Opt.-Mekh. Prom-st., (9) (1983) 28.
237. T.H. Allen, Proc. Int. Ion Eng. Congr., 2 (1983) 1305.
238. J.R. Sites, P. Gilstrap and R. Rujkorakarn, NBS Spec. Publ. (U.S.) 669 (1984) 243.
239. J.R. Sites, P. Gilstrap and R. Rujkorakarn, NBS Spec. Publ. (U.S.) 669 (1984) 243.
240. Z. Hong and S. Meng, Fenzi Kexue Yu Huaxue Yanjiu, 4 (1984) 131.
241. H. Yang, X. Dai, Q. Gao and B. Sun, Shanghai Jiaotong Daxue Xuebao, (4) (1983) 123.
242. M.S. Ioffe, G.S. Salitra, A.P. Pivovarov and Yu.G. Borod'ko, Khim. Fiz., 3 (1984) 1012.
243. N.M. Klimenko, D.G. Musaev and O.P. Charkin, Zh. Neorg. Khim., 29 (1984) 835.
244. S. Munnix and M. Schmeits, Phys. Rev. B: Condens. Matter, 28 (1983) 7342.
245. L.A. Bursill and M.G. Blanchin, J. Solid State Chem., 51 (1984) 321.
246. L.A. Bursill and S.G. Jun, Optik (Stuttgart), 66 (1984) 251.
247. M.G. Blanchin, L.A. Bursill and D.J. Smith, Proc. R. Soc. London, [Ser.] A, 391 (1984) 351.
248. K. Aizawa, E. Iguchi and R.J.D. Tilley, Proc. R. Soc. London, A, 394 (1984) 299.
249. J. Woning and R.A. Van Santen, Chem. Phys. Lett., 101 (1983) 541.
250. B. Morosin and R.A. Graham, Shock Waves Condens. Matter, Proc. Am. Soc. Top. Conf. 1983 (Pub. 1984) 355.
251. H. Seki, N. Ishazawa, N. Mizutani and M. Kato, Yogyo Kyokaishi, 92 (1984) 219.
252. D.M. Ovchinnikov and T.L. Luk, Vestn. Belorus. Un-ta, Ser. 2, (1984) 22.
253. Y. Suwa, M. Inagaki and S. Naka, J. Mater. Sci., 19 (1984) 1397.
254. D.K. Arkhipenko, Ya.S. Bobovich and M. Ya. Tsenter, Zh. Prikl. Spektrosk., 41 (1984) 304.
255. G. Rocker, J.A. Schaefer and W. Goepel, Phys. Rev. B: Condens. Matter, 30 (1984) 3704.
256. K. Sato, Surf. Technol., 23 (1984) 179.
257. S.M. Rossanagel and J.R. Sites, J. Vac. Sci. Technol., A, 2 (1984) 376.
258. Y. Baba and T.A. Sasaki, Nippon Genshiryoku Kenkyusho [Rep.] JAERI-M, JAERI-M-84-005 (1984) 45pp.
259. M.A. Vannice, P. Odier, M. Bujor and J.J. Fripiat, Prepr.- Am. Chem. Soc., Div. Pet. Chem., 29 (1984) 736.
260. W. Goepel, J.A. Anderson, D. Frankel, M. Jaehnig, K. Phillips, J.A. Schaefer and G. Rocker, Surf. Sci., 139 (1984) 333.

261. M.J. Carr, R.A. Graham, B. Morosin and F.L. Venturini, Mater. Res. Soc. Symp. Proc., 24(Defect Prop. Process. High-Technol. Nonmet. Metal) (1984) 543.
262. R. Kozlowski, R.F. Pettifer and J.M. Thomas, J. Phys. Chem., 87 (1983) 5172.
263. G.A. Royce and R.B. Kay, Appl. Opt., 23 (1984) 1975.
264. E. Michiels, T. Mauney, F. Adams and R. Gijbels, Int. J. Mass. Spectrom. Ion Processes, 61 (1984) 231.
265. S. Lugomer, M. Stipancic and A. Persin, Appl. Opt., 22 (1983) 3314.
266. G.A. Kazaryan, V.A. Polushkin, A.V. Vlasov, B.L. Tsetlin and P.A. Chakhoyan, Kolloidn. Zh., 46 (1984) 567.
267. H.G. Walther and G. Schirmer, Ann. Phys. (Leipzig), 41 (1984) 12.
268. D. Bahnemann, A. Henglein, J. Lilie and L. Spanhel, J. Phys. Chem., 88 (1984) 709.
269. A.K. Rakhmanov, N.I. Kuntsevich, V.V. Sviridov and V.G. Sokolov, Zh. Nauchn. Prikl. Fotogr. Kinematogr., 28 (1983) 459.
270. S.G. Saxe, M.J. Messerly, B. Bovard, L. DeSandre, F.J. Van Milligen and H.A. Macleod, Appl. Opt., 23 (1984) 3635.
271. S. Yolou and L. Nadjo, J. Electroanal. Chem. Interfacial Electrochem., 159 (1983) 449.
272. S.D. Babenko, V.A. Denderskii, Yu.G. Borod'ko, A.N. Rukin and G.S. Salitra, Khim. Fiz., 3 (1984) 584.
273. E.I. Vasilevskaya, N.I. Kuntsevich and T.L. Luk, Zh. Nauchn. Prikl. Fotogr. Kinematogr., 29 (1984) 277.
274. E.I. Vasilevskaya, N.I. Kuntsevich, T.L. Luk, A.I. Kulak, V.V. Sviridov and I.A. Shingel, Zh. Nauchn. Prikl. Fotogr. Kinematogr., 29 (1984) 23.
275. C.V. D'Alkaine, R.M.B. Rodrigues and F.C. Nart, An. Simp. Bras. Eletroquim. Eletroanal., 4th, (1984) 431.
276. G.I. Marinina, D.M. Shub and S. Yu. Prochankin, Izv. Vyssh. Uchebn. Zaved., Khim. Khim. Tekhnol., 27 (1984) 900.
277. P. Salvador and C. Gutierrez, J. Phys. Chem., 88 (1984) 5696.
278. M. Takeuchi, F. Shimizu, F. Kaneko and H. Nagasaka, Proc. Int. Ion Eng. Congr., 2 (1983) 927.
279. J. Taniguchi, R. Hayashida, K. Matsuochi, M. Yoshioka, H. Yamaguchi and K. Yasukouchi, Denko Kagaku oyobi Kogyo Butsuri Kagaku, 52 (1984) 300.
280. G. Betz, H. Tributsch and R. Marchand, J. Appl. Electrochem., 14 (1984) 515.
281. C. Bartels, M.M. Lohrengel and J.W. Schultze, Proc. -Electrochem. Soc., 84-3(Fundam. Aspects Corros. Prot. Surf. Modif.) (1984) 205.
282. K.H. Yoon and S.O. Yoon, Jpn. J. Appl. Phys., Part 1, 23 (1984) 1137.
283. L.M. Williams and D.W. Hess, Thin Solid Films, 115 (1984) 13.
284. Y. Shi, H. Yang, X. Dai, Q. Gao and B. Shi, Sol. World Congr., Proc. Bienn. Congr. Int. Sol. Energy Soc., 8th, 1983, (Pub. 1984) 3, 2048.
285. I.A. Abdullin, Elektron. Obrab. Mater., (1983) 47.
286. S. Meguro, B. Ise, O. Takagi and S. Toshima, Tohoku Kogyo Daigaku Kiyo,1, 4 (1984) 187.
287. L. Fornarini, A.J. Nozik and B.A. Parkinson, J. Phys. Chem., 88 (1984) 3238.
288. A.V. Alekseev and V.N. Filimonov, Zh. Fiz. Khim., 58 (1984) 2023.
289. G.N. Kuz'min, M.V. Knat'ko and S.V. Kurganov, React. Kinet. Catal. Lett., 23 (1983) 315.
290. V.K. Tiwari, Natl. Acad. Sci. Lett. (India), 6 (1983) 159.
291. J. Phillips and J.A. Dumesic, ACS Symp. Ser., 248(Catal. Mater.: Relat. Struct. React.) (1984) 3.
292. T. Nguyen and D.F. Ollis, J. Phys. Chem., 88 (1984) 3386.
293. D.F. Ollis, C.Y. Hsiao, L. Budiman and C.L. Lee, J. Catal., 88 (1984) 89.
294. S. Ahmed and D.F. Ollis, Sol. Energy, 32 (1984) 597.
295. N. Kikykawa, M. Makino, H. Matsumoto and M. Horie, Kogai Shigen Kenkyusho Iho, 13 (1983) 13.
296. G.T. Brown and J.R. Darwent, J. Chem. Soc., Faraday Trans. 1, 80 (1984) 1631.

297. H. Yoneyama, N. Matsumoto, T. Furusawa and H. Tamura, Nippon Kagaku Kaishi, (1984) 253.
298. E.A. Shishkina, I.S. Kolomnikov, T.V. Lyasyak, A.V. Rudnev, E.P. Kalyazin and Yu.Ya. Kharitonov, Zh. Neorg. Khim., 29 (1984) 2143.
299. M.A. Malati and W.K. Wong, Surf. Technol., 22 (1984) 305.
300. V.V. Shimanovskaya, L.G. Svintsova, A.A. Dvernyakova, G.N. Novitskaya and G.I. Golodets, React. Kinet. Catal. Lett., 23 (1983) 37.
301. T. Nakajima, H. Miyata and Y. Kubokawa, J. Chem. Soc., Faraday Trans. 1, 79 (1983) 2559.
302. V.V. Viktorov, V.E. Gladkov, A.A. Fotiev and V.T. Ivashinnikov, Izv. Akad. Nauk SSSR, Neorg. Mater., 20 (1984) 686.
303. S. Suzuki, N. Horiuchi, M. Matsumoto and Y. Hori, Taiki Osen Gakkaishi, 18 (1983) 579.
304. R.S. Davidson and J.E. Pratt, Tetrahedron Lett., 24 (1983) 5903.
305. Y. Shimamura, H. Misawa, T. Oguchi, T. Kanno, H. Sakuragi and K. Hiroaki, Chem. Lett., (1983) 1691.
306. M.A. Fox, C.C. Chen and J.N.N. Younathan, J. Org. Chem., 49 (1984) 1969.
307. G.T. Brown and J.R. Darwent, J. Phys. Chem., 88 (1984) 4955.
308. R.W. Matthews, J. Chem. Soc., Faraday Trans. 1, 80 (1984) 457.
309. M. Anpo, N. Aikawa, S. Kodama and Y. Kubokawa, J. Phys. Chem., 88 (1984) 2569.
310. E. Santacesaria, R.C. Pace and S. Carra, Congr. Naz. Chim. Inorg., [Atti], 16th, (1983) 295.
311. A.A. Gurov, O.A. Sinegribova and G.A. Yagodin, Zh. Neorg. Khim., 29 (1984) 1164.
312. V.P. Titov, N.S. Dyachenko and F.L. Fisher, Vesti Akad. Navuk BSSR, Ser. Khim. Navuk, (1984) 106.
313. K.J. Hartig and N. Getoff, Hydrogene Mater., Congr. Int., 3rd, 2 (1982) 947.
314. E. Borgarello and E. Pelizzetti, Inorg. Chim. Acta, 91 (1984) 295.
315. H.D. Duong, N. Serpone and M. Graetzel, Helv. Chim. Acta, 67 (1984) 1012.
316. H. Muraki, T. Saji, M. Fujihira and S. Aoyagui, J. Electroanal. Chem. Interfacial Electrochem., 169 (1984) 319.
317. R.S. Davidson, C.L. Morrison and J. Abraham, J. Photochem., 24 (1984) 27.
318. M.M. Kosanic, R.P. Djajic-Jovanovic and A.D. Nikolic, Glas. Hem. Drus. Beograd, 48 (1983) 229.
319. M. Herman and L.M. Kovba, Izv. Akad. Nauk SSSR, Neorg. Mater., 19 (1983) 1941.
320. L.C. Otero-Diaz and B.G. Hyde, Acta Crystallogr., Sect. B: Struct. Sci., B40 (1984) 237.
321. L.C. Otero-Diaz, J. Soria and M.A. Alario-Franco, Phys. Status Solidi A, 82 (1984) 379.
322. R. Kozlowski, R.F. Pettifer and J.M. Thomas, J. Phys. Chem., 87 (1983) 5176.
323. K. Mori, M. Miura, A. Miyamoto and Y. Murakami, J. Phys. Chem., 88 (1984) 5232.
324. K. Mori, A. Miyamoto and Y. Murakami, J. Phys. Chem., 99 (1984) 2735.
325. M. Gasior, B. Grzybowska and M. Czerwenka, Geterog. Katal., 5th, Part 1, (1983) 75.
326. M. Rusiecka, B. Grzybowska and M. Gasior, Appl. Catal., 10 (1984) 101.
327. A.J. Van Hengstum, J.G. Van Ommen, H. Bosch and P.J. Gellings, Appl. Catal., 8 (1983) 369.
328. A.J. Van Hengstum, J. Pranger, J.G. Van Ommen and P.J. Gellings, Appl. Catal., 11 (1984) 317.
329. H. Miyata, Y. Nakagawa, T. Ono and Y. Kubokawa, J. Chem. Soc., Faraday Trans. 1, 79 (1983) 2343.
330. H. Miyata, Y. Nakagawa, T. Ono and Y. Kubokawa, from Ref. Zh., Khim., (1984) Abstr. No. 4B4220.
331. Y. Nakagawa, T. Ono, H. Miyata and Y. Kubokawa, J. Chem. Soc., Faraday Trans. 1, 79 (1983) 2929.

332. P.B. Vorob'ev, N.R. Bukeikhanov, A.G. Lyubarskii, A.G. Gorelik, O.N. Sal'nikova and B.V. Suvorov, Izv. Akad. Nauk Kaz., SSR, Ser. Khim., (5) (1985) 34.
333. A. Miyamoto, M. Inomata, K. Mori, T. Ui, K. Kobayashi and Y. Murakami, Sov.-Yaponskii Semin. Katal., Sb. Dokl., 7th, (1985) 142.
334. W.C. Wong and K. Nobe, Ind. Eng. Chem. Prod. Res. Dev., 23 (1984) 564.
335. S. kasaoka, E. Sasaoka and H. Nanba, Nippon Kagaku Kaishi, (1984) 486.
336. J. Kiwi, J.T. Suss and S. Szapiro, Chem. Phys. Lett., 106 (1984) 155.
337. L.A. Bursill and S.G. Jun, J. Solid State Chem., 51 (1984) 388.
338. E.V. Avagyan, V.A. Atsarkin and G.A. Vasneva, Zh. Eksp. Teor. Fiz., 85 (1983) 1790.
339. G.N. Yagodkina, G.A. Duntsig and E.A. Boevskaya, Zh. Prikl. Khim. (Leningrad), 57 (1984) 1876.
340. D.M. Hercules, Report (1984) DOE/ER/10485-T4; order no. DE84004210, 15pp.
341. K. Miyahara, Chem. Lett., (1983) 1871.
342. T. Ono, Y. Nakagawa, H. Miyata and Y. Kubokawa, Bull. Chem. Soc. Japan, 57 (1984) 1205.
343. N. Kh. Allakhverdova, F.B. Kasumov, K. Ya. Adzhamov and T.G. Alkhazov, Kinet. Katal., 25 (1984) 684.
344. J.G. Van Ommen, K. Hoving, H. Bosch, A.J. Van Hengstum and P.J. Gellings, Z. Phys. Chem. (Wiesbaden), 134 (1983) 99.
345. A. Grandin, M.M. Borel, C. Michel, N. Nguyen and B. Raveau, Mater. Chem. Phys., 10 (1984) 445.
346. S.H. Chien, J.C. Chang, K.L. Lu and J.N. Wang, Bull. Inst. Chem., Acad. Sin., 31 (1984) 17.
347. L.M. Tau and C.O. Bennett, J. Catal., 89 (1984) 285.
348. S. Levine, F.T. Liou, K. Hakim and C. Yang, Report (1983), DOE/ET/25209-1; order no. DE84005168, 157pp.
349. P. Salvador, C. Gutierrez, P. Triggs and F. Levy, Mater. Res. Bull., 19 (1984) 643.
350. L.J.J. Janssen, Mod. Chlor-Alkali Technology, [Pap. Int. Chlorine Symp.], 3rd, 1982 (Pub. 1983) 271.
351. R.G. Erenburg, L.I. Krishtalik and N.P. Rogozhina, Elektrokhimiya, 20 (1984) 1183.
352. M.D. Spasojevic, N.V. Krstajic and M.M. Jaksic, J. Res. Inst. Catal. Hokkaido Univ., 31(2-3) (1984) 77.
353. F.V. Kupovich, T.Ya. Krasilova and V.L. Kubasov, Zh. Prikl. Khim. (Leningrad), 56 (1983) 2536.
354. V.V. Gorodetskii, Yu.Ya. Tomashpol'skii, L.B. Gorbacheva, N.V. Sadovskaya, M.M. Pecherskii, S.V. Evdokimov, V.B. Busse-Machukas, V.L. Kubasov and V.V. Losev, Elektrokhimiya, 20 (1984) 1045.
355. V.V. Gorodetskii, M.M. Pecherskii, N. Ya. Bune, S.V. Evdokimoc, V. Busse-Macukas, V.L. Kubasov, Yu.Ya. Tomashpol'skii and V.V. Losev, Nov. Napravleniya v Pr-ve Khlora, Kaust. Sody i Konstruir. Elektrolizerov Tr. Simpoz., Moskva, 29 Sent.-3 Okt., 1981, M (1983) 102.
356. J.A. Harrison, Mod. Chlor-Alkali Technology, [Pap. Int. Chlorine Symp.], 3rd, 1982 (Pub. 1983) 246.
357. E. Kikuchi, H. Nomura, M. Matsumoto and Y. Morita, Pan-Pac. Synfuels Conf., 1 (1982) 216.
358. E. Kikuchi, M. Matsumoto, T. Takahashi, A. Machino and Y. Morita, Appl. Catal., 10 (1984) 251.
359. M. Halmann, V. Katzir, E. Borgarello and J. Kiwi, Sol. Energy Mater., 10 (1984) 85.
360. B.I. Ikhlasova and Z.M; Aliev, Deposited Doc., (1982) SPSTL 1281 Khp-D82, 10pp.
361. V.E. Kazarinov, Kh.A. Maksimov, G.A. Tedoradze and L.T. Gorokhova, Elektrokhimiya, 20 (1984) 594.
362. D.V. Kokulina and L.V. Bunakova, J. Electroanal. Chem. Interfacial Electrochem., 164 (1984) 377.

363. T. Sakata, K. Hashimoto and T. Kawai, J. Phys. Chem., 88 (1984) 5214.
364. C. Minero, E. Lorenzi, E. Pramauro and E. Pelizzetti, Inorg. Chim. Acta, 91 (1984) 301.
365. E. Yesodharan and M. Graetzel, Helv. Chim. Acta, 66 (1983) 2145.
366. S. Takasaki, H. Suzuki, K. Takahashi, S. Tanabe, A. Ueno and Y. Kotera, J. Chem. Soc., Faraday Trans. 1, 80 (1984) 803.
367. R.C. Reuel and C.H. Barthoolomew, J. Catal., 85 (1984) 78.
368. S. Tanabe, T. Ida, H. Tsuiki, A. Ueno, Y. Kotera, K. Tohji and Y. Udagawa, Chem. Lett., (1984) 1271.
369. J.C. Vis, H.F.J. Van't Blik, T. Huizinga, J. Van Grondelle and R. Prins, J. Mol. Catal., 25 (1984) 367.
370. J.C. Conesa, P. Malet, G. Munera, J. Sanz and J. Soria,J. Phys..Chem., 88 (1984) 2986.
371. T. Ichikawa, S. Fujimoto and H. Yoshida, Chem. Phys. Lett., 103 (1983) 80.
372. D.N. Belton, Y.M. Sun and J.M. White, J. Am. Chem. Soc., 106 (1984) 3059.
373. D.E. Resasco and G.L. Haller, Appl. Catal., 8 (1983) 99.
374. A. Erdohelyi and F. Solymosi, J. Catal., 84 (1983) 446.
375. H. Orita, S. Naito and K. Tamaru, Chem. Lett., (1983) 1161.
376. A. Deluzarche, J.P. Hindermann, R. Kieffer, R. Breault and A. Kiennemann, J. Phys. Chem., 88 (1984) 4993.
377. A.J. Simoens, R.T.K. Baker, D.J. Dwyer, C.R.F. Lund and R.J. Madon, J. Catal., 86 (1984) 359.
378. L. Pejryd, Acta Chem. Scand., Ser. A, A38 (1984) 241.
379. L.T. Prahov, J. Disdier, J.M. Herrmann and P. Pichat, J. Hydrogen Energy, 9 (1984) 397.
380. M. Malinowski, R. Makowski, R. Muranyi and J. Wild, Geterog. Katal., 5th (1982) Part 2, 69.
381. G.B. Raupp and J.A. Dumesic, J. Phys. Chem., 88 (1984) 660.
382. C.C. Kao, Diss. Abstr. Int. B, 44 (1984) 3489.
383. M.A. Vannice, Pan-Pac. Synfuels Conf., 1 (1982) 208.
384. Y. Chung, G. Ziong and C. Kao, J. Catal., 85 (1984) 237.
385. S. Takatani and Y.W. Chung, J. Catal., 90 (1984) 75.
386. Z. Bastl and P. Mikusik, Czech. J. Phys., B34 (1984) 989.
387. R.T.K. Baker, E.B. Prestridge and G.B. McVicker, J. Catal., 89 (1984) 422.
388. H.D. Gesser and L. Kruczynski, J. Phys. Chem., 88 (1984) 2751.
389. G. Carturan, G. Facchin, G. Navazio, V. Gottardi and G. Cocco, Ultrastruct. Process. Ceram., Glasses, Compos., [Proc. Int. Conf.], 1983 (Pub. 1984) 197.
390. R. Galicia, Rev. Inst. Mex. Pet., 14 (1982) 26.
391. V.E. Henrich, J. Catal., 88 (1984) 519.
392. J.A. Horseley, J. Am. Chem. Soc., 101 (1979) 2870.
393. J.A. HOrsley, J. Catal., 88 (1984) 549.
394. D.D. Beck and J.M. White, J. Phys. Chem., 88 (1984) 2764.
395. D.D. Beck and J.M. White, J. Phys. Chem., 88 (1984) 174.
396. D.D. Beck, A.O. Bawagan and J.M. White, J. Phys. Chem., 88 (1984) 2771.
397. H. Courbon, J.M. Herrmann and P. Pichat, J. Phys. Chem., 88 (1984) 5210.
398. T. Huizinga, J. Van Grondelle and R. Prins, Appl. Catal., 10 (1984) 199.
399. D.N. Belton, Y.M. Sun and J.M. White, J. Phys. Chem., 88 (1984) 5172.
400. T. Huizinga, J.C. Vis, H.F.J. Van't Blik and R. Prins, Recl.; J.R. Neth. Chem. Soc., 102 (1983) 496.
401. T. Huizinga, H.F.J. Van' Blik, J.C. Vis and R. Prins, Surf. Sci., 135 (1983) 580.
402. C. Sungbom, M. Kawai and K. Tanaka, Bull. Chem. Soc. Japan, 57 (1984) 871.
403. M. Koudelka, A. Monnier, J. Sanchez and J. Augustynski, J. Mol. Catal., 25 (1984) 295.
404. X. Huang, H. Liu, J. Ren and Y. Chen, Cuihua Xuebao, 4 (1983) 307.

405. T.J. Lee and Y.G. Kim, Proc. - Pac. Chem. Eng. Congr., 3rd, 2 (1983) 250.
406. A.R. Berzins, M.S.W. Lau Vong, P.A. Sermon and A.T. Wurie, Adsorpt. Sci. Technol., 1 (1984) 51.
407. M.A. Vannice and C. Sudhakar, J. Phys. Chem., 88 (1984) 2429.
408. Z. Hong and Y. Chen, Huaxue Tongbao, (1984) 19.
409. V.M. Kolchanova and E.P. Mikheeva, React. Kinet. Catal. Lett., 24 (1984) 207.
410. S. Sato and K. Kunimatsu, J. Phys. Chem., 88 (1984) 175.
411. M. Koudelka, A. Monnier and J. Augustynski, J. Electrochem. Soc., 131 (1984) 745.
412. K. Tanaka, K. Miyahara and I. Toyoshima, J. Phys. Chem., 88 (1984) 3504.
413. C.H. Langford, C. Saint Joly, E. Pelletier and C. Arbour, Inorg. Chim. Acta, 87 (1984) L31.
414. M. Ampo, N. Aikawa and Y. Kubokawa, J. Phys. Chem., 88 (1984) 3998.
415. M. Tefek, Madencilik, 22 (1983) 25.
416. K. Yamaguti and S. Sato, Nippon Kagaku Kaishi, (1984) 258.
417. S. Nakabayashi, A. Fujishima and K. Honda, Chem. Phys. Lett., 102 (1983) 464.
418. K. Fujimoto, H. Kawai, S. Nonomura, H. Okamoto and Y. Hamakawa, Comm. Eur. Communities, [Rep] EUR (1984) 9007, Photovoltaic Sol. Energy Conf., Proc. Int. Conf., 5th, 1985, 815.
419. R.R. Seyedmonir, D.E. Strohmayer, G.L. Geoggroy, M.A. Vannice, H.W. Young and J.W. Linowski, J. Catal., 87 (1984) 424.
420. E.A. Strel'tsov, A.I. Kulak and R.M. Lazorenko-Manevich, Elektrokhimiya, 20 (1984) 211.
421. B.E. Yoldas and T. O'Keefe, Appl. Opt., 23 (1984) 3638.
422. A.K. Rakhmanov, N.I. Kuntsevich and V.G. Sokolov, Zh. Nauchn. Prikl. Fotogr. Kinematogr., 29 (1984) 262.
423. K. Fujimoto, H. Kawai, H. Okamoto and Y. Hamakawa, Sol. Cells, 11 (1984) 357.
424. J. Kubicki and B. Szczygiel, Powloki Ochr., 11 (1983) 27.
425. A. Albu-Yaron, D. Cahen and G. Hodes, Thin Solid Films, 112 (1984) 349.
426. S. Okazaki, A. Kurosaki and S. Suzaki, Bull. Chem. Soc. Japan, 57 (1984) 1046.
427. N.I. Ivashchenko, I.A. Yursha and T.I. Larionova, Deposited Doc., (1982) VINITI 6545-82, 150.
428. G. Kh. Mezhinskii, Ya.Ya. Bol'shii and E.A. Chodar, Neorg. Stekla Pokrytiya Mater., 6 (1983) 19.
429. H. Schwiecker, Vide, Couches Minces, 39 (1984) 175.
430. C.Y. Ting, M. Wittmer, S.S. Iyer and S.B. Brodsky, Proc. Electrochem. Soc., 84-7(VLSI Sci. Technol.) (1984) 397.
431. R. Vithanage and H.O. Finklea, J. Electrochem. Soc., 131 (1984) 799.
432. J.P. Boilot, P. Colomban and N. Blanchard, Solid State Ionics, 9-10, Pt. 1 (1983) 659.
433. G.J. Exarhos and W.T. Pawlewicz, Appl. Opt., 23 (1984) 1986.
434. T.A. Egerton, G.D. Parfitt, Y. Kang and J.P. Wightman, Colloids Surf., 7 (1983) 311.
435. A.I. Kulak and S.K. Poznyak, Elektrokhimiya, 20 (1984) 929.
436. M. Berti, A.V. Drigo, C. Cohen, J. Siejka, G.G. Bentini, R. Nipoti and S. Guerri, J. Appl. Phys., 55 (1984) 3558.
437. G.G. Bentini, M. Berti, C. Cohen, A.V. Drigo, S. Guerri, R. Mo=pto amd J. Siejka, Mater. Res. Soc. Symp. Proc., 25(Thin Films Interfaces 2) (1984) 137.
438. N.I. Min'ko and V.E. Trunaev, Fiz.-Mat. Metody v Issled. Sv-v Stroitel'nykh Materialov i v ikh Pr-ve, M., (1982) 148.
439. M.M. Shul'ts, A.V. Andreenko and A.M. Pisarevskii, Dokl. Akad. Nauk SSSR, 274 (1984) 1430.
440. M. Ichikawa, K. Shikakura and M. Kawai, China-Jpn.-U.S. Symp. Heterog. Catal. Relat. Energy Probl., (1982) A08J, 5pp.
441. F. Hine and M. Yasuda, Trans. SAEST, 19 (1984) 83.

442. H. Hirashima and T. Yoshida, Nippon Kagaku Kaishi, (1984) 823.
443. V.P. Titov, A.V. Pavlov and L.V. Lapteva, Izv. Akad. Nauk SSSR, Neorg. Mater., 19 (1983) 1903.
444. A. Radde and L. Kolditz, Z. Chem., 23 (1983) 436.
445. N.I. Zaginaichenko, E.B. Panasenko, V.A. Masloboev and M.P. Shul'gina, Issled. Fiz.-Khim. Osn. Tekhnol. Pererab. Miner. Syr'ya, (1983) 83.
446. M. German and L.M. Kovba, Vestn. Mosk. Univ., Ser. 2: Khim., 25 (1984) 276.
447. P. Meteniowski, React. Kinet. Catal. Lett., 23(3-4) (1983) 355.
448. I.M. Maister, L.M. Lopato, A.V. Shevchenko and I.E. Kir'yakova, Izv. Akad. Nauk SSSR, Neorg. Mater., 19 (1983) 1512.
449. R. Kuentzler, R.M. Waterstrat, P. Turek and A. Bieber, Mater. Res. Soc. Symp. Proc., 21(Phase Transform. Solids) (1984) 393.
450. T.P. Chow, W. Katz and R. Goehner, Proc. - Electrochem. Soc., 84-7(VLSI Sci. Technol.) (1984) 465.
451. S. Iyer, C.Y. Ting and P.M. Fryer, Proc. - Electrochem. Soc., 84-7(VLSI Sci. Technol.) (1984) 381.
452. D. Khatamian, G.C. Weatherly and F.D. Manchester, Acta Mettal., 31 (1983) 1771.
453. C.N. Park and J.Y. Lee, J. Less-Common Met., 96 (1984) 177.
454. A. Bernis and A. Storck, Entropie, 20 (1984) 58.
455. H. Tange, Y. Yamada and M. Goto, J. Phys. Soc. Jpn., 53 (1984) 2092.
456. P. Shen, G. Wang, Z. Zhou and D. Yan, Daodeng Xuexiao Huaxue Xuebao, 4 (1983) 673.
457. J.V. Yakhmi, I.K. Gopalakrishnan and A.K. Grover, Phys. Status Solidi A, 85 (1984) K89.
458. U. Bardi, G.A. Somorjai and P.N. Ross, J. Catal., 85 (1984) 272.
459. M. Thoma, Annu. Tech. Conf. Proc. - Am. Electroplat. Soc., 7th, A-6 (1983), 9pp.
460. E.M. Rumyantsev, O.I. Nevskii, V.I. Volkov and E.P. Grishina, Elektron. Obrab. Mater., (1984) 67.
461. A.M. Sedenkov, D.R. Berezovskii and V.S. Kuzub, Elektrokhimiya, 20 (1984) 1004.
462. Yu.S. Ruskol, M.N. Fokin and L.I. Viter, Zashch. Met., 20 (1984) 420.
463. V.V. Mel'nik, V.V. Sokolov, R.Sh. Spivak and V.M. Sorokin, Deposited Doc. (1982) SPSTL 693 Khp-D82, 8pp.
464. N. Koyanagi, Kogyo Reametaru,(83) (1984) 31.
465. T. Yoshinaga, K. Kawano, K. Yanagase and H. Murakami, Denko Kagaku oyobi Kogyo Butsuri Kagaku, 51 (1983) 493.
466. V.P. Gomozov, B.I. Bairachnyi and F.K. Andryushchenko, Zh. Prikl. Khim. (Leningrad), 56 (1983) 2533.
467. O.R. Camara, C.P. De Pauli and M.C. Giordano, Electrochim. Acta, 29 (1984) 1111.
468. L.D. Burke and M. McCarthy, Electrochim. Acta, 29 (1984) 211.
469. R.I. Mostkova, N.F. Nikol'skaya and L.I. Krishtalik, Elektrokhimiya, 19 (1983) 1608.
470. N.I. Kavardakov, V.I. Kichigin and V.V. Kuznetsov, Elektrokhimiya, 20 (1984) 486.
471. T. Loucka and S. Papez, Chem. Prum., 34 (1984) 345.
472. A.P. Brynza, E.Ya. Balbarova, L.P. Sushchenko and E.A. Filippova, Zashch. Met., 20 (1984) 261.
473. O.A. Nikitina and B.N. Mikhailov, Fiz. Khim. Elektrokhim. Redk. Met. Solevykh Rasplavakh, (1984) 64.
474. O.A. Ninikina and B.N. Mikhailov, Fiz. Khimiya i Elektrokhimiya Redk. Med. v Solev. Rasplavakh, Apatity, (1983) 64.
475. T.A. Krapivkina, Zashch. Met., 20 (1984) 258.
476. T.A. Krapivkina and I.Yu. Dobrovol'skaya, Zashch. Met., 20 (1984) 260.
477. Yu. S. Ruskol, Titan v Khim. Pr-vakh, M., (1983) 4.
478. Yu.S. Ruskol and L.I. Viter, Protivokorroz. Zashchita v Khim. Prom-sti, M., (1983) 33.

479. I.V. Riskin, V.B. Torshin, Ya.B. Skuratnik and M.A. Dembrovskii, Corrosion (Houston), 40 (1984) 266.
480. Yu.G. Dikunov, V.D. Tkhai and I.N. Ozeryanaya, Khim. Elektrokhim. Redk. Met. Solevykh Rasplavakh, (1984) 60.
481. S.S. Chouthai and K.S. Gadiyar, J. Electrochem. Soc. India, 33 (1984) 15.
482. L.I. Tungusova, V.A. Gerasimova, I.L. Kurbatova, P. Lapchenko and E.Ya. Semenyuk, Titan v Khim. Pr-vakh, M., (1983) 98.
483. V.S. Zotikov, V.A. Gerasimova, L.V. Pomyalova and E. Ya. Semenyuk, Zh. Prikl. Khim. (Leningrad), 57 (1984) 1139.
484. L.I. Gerasyutina, A.P. Brynza, L.G. Karyaka and V.P. Fedash, Zashch. Met., 20 (1984) 451.
485. I.V. Riskin, Titan v Khim. Pr-vakh, M., (1983) 37.
486. V.N. Balitskii, A.S. Gorbachev, A.F. Mazanko and S.V. Savinkov, Titan v Khim. Pr-vakh, M., (1983) 55.
487. V.S. Balikhin and S.B. Makarov, Izv. Akad. Nauk SSSR, Met., (1983) 49.
488. S.B. Makarov and A.V. Balikhin, Ukr. Khim. Zh. (Russ. Ed.), 50 (1984) 498.
489. Q. Yang and G. Liu, Gaodeng Xuexiao Huaxue Xuebao, 5 (1984) 215.
490. V.S. Balikhin and S.B. Makarov, Elektrokhimiya, 20 (1984) 696.
491. V.V. Volcinik, Yu.G. Olesov, V.G. Galochka, I.E. Lukoshnikov and V.V. Pavlov, Ukr. Khim. Zh. (Russ. Ed.), 50 (1984) 407.
492. Yu.G. Dikunov, V.D. Tkhai and I.N. Ozeryanaya, Fiz. Khimiya i Elektrokhimiya Redk. Met. v Solev. Rasplavakh, Apatity, (1983) 60.
493. V.I. Shapoval, V.I. Taranenko, V.V. Nerubashchenko, L.L. Kaidanovich, N.N. Uskova and N.Ya. Kholod, Fiz. Khim. Elektrokhim. Redk. Met. Solevykh Rasplavakh, (1984) 108.
494. I.A. Barannik, G.P. Dovgaya and E.A. Kitaigorodskii, Fiz. Khim. Elektrokhim. Redk. Met. Solevykh Rasplavakh, (1984) 54.
495. I.A. Barannik, G.P. Dovgaya and E.A. Kitaigorodskii, Fiz. Khimiya i Elektrokhimiya Redk. Met. v Solev. Rasplavakh, Apatity, (1983) 54.
496. D.G. Lovering and D.P.D. Clark, Proc.-Electrochem. Soc., 84-2(Molten Salts) (1984) 603.
497. E.B. Lobkovskii, G.L. Soloveichik, A.I. Sisov, B.M. Bulychev, A.I. Gusev, N.I. Kirillova, J. Organomet. Chem., 265 (1984) 167.
498. T.L. Chen, T.H. Chan and A. Shaver, J. Organomet. Chem., 268 (1984) C1.
499. S. Wu, C. Zhao, Y. Zhao and R. Hu, Lanzhou Daxue Xuebao, Ziran Kexuehan, 19(Huaxue Jikan) (1983) 206.
500. H.S. Lee, K. Isagawa and Y. Otsuji, Chem. Lett., (1984) 363.
501. O.N. Krasochka, A.F. Shestakov, G.G. Tairova, Yu.A. Shvetsov, E.F. Kvashina, V.I. Ponomarev, L.O. Atovmyan and Yu.G. Borod'ko, Khim. Fiz., (1983) 1459.
502. G. Plesch, Chem. Zvesti, 38 (1984) 33.
503. T. Nerskovitz, J. Polym. Sci., Polym. Chem. Ed., 22 (1984) 657.
504. A. Sousa, A. Macias, M. Gayoso and J. Romero, An. Quim., Ser. B, 79 (1983) 48.
505. D. Wang and G. Wu, Kexue Tongbao (Foreign Lang. Ed.), 29 (1984) 481.
506. H.O. Froehlich and K.H. Mann, Wiss. Z.-Friedrich-Schiller-Univ. Jena, Math.-Naturwiss. Reihe, 33 (1984) 186.
507. M. Hoshino, M. Imamura, S. Watanabe and Y. Hama, J. Phys. Chem., 88 (1984) 45.
508. A. Deronzier and J.M. Latour, Nouv. J. Chim., 8 (1984) 393.
509. D. Chang, Diss. Abstr. Int. B, 44(12, Pt. 1) (1984) 3762.
510. H. Inoue and E. Fluck, Z. Naturforsch, B: Anorg. Chem., Org. Chem., 39B (1984) 185.
511. N.S. Biradar, M.C. Divakar and T.M. Aminabhavi, Indian J. Chem., Sect. A, 23A (1984) 586.
512. K.C. Malhotra, K.C. Mahajan and S.C. Chaudhry, J. Indian Chem. Soc., 60 (1983) 636.
513. K.C. Malhotra, K.C. Mahajan and S.C. Chaudhry, Indian J. Chem., Sect. A, 23A (1984) 348.

514. K.C. Malhotra, K.C. Mahajan and S.C. Chaudhry, Indian J. Chem., Sect. A, 23A (1984) 246.
515. K.C. Malhotra, K.C. Mahajan and S.C. Chaudhry, Indian J. Chem., Sect. A, 23A (1984) 614.
516. E. Giannetti and E. Albizzati, Inorg. Chim. Acta, 74 (1983) 215.
517. S.L. Chadha and P.K. Gupta, Res. Bull. Panjab Univ., Sci., 34 (1983) 53.
518. B.L. Gorsi and R.C. Mehrotra, J. Indian Chem. Soc., 61 (1984) 189.
519. S.C. Goel, Synth. React. Inorg. Met.-Org. Chem., 13 (1983) 725.
520. M. Bei, L. Yuan, Y. Wu, H. Guo, Youji Huaxue, (1984) 43.
521. V.I. Zhukov, V.Ya. Ivolgin, G.P. Belov and N.V. Kartasheva, Kompleksn. Metalloorg. Katal. Polim. Olefinov, 8 (1983) 106.
522. F. Pilati, P. Manaresi, B. Fortunato, A. Munari and P. Monari, Polymer, 24 (1983) 1479.
523. V.Z. Maslosh, N.K. Bushueva and Yu.P. Kudyukov, Izv. Vyssh. Uchebn. Zaved., Khim. Khim. Tekhnol., 26 (1983) 1126.
524. J.C. Schra and S. Gundiah, Makromol. Chem., 185 (1984) 1117.
525. E. Nakamura, J. Shimada, Y. Koriguchi and I. Kuwajima, Tetrahedron Lett., 24 (1983) 3341.
526. P. Chaudhuri and H. Diebler, Z. Phys. Chem. (Munich), 139 (1984) 191.
527. A.S. Kereichuk, O.G. Lekhanova and L.N. Morozova, Probl. Sovrem. Anal. Khim., 4 (1983) 23.
528. A. Kitani and K. Sasaki, Denki Kagaku oyobi Kogyo Butsuri Kagaku, 52 (1984) 302.
529. R. Balachandran and T.R.N. Kutty, Mater. Chem. Phys., 10 (1984) 287.
530. A. Uri, Org. React. (Tartu), 20 (1983) 444.
531. L.S. Vol'dman and V.M. Berdnikov, Koord. Khim., 9 (1983) 1480.
532. M. Castillo and E. Ramirez, Transition Met. Chem. (Weinheim, Ger.), 9 (1984) 268.
533. M.F. Grigor'eva and M.G. Ivan'ko, Zh. Obshch. Khim., 53 (1983) 2233.
534. W. Jabs and W. Gäube, Z. Anorg. Allg. Chem., 514 (1984) 185.
535. Ya.I. Tur'yan, Elektrokhimiya, 19 (1983) 1615.
536. V.I. Krupenskii, Izv. Vyssh. Uchebn. Zaved., Lesn. Zh., (1984) 130.
537. A.N. Glebov, P.A. Vasil'ev and V.V. Ustyak, Fiz.-khim. Issled. Neorgan. Soedinen., Cheboksary, (1983) 39.
538. P.A. Awesarkar, S. Gopinathan and C. Gopinathan, Indian J. Chem., Sect. A, 22A (1983) 1076.
539. H. Kaneko, J. Electroanal. Chem. Interfacial Electrochem., 169 (1984) 221.
540. A.N. Glevov, Yu.I. Sal'nikov and V.V. Ustyak, Zh. Neorg. Khim., 28 (1983) 2691.
541. G.S. Sodhi, R.K. Majaj and N.K. Kaushik, Inorg. Chim. Acta, 92 (1984) L27.
542. S. Kumar, R.K. Mahajan and V.P. Kapila, Indian J. Chem., Sect. A, 22A (1983) 490.
543. A.I. Tolkuev, I.A. Vinokurov and V.I. Kravtsov, Vestn. Leningr. Univ., Fiz., Khim., (1984) 70.
544. A.I. Nikolaev, N.I. Kasikova, E.G. Il'in, and M.E. Ignatov, Zh. Neorg. Khim., 29 (1984) 2062.
545. B. Singh and H.N. Tiwari, J. Indian Chem. Soc., 60 (1983) 526.